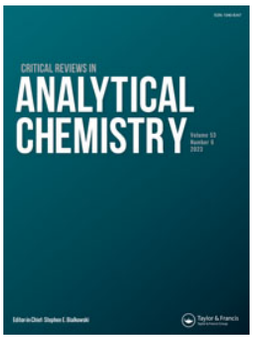

Taylor & Francis
Taylor & Francis Group

Critical Reviews in Analytical Chemistry

ISSN: (Print) (Online) Journal homepage: https://www.tandfonline.com/loi/batc20

Recent Advancements in Colorimetric and Fluorescent pH Chemosensors: From Design Principles to Applications

Dipanjan Banik, Saikat Kumar Manna, Anwesha Maiti & Ajit Kumar Mahapatra

To cite this article: Dipanjan Banik, Saikat Kumar Manna, Anwesha Maiti & Ajit Kumar Mahapatra (2023) Recent Advancements in Colorimetric and Fluorescent pH Chemosensors: From Design Principles to Applications, Critical Reviews in Analytical Chemistry, 53:6, 1313-1373, DOI: 10.1080/10408347.2021.2023002

To link to this article: https://doi.org/10.1080/10408347.2021.2023002

Published online: 28 Jan 2022.

CRITICAL REVIEWS IN ANALYTICAL CHEMISTRY
2023, VOL. 53, NO. 6, 1313–1373
https://doi.org/10.1080/10408347.2021.2023002

Recent Advancements in Colorimetric and Fluorescent pH Chemosensors: From Design Principles to Applications

Dipanjan Banik[a], Saikat Kumar Manna[b], Anwesha Maiti[a], and Ajit Kumar Mahapatra[a]

[a]Department of Chemistry, Indian Institute of Engineering Science and Technology, Shibpur, Howrah, West Bengal, India; [b]Department of Chemistry, Haldia Government College, Purba Medinipur, West Bengal, India

ABSTRACT

Due to the immense biological significance of pH in diverse living systems, the design, synthesis, and development of pH chemosensors for pH monitoring has been a very active research field in recent times. In this review, we summarize the designing strategies, sensing mechanisms, biological and environmental applications of fluorogenic and chromogenic pH chemosensors of the last three years (2018–2020). We categorized these pH probes into seven types based on their applications, including 1) Cancer cell discriminating pH probes; 2) Lysosome targetable pH probes; 3) Mitochondria targetable pH probes; 4) Golgi body targetable pH probes; 5) Endoplasmic reticulum targetable pH probes; 6) pH probes used in nonspecific cell imaging; and 7) pH probes without cell imaging. All these different categories exhibit diverse applications of pH probes in biological and environmental fields.

KEYWORDS

Colorimetric and fluorometric; pH chemosensors; biological and environmental applications

GRAPHICAL ABSTRACT

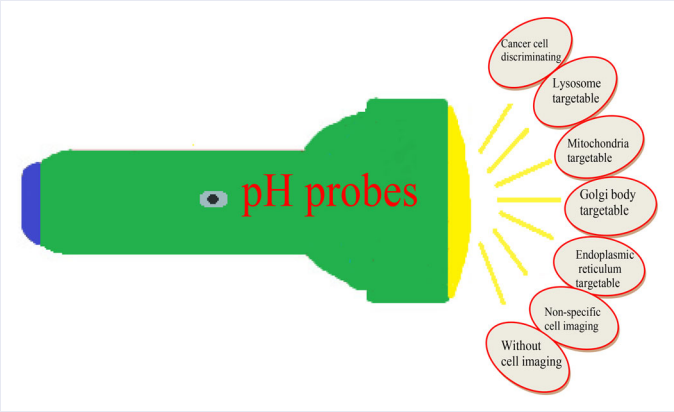

Introduction

pH is the power of hydrogen ion in aqueous solution expressed as $-\log_{10}[H^+]$ at a particular temperature. pH values are of utmost importance in all fields of chemical sciences, together with agriculture, wastewater treatment, industrial processes, environmental monitoring and in biological systems including physiological and pathological processes.[1] In this review pH values in aqueous-organic mixed solvents, when stated, refer to pH meter readings. Different biological processes like cell growth, cell metabolism, cellular proliferation and apoptosis,[2] enzymatic activity,[3] muscle contraction,[4] ion transport,[5] homeostasis,[6] endocytosis,[7] multidrug resistance,[8] receptor-mediated signal transduction,[9] are directly related to intracellular pH. Similarly, different subcellular organelles must maintain their individual intracellular pH levels, such as lysosomes (pH 4.0–5.5)[10] and Golgi apparatus (pH = 6.0–6.7)[11] need an acidic environment, whereas the cell nucleus (pH = 7.2–7.4)[12] and mitochondria (pH ≈ 8.0)[13] require midly alkaline environment for their optimal subcellular activity and metabolic processes.

However, abnormal or irregular pH can severely affect the normal and proper activity of subcellular organelles as well as various biological processes. Any fluctuation of normal pH leads to cellular dysfunctions[14] which are responsible for various fatal diseases like cystic fibrosis,[15] Alzheimer's disease,[16] cancer,[17] lysosomal storage disorder,[18] cardiopulmonary disease[19] and neurodegenerative diseases.[20] For example, under normal physiological conditions, the pH of extracellular fluid is nearly basic (pH 7.4)

CONTACT Ajit Kumar Mahapatra akmahapatra@rediffmail.com Department of Chemistry, Indian Institute of Engineering Science and Technology, Shibpur, Howrah, 711103 West Bengal, India; Saikat Kumar Manna saikat.manna.chem@gmail.com Department of Chemistry, Haldia Government College, Debhog, Haldia, Purba Medinipur- 721657, West Bengal, India

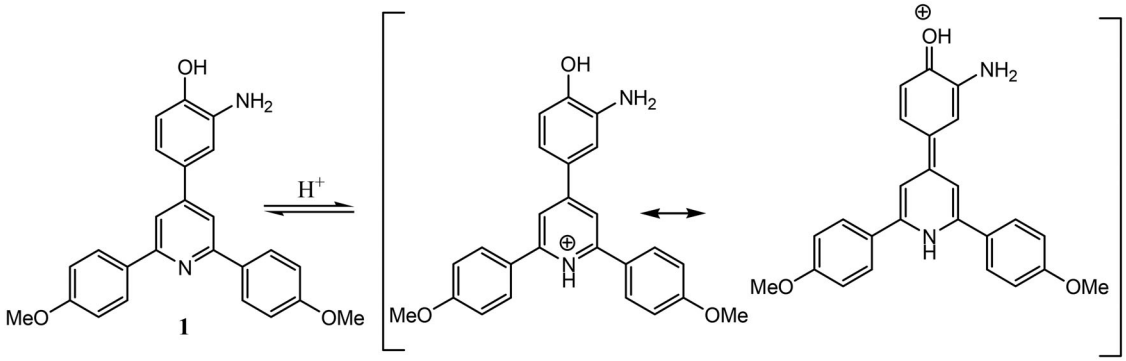

Figure 1. Chemical structure of cancer cell discriminating two-photon fluorescent probe **1** and its pH-controlled sensing process.

whereas it becomes acidic (pH= 6.2–6.9) in case of tumor formation. Lysosomal pH fluctuation can lead to aging, inflammation, lysosomal storage diseases, tumors. Similarly, slight changes in the alkaline environment in mitochondria can cause excess reactive oxygen species (ROS) production which is associated with cancer, aging, neurodegenerative and cardiopulmonary diseases. Hence, as pH values act as a key indicator of cell status linked with various cellular functions and metabolic processes, accurate and quantitative measurement of intracellular pH is necessary to diagnose various diseases and to properly understand related physiological and pathological processes.[21,22]

Various traditional methods like microelectrodes,[23] nuclear magnetic resonance (NMR),[24] absorption spectroscopy,[25] acid-base indicator titration, and potentiometric titration[26] are used for pH measurement, but these are complicated, costly and have low sensitivity.[27] Besides this, fluorescence imaging methods are more promising due to excellent sensitivity, low cost, simplicity of operation, rapid real-time response, high selectivity, low signal-to-noise ratio, noninvasive detection and high spatiotemporal resolution.[28–34]

Various reviews on pH probes have already been published.[35–40] However, because of the widespread interest and quick growth of this issue, the most current research achievements on fluorescent pH chemosensors must be discussed. In addition to the considerable progress of lysosome and mitochondrial targeted pH probes, Golgi and ER specific pH probes have recently been reported. As a result, in this study, we will properly and accurately summarize fluorescent pH probes published from 2018 to 2020, together with their design methods, sensing processes, and applications.

We classified the chemosensors into seven categories according to their applications. These are as follows: 1) Cancer cell discriminating pH probes; 2) Lysosome targetable pH probes; 3) Mitochondria targetable pH probes; 4) Golgi body targetable pH probes; 5) Endoplasmic reticulum targetable pH probes; 6) pH probes used in nonspecific cell imaging; and 7) pH probes without cell imaging.

pH probes with various applications

Cancer cell discriminating pH probes

During cancer chemotherapeutic therapy, neighboring healthy cells, as well as cancer cells, are damaged or destroyed, which might result in serious health consequences. So, in order to specifically find cancer cells, enhance the diagnostic process, and deliver medicines to target cells, cancer cells must be distinguished from normal cells based on the pH differential in their cell's microenvironment. To meet this need, it is important to develop highly sensitive, selective and biocompatible pH probes with good cell permeability. In this section, we summarize pH probes (**1** to **6**) which were applied to differentiate cancer cells using the fluorometric method.

In 2018, by using the advantages of an easy synthetic procedure, good thermal stability, and high quantum yield of the rarely reported 2,4,6-trisubstituted pyridine moiety, Ma *et al.* reported pH probe **1** to discriminate cancer cells from normal cells by using two-photon fluorescence microscopy.[41] On decreasing the pH from 7.00 to 2.20, the probe displayed 450-fold fluorescence enhancement at 475 nm with 121 nm of large stoke shift and this was due to protonation of pyridine "N" on increasing acidity. The probe showed good linearity within the pH range of 2.40 to 4.00 with a pK_a value of 3.22. The probe was found to be photo-stable and reversible and also exhibited good selectivity, as various ions, biologically relevant molecules did not show significant interference in pH monitoring except excess concentration of Hg^{2+} which caused a 20% decrease in fluorescence intensity when investigated at pH = 3.20 and pH = 4.20. Most importantly, the probe successfully differentiated HeLa cancer cells from normal 293 T cells by two-photon fluorescence imaging on excitation at 700 nm (Figure 1).

In the same year, Tian and coworkers reported a xanthene-based pH probe **2** contained electron withdrawing malonitrile moiety and phenolic –OH group for ratiometric monitoring of pH fluctuation.[42] To maintain the pK_a value within the physiological pH range, an electron- withdrawing malonitrile moiety was incorporated into the probe, and that made it suitable for tracking intracellular pH change in this range. When pH increased from 5.0 to 9.0, strong intramolecular charge transfer (ICT) was observed and that was due to alkali induced deprotonation of phenolic –OH group of the probe. There occurred a red shift in the absorption maxima (520 nm to 600 nm) with a color change from pink to vivid blue and an isosbestic point was found at 536 nm. Under similar condition, a ratiometric change was found in emission spectra where fluorescence intensity ratio (I_{623}/I_{572}) showed a 95-fold increment along with an increase in

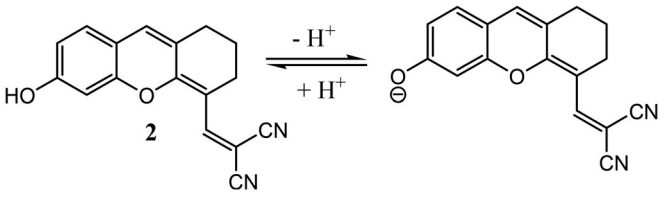

Figure 2. Chemical structure of xanthene-based pH probe **2** and its pH dependent structural alterations.

fluorescence quantum yield from 0.06 to 0.36. With good photo-stability and reversibility, the probe was found to be selective over various ions and amino acids. The probe was found to have good linear response with excellent sensitivity as within the pH range of 7.0–8.0 it exhibited up to 31.2% fluorescence signal change per 0.1 pH unit. Further, with more than 80 % cell viability and a pK_a value of 7.45, the probe was used to monitor pH variation in living HUVEC cells. More importantly, the probe could successfully differentiate tumor HeLa cells from normal HUVEC and Vero cells with 3.13- and 3.75-times fluorescence brightness than tumor cells respectively (Figure 2).

Saha's group reported another cancer cell discriminating pH probe **3** based on aminoquinoline moiety.[43] When investigated in Britton–Robinson buffer, the probe showed increase in absorption peak at 330 nm with a decrease of peak at 400 nm on changing the pH from 7.0 to 2.0. Again, on increasing pH from 7 to 11, the reverse observation was displayed in the absorption spectrum with a change in color from colorless to light yellow. In emission spectra, the fluorescence intensity showed gradual enhancement at 460 nm on changing the pH from 7.0 to 2.0, whereas on increasing pH from 7.5 to 9.5, intensity declined with broadening of the peak. Strong blue fluorescence was observed within pH 2–5 and within pH 6–9 fluorescence was weak. Strong fluorescence in acid medium was due to inhibition of photoinduced electron transfer (PET) process as imine "N" of the probe got protonated and this was further validated by nuclear magnetic resonance (NMR), density functional theory (DFT) and time-dependent density functional theory (TDDFT) study. The fluorescence quantum yield and fluorescence lifetime increased from neutral to acid medium and the pK_a value was 5.7. The probe was found to be highly selective as various cations (Na^+, K^+, Ca^{2+}, Mn^{2+}, Fe^{3+}, Co^{2+}, Ni^{2+}, Cu^{2+}, Zn^{2+} and Cd^{2+}) and anions (NO_3^-, Cl^-, SO_4^{2-}, PO_4^{3-}, PF_6^- and SO_3^{2-}) did not exhibit significant interference in pH sensing. Importantly, cancerous, MDA-MB 468 cells were successfully differentiated from normal HEK cells by fluorescence microscopy study (Figure 3).

She *et al.* has reported a cyanine dye based near-infrared (NIR) pH probe **4** for discriminating cancerous cell, tissue and living animal.[44] When the pH was reduced from 7.4 to 5, the probe displayed a red shift of 190 nm in the absorption spectra, with the color changing from red to green. Also 20-fold enhancement of fluorescence intensity at 780 nm in emission spectra was observed with pK_a value of 6.14. The protonation of one indole "N" of the probe in acid medium exhibited large π-conjugation which was responsible for this spectral change and it was confirmed by

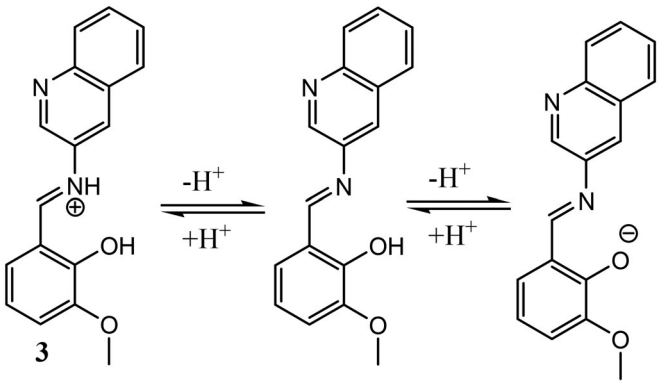

Figure 3. Chemical structure of cancer cell discriminating aminoquinoline-based pH probe **3** and its pH dependent structural alterations.

DFT study and mass spectroscopy. Again, the probe was found to be reversible within the same pH range and selective toward pH over various analytes. Fluorescence imaging in living cells successfully differentiated cancerous HCT116 cells from normal FHC cells, liver tissue of tumor mouse from normal mouse and a strong fluorescence at tumor site was observed when the probe was injected in HCT116-xenograft tumor mouse (Figure 4).

To investigate the effect of the small aromatic ring on the pH sensing abilities of the probes and to check whether two isomeric probes exhibit any difference in their sensing properties, Roy and coworkers have synthesized two reversible pH probes, **5** and **6**, by appending two different isomers of aminopyridine with 4-methyl-2,6-diformylphenol through condensation reaction.[45] On changing the pH from 4.0 to 10.0, both the probes displayed enhancement in fluorescence intensity by 195-fold for **6** and 66-fold for **5** at 530 nm along with an increase in fluorescence lifetime and quantum yield. A naked eye detectable color change from colorless to yellow in visible light and colorless to yellowish-green under UV-light appeared at pH 6.5 as well as it gradually got intense on increasing pH. This was mainly due to phenolic –OH de-protonation in alkaline medium and it was verified by ^{1}H-NMR and theoretical studies. These probes exhibited good selectivity over various ions and the pK_a value of both the probes **5** and **6** were found to be 7.15 and 6.57 respectively. More importantly, both the probes were used to discriminate HepG2 cancer cells (pH = 5.5) from normal WI38 cells (pH = 7.4) with negligible toxicity (Figure 5).

Lysosome targetable pH probes

Lysosomes are important subcellular acidic organelle of eukaryotic cell and its acidic pH (4.5–5.5) is maintained *via* proton pump from cytosol to lysosomal lumen by V-type ATP-ase.[46,47] This acidic environment helps in many cellular biological events such as digestion and degradation of damaged organelles and proteins, phagocytosis, plasma membrane repairing, energy metabolism.[48,49] Hence slight pH fluctuation in lysosome can induce adverse effect on cell function and can cause aging, inflammation, lysosomal storage diseases, rheumatoid arthritis, mucolipidoses, neurodegenerative diseases and tumors.[50–54] Additionally, recent

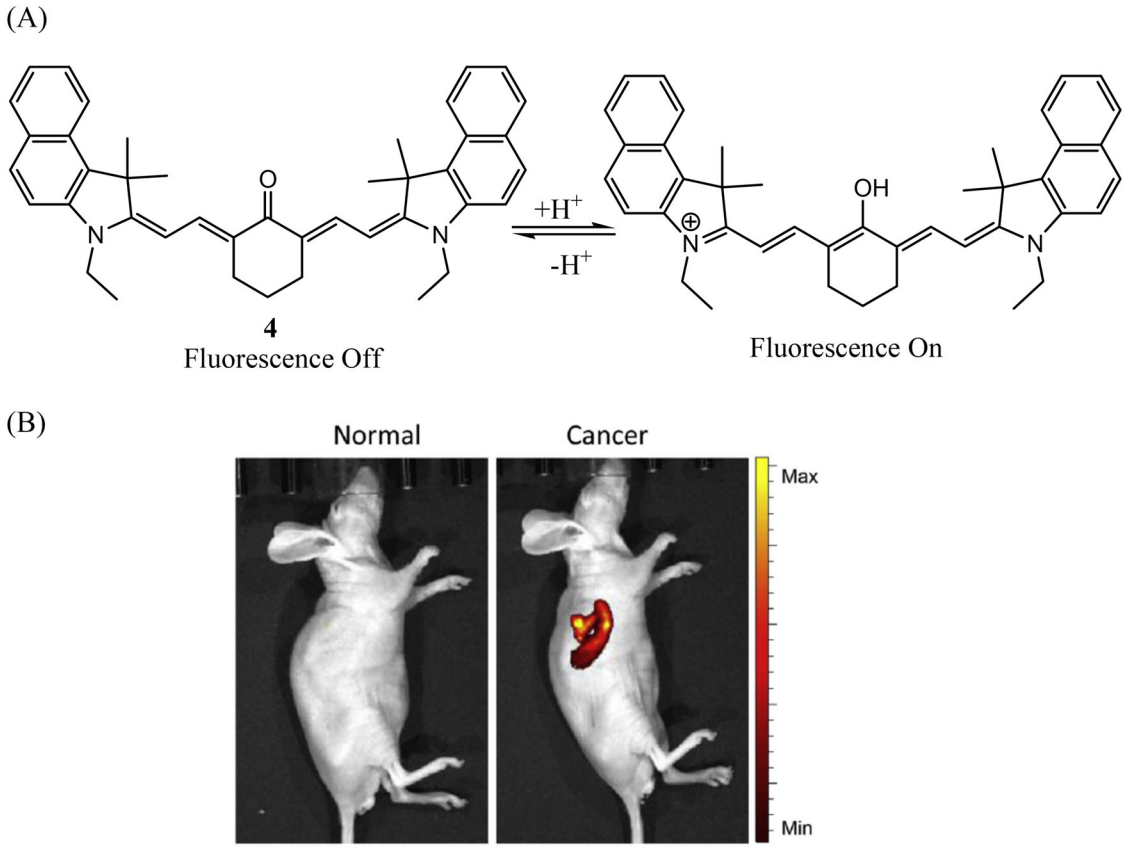

Figure 4. (A) Chemical structure of cancer cell discriminating NIR fluorescence pH probe **4** and its pH dependent structural alterations. (B) Fluorescence imaging of normal and HCT116-xenograft tumor mouse in presence of probe **4** (10 μM) [λ_{ex} = 715 nm, λ_{em} = 750–850 nm]. Reprinted from Ref. [44] Copyright (2020), with permission from Elsevier.

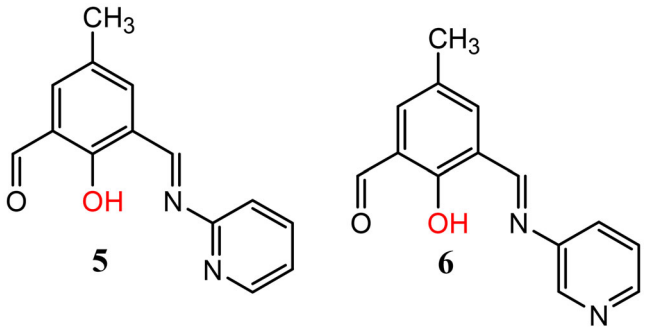

Figure 5. Chemical structures of cancer cell discriminating pH probes **5** and **6**.

studies have found that mitophagy and heat stress can cause lysosomal pH rise through increasing membrane permeability of lysosome and activating the lysosomal-mitochondrial apoptotic pathway.[55,56] Thus, it is necessary to monitor lysosomal pH accurately to understand its function and diseases related to it. Generally lipophilic molecules with alkalescence moieties are lysosome permeable and after protonation inside the lysosome it gets trapped due to its positive charge and become membrane impermeable. Commercially used lysotrackers are LTR (*Lyso Tracker Red)* and LTG (*Lyso Tracker Green)* whereas morpholine, dimethylamino, cyanide and methyl carbitol moieties are used in probes by researchers to locate lysosome. In this section we reviewed various lysosome targeted pH probe reported in last 3 years.

A two-photon pH probe **7** having lysosome targeting methylcarbitol unit and pH-responsive benzimidazole moiety was designed by Ge *et al.* for ratiometric monitoring of pH variance in lysosome of living cells and cancer tissues.[57] When investigated in H_2O/DMSO (4/1, v/v) medium by lowering the pH from 6.80 to 2.50, acid induced protonation of benzimidazole "N" of the probe caused enhancement of ICT from donor carbazole to acceptor benzimidazolium unit. As a result, red shift was observed in both absorption spectra (359 nm to 397 nm) and emission spectra (454 nm to 514 nm) with detectable color change from colorless to yellow as well as fluorescence change from blue to green. Having large stoke shift in both acid and basic medium, the emission intensity ratio ($F_{454\,nm}/F_{514\,nm}$) showed a good linear relationship within pH 5.0–3.82 with a pK_a value of 4.46. The two-photon fluorescence measurement showed enhancement of fluorescence intensity at 525 nm with a gradual decrease at 485 nm on decreasing pH. With good selectivity, reversibility and photo-stability, the probe was found to be lysosome targeting when co-localised with Lyso Tracker Red DND-99 in HeLa cells. Ratiometric two-photon fluorescence imaging in live HeLa cells and living tissues from the liver of cancerous mouse proved the probe's capability to monitor intracellular pH fluctuation. Furthermore, the probe was used to track lysosomal pH change induced by NH_4Cl, H_2O_2 and NAC(N-acetylcysteine) (Figure 6).

Liu's group reported two pH probes (**8** and **9**) constructed by connecting coumarin and NIR hemicyanine

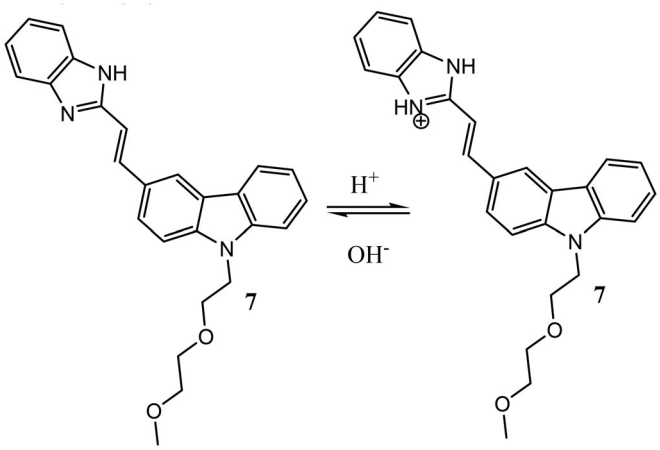

Figure 6. Chemical structure of lysosome targetable two-photon ratiometric fluorescent pH probe **7** and its pH dependent structural alterations.

moiety modified with lysosome targetable morpholine and *o*-diaminebenzene unit.[58] When pH was changed from 7.0 to 2.5, the acid induced opening of spirolactam rings of both the probes caused enhancement of π-conjugation. Consequently, a ratiometric reversible fluorescence change took place where hemicyanine fluorescence increased at 755 nm for probe **8** and 740 nm for probe **9** with simultaneous lowering of coumarin fluorescence at 528 nm for probe **8** and 515 nm for probe **9**. The probes were found to be selective, photo-stable and the pK_a values were 4.2 and 4.8 for probe **8** and **9** respectively. With negligible cytotoxicity, the probe **8** was found to be lysosome targeting and both the probes were used to monitor pH change in living HeLa cells ratiometrically (Figure 7).

Liu *et al.* designed three NIR pH probes **10**, **11** and **12** by connecting aggregation-induced emission (AIE) containing tetraphenylethylene (TPE) moiety as donor with hemicyanine moiety as acceptor *via* through bond energy transfer (TBET) (probe **10**) and π-conjugation modulation (probe **11** and **12**) strategy with incorporation of morpholine residue to target lysosome.[59] When the pH was reduced from 7.4 to 2.5, all three probes showed a ratiometric fluorescence response with a decrease in donor TPE fluorescence and an increase in acceptor hemicyanine fluorescence due to large π-conjugation caused by acid induced spirolactam ring opening. Among three probes, probe **10** showed better ratiometric response with 238-fold enhancement of fluorescence intensity ratio (I_{737} nm/I_{510} nm) due to its high TBET from donor to acceptor on excitation at 420 nm. Further, with good selectivity and photostability, all the probes were found to have excellent membrane permeability and lysosome staining ability. Finally, probe **10** showed better ratiometric fluorescence imaging of intracellular pH in living HeLa cells (Figure 8).

A rhodamine-based pH probe **13** was developed by Yoon's group by incorporating lysosome targeting weakly basic N-(2-aminophenyl) aza-18-crown-6 moiety.[60] The author showed that after the introduction of the crown ether ring, the probe exhibited better water solubility and could track acidic pH. Acid induced spirolactam ring opening of rhodamine caused more than 230-fold enhancement in fluorescence intensity at 588 nm and an increase in absorption peak was observed at 570 nm with a color change from colorless to pink on increasing acidity (pH 7.0 to 3.0) in 1 % MeCN containing Britton-Robinson (BR) buffer. The fluorescence quantum yield also increased from 0.05 (pH 7.0) to 0.46 (pH 4.0). Being reversible (within pH 4.0–7.0) with high selectivity over cations and amino acids, the probe showed good linear response within pH 4.2–6.0 and the pK_a value was 4.10. Furthermore, the probe was used to monitor lysosomal pH increase induced by chloroquine and dexamethasone as well as lysosomal pH decrease induced by artesunate in HeLa cells with negligible cytotoxicity and good photostability (Figure 9).

Wu *et al.* utilized the hemicyanine moiety to develop a pH probe **14** for ratiometric detection of pH changes in the lysosome.[61] They used a morpholine unit as an anchor to tergate lysosomes, and that could prevent the leakage of the probe during heat shock. Deprotonation of phenol moiety induced a decrease in emission intensity at 522 nm along with an increase at 557 nm with pH change from 3 to 11. The maximum emission intensity ratio (F_{522}/F_{557}) changed from 0.18 to 1.2 on decreasing the pH from 11 to 3 with good reversibility and the pK_a value was 5.96. Co-localization experiment by using LysoTracker Deep Red revealed the probe's lysosome targeting ability. Further lysosomal pH increase during heat shock and its reversibility with uneven pH distribution in lysosomes was successfully monitored by using the fluorescence intensity ratio of two channels (green, 500–550 nm and yellow, 570–620 nm) in HeLa cells (Figure 10).

Zhang *et al.* synthesized three NIR rhodamine dyes among which probe **15** was successfully used to monitor lysosomal pH changes.[62] The introduction of an extra amine group in the rhodamine moiety of probe **15** improved its electron donation ability and photophysical properties. Enhancement in absorption peak at 587 nm and emission peak at 655 nm with turn-on fluorescence response was caused by acid induced spirolactam ring opening of probe **15** when pH changed from 7.6 to 2.0. Large steric hindrance between amine moiety and xanthene moiety in probe **15** made it to have a quick and selective response toward pH change with a high pk_a value of 5.4. Co-culturing of probe **15** with lysotracker green in HeLa cells revealed its lysosome targeting ability and further experiment demonstrated that probe **15** could image pH increase in the lysosome due to H_2O_2 and N-ethylmaleimide induced oxidative stress. Again, NH_4Cl and chloroquine induced alkalification was also tracked by the probe. Furthermore, intracellular pH change in MCF7 human breast cells and HeLa cells was monitored by probe **15** with good photostability and low toxicity (Figure 11).

By incorporating pH sensitive dimethylamino groups and lysosome anchoring morpholine unit in boron-dipyrromethene (BODIPY) fluorophore, Zhu *et al.* synthesized two acidic pH responsive probes **16** and **17**.[63] When investigated in THF/H_2O (1:1, v/v) by decreasing pH from 6.83 to 0.82, protonation of dimethylamino groups in both the probes inhibited the ICT process and that caused large blue

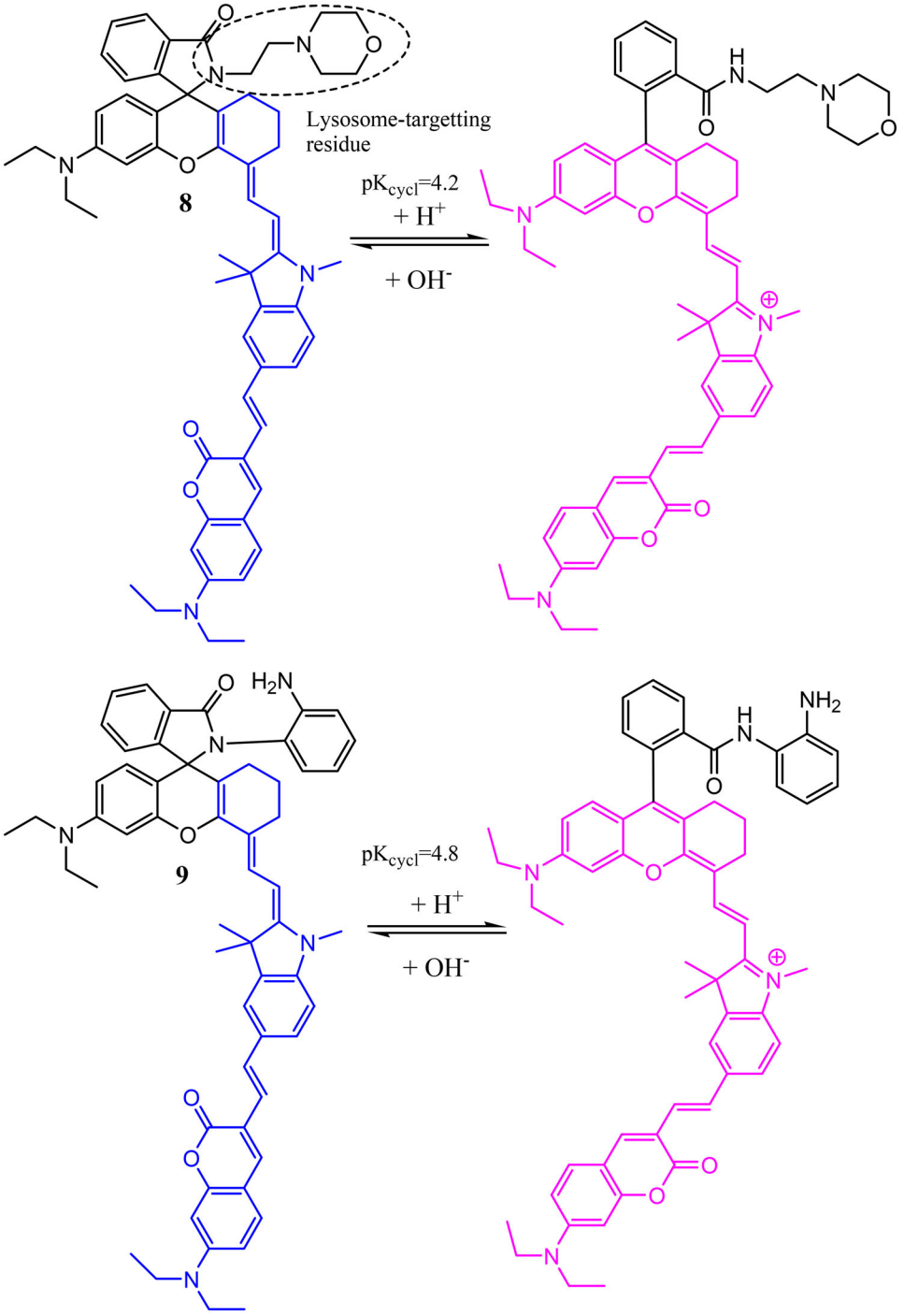

Figure 7. Chemical structure of lysosome targetable probes **8** and **9** and their pH-dependent structural alterations.

shift in both absorption and emission spectra. There occurred a 300-fold increase in emission intensity ratio (I_{515}/I_{665}) of probe **16** with pK_a value of 2.0 under similar condition. Probe **17** also showed an increase in emission intensity ratio (I_{520}/I_{730}) from 0.63 (pH = 6.83) to 924 (pH = 0.82) with two pK_a values of 3.3 and 1.5. Both the probes were found to be lysosome specific when co-localized with commercial LysoTracker^{TM} Blue DND-22 in A549 cells and also exhibited more than 85% cell viability under 20 μM. Further both the probes displayed significant ratiometric change within pH 4.0–3.0 in intracellular pH monitoring (Figure 12).

In 2018, Lin and coworkers reported a two-photon pH probe **18** by modifying naphthalimide moiety with pH sensitive, lysosome targeting morpholine and piperazine units.[64] When investigated in B-R buffer by increasing pH from 2.0 to 10.0, the probe exhibited a decrease of absorption peak at 396 nm and 52-fold decrease of emission peak at 531 nm. Protonation of morpholine "N" and piperazine "N" in acid medium induced PET off and caused strong fluorescence. The probe **18** was found to be selective over various bioactive molecules and ions (Mg^{2+}, Ca^{2+}, H_2O_2, GSH and Cys) and also showed reversible behavior between pH 5.5 and 7.4 up to more than six cycles. Co-localization with

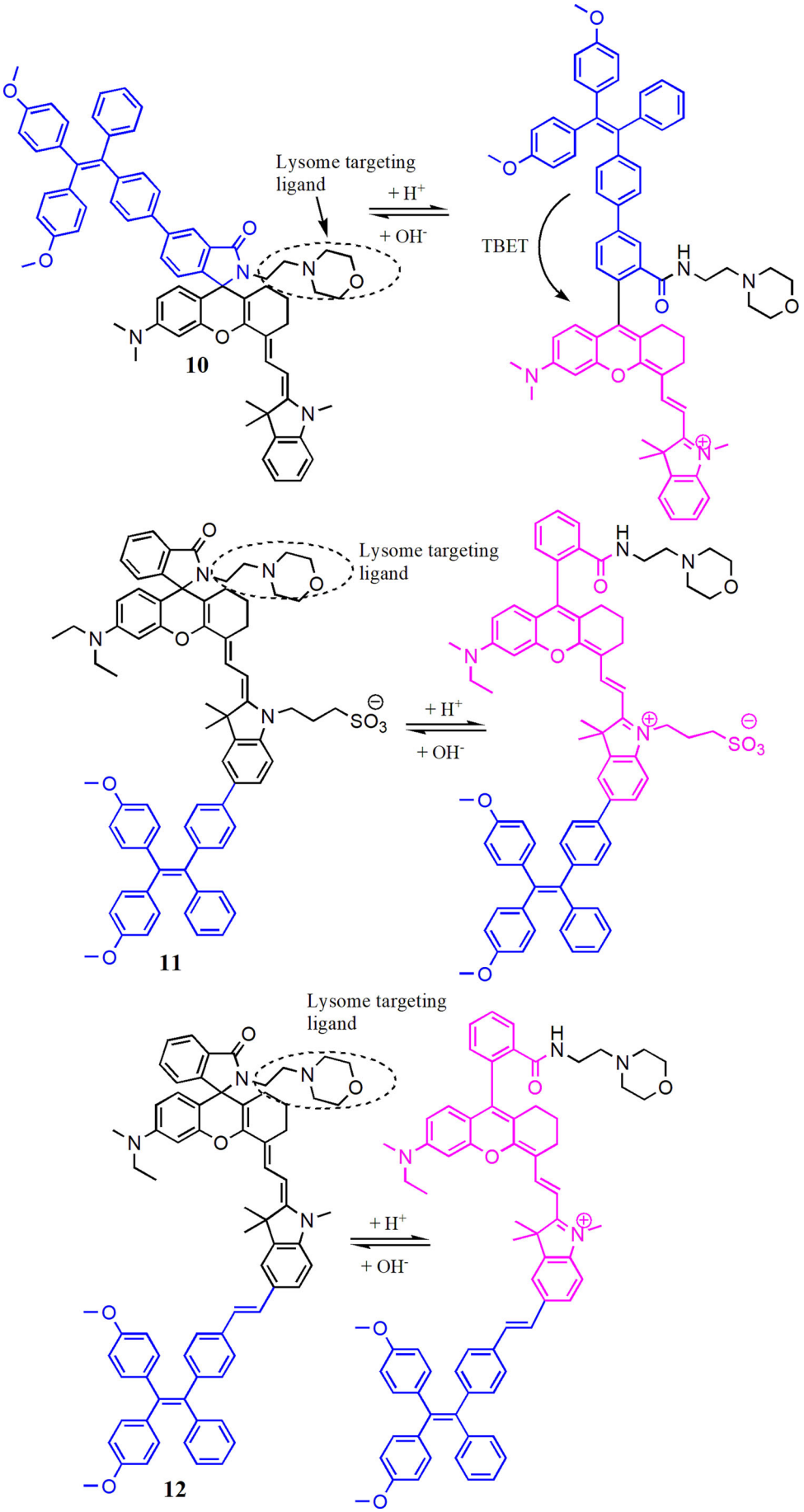

Figure 8. Chemical structures of lysosome targetable ratiometric NIR probes **10**-**12** and their pH-dependent structural alterations.

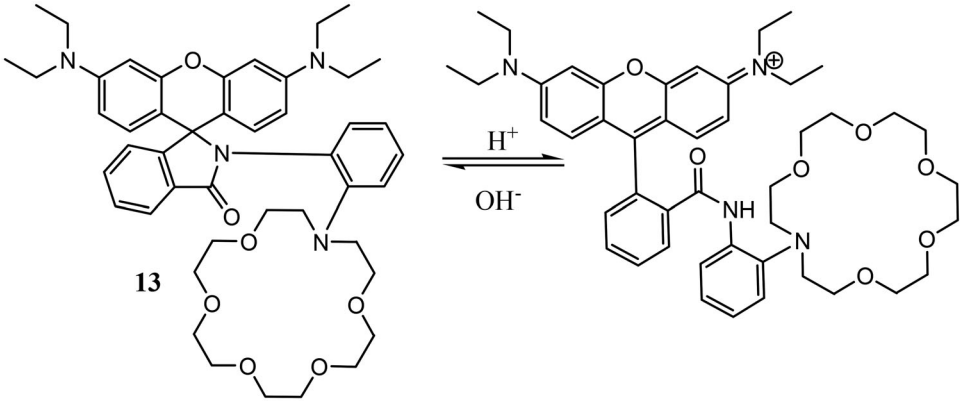

Figure 9. Chemical structure of rhodamine-based lysosome targetable pH probe **13** and its pH-dependent structural alterations.

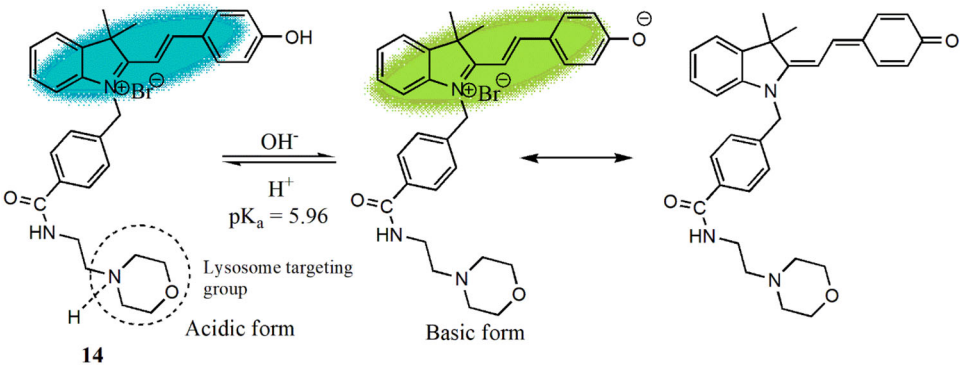

Figure 10. Chemical structure of lysosome targetable ratiometric fluorescent probe **14** and its pH-dependent structural alterations.

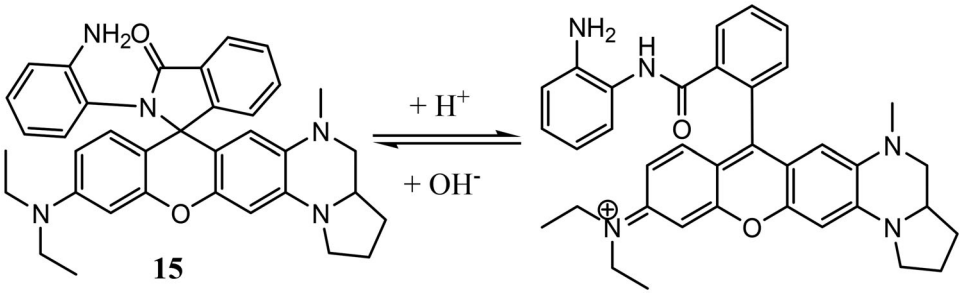

Figure 11. Chemical structure of lysosome targetable rhodamine based NIR pH probe **15** and its pH-dependent structural alterations.

LysoTracker Red® displayed the probe's lysosome labeling ability and two-photon imaging of chloroquine induced lysosomal pH change was successfully done by the probe **18** (Figure 13).

Liu *et al.* reported two NIR pH probes **19** and **20** for monitoring lysosomal pH fluctuation in living cells by using both stoke-shift and anti-stoke shift fluorescence measurement.[65] Both the probes contained lysosome targeting morpholine unit whereas the mannose unit of probe **20** made it bio-compatible and enhanced its solubility in aqueous solution. On decreasing pH from 7.22 to 2.76, both the probes showed enhancement at 699 nm and 693 nm in stokes and anti-stoke shift fluorescence measurement respectively with good reversible response and this was due to enhancement of π-conjugation resulted from acid induced spirolactam ring opening. The pK_a values for both the probes were 4.80 (**19**) and 4.40 (**20**). Being photostable with minimum photo bleaching issues, both the probes showed good selectivity toward pH over various bio-relevant species. Both the probes targeted the lysosome when co-cultured with LysoTracker green in HeLa cells where probe **20** showed comparatively low toxicity and stronger fluorescence due to its mannose unit. Both the probes were applied to visualize pH change in lysosome by using stoke and single photon anti-stoke shift fluorescence measurement in HeLa and KB cells. Additionally, stoke shift fluorescence measurement of lysosomal pH change was also investigated in HUVEC-C and MDA-MB231 breast cancer cells (Figure 14).

Zhang *et al.* synthesized a rhodamine based NIR pH probe **21** and a Förster or fluorescence resonance energy transfer (FRET) based NIR pH probe **22** where probe **22** was designed by connecting rhodamine as FRET donor with cyanine as FRET acceptor through ethylene-diamino linkage.[66] Acid induced spirolactam ring opening of probe **21** led to increase of emission peak at 623 nm on decreasing pH from 7.0 to 2.4 and the pK_a value was calculated to be

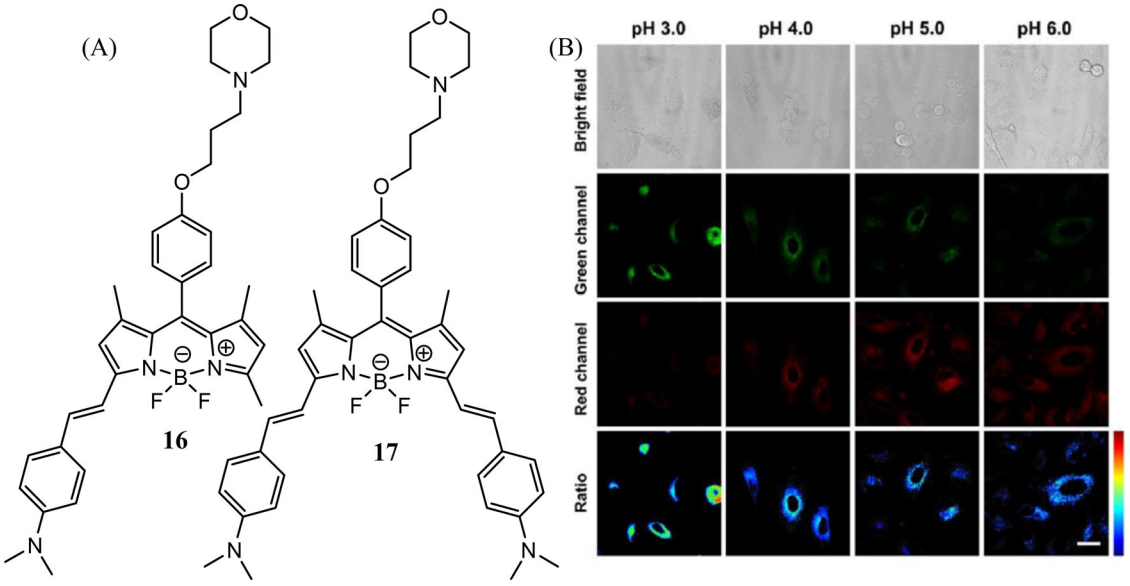

Figure 12. (A) Chemical structures of lysosome targetable BODIPY based ratiometric fluorescent pH probes **16** and **17.** (B) Fluorescence imaging of probe **16** (5 μM) in A549 cells at several pH [Green channel (λ_{em} = 515–565 nm), red channel (λ_{em} = 650–700 nm), λ_{ex}=488 nm, Ratio images show the fluorescence intensity ratio between the green and red channels (I_{green}/I_{red})]. Reproduced/Adapted from Ref. [63] with permission from The Royal Society of Chemistry.

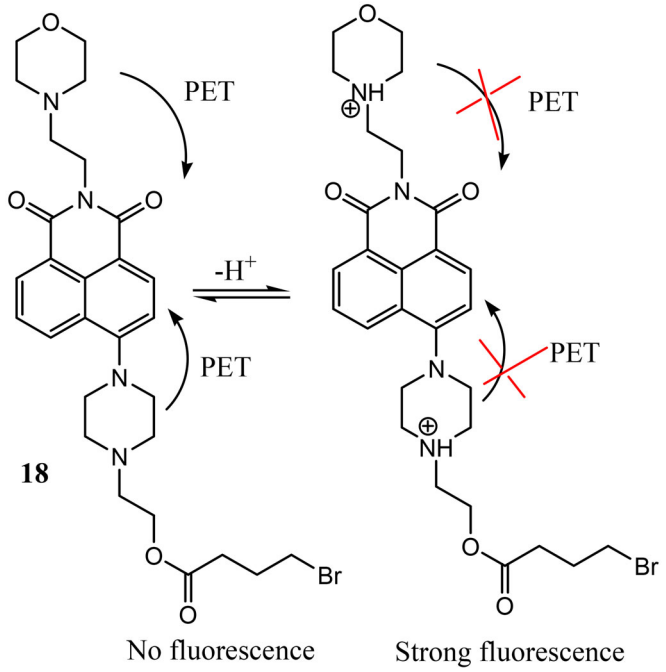

Figure 13. Chemical structures of lysosome targetable two-photon fluorescent probe **18** and its pH-dependent structural alterations.

5.15. Similarly, protonation of N atom led to spirolactam ring opening of probe **22** in acidic pH which induced the enhancement of emission peak at 616 nm and 743 nm on excitation at 450 nm with two pK_a values of 4.0 (from rhodamine donor) and 7.4 (from cyanine acceptor). Finally, with reversibility and selectivity over various metal ions, anions and biologically relevant small molecules both the probes were found to be lysosome targetable and could monitor intracellular pH change in living HeLa cells (Figure 15).

Wang *et al.* synthesized three NIR pH probes **23**, **24** and **25** by connecting AIE fluorophore TPE with NIR fluorophore rhodamine for ratiometric monitoring of pH variation through both TBET and FRET mechanism.[67] All the three probes responded within pH 7.4 – 3.0 where on increasing acidity, acid induced spirolactam ring opening caused decrease of donor TPE emission and simultaneous increase of acceptor rhodamine emission due to energy transfer occurred through both TBET and FRET. Signal-to-background emission ratios in terms of donor to acceptor showed 365, 1762 and 131-fold enhancement and the pK_a values found to be 4.4, 4.6 and 4.8 for **23**, **24** and **25** respectively. The probes exhibited good photostability and reversibility and no significant interference was observed from cations, anions and bioactive molecules in pH determination. Being consistent with the fluorescence spectra in buffer solution, all the three probes ratiometrically detect pH variation in living HeLa cell and stained lysosome with high Pearson's coefficients. Furthermore, probe **25** was applied to monitor lysosomal pH increase induced by chloroquine (Figure 16).

Ning *et al.* reported a ratiometric two-photon fluorescent probe **26** which contained pH-responsive benzimidazole and lysosome targeting morpholine moiety.[68] The probe exhibited a red-shift (340 nm to 385 nm) in absorption spectra with isosbestic point at 370 nm on changing pH from 8.2 to 3.2. In emission spectra there also occurred a 65 nm red shift (410 nm to 475 nm) with fluorescence change from weak blue to green and fluorescence intensity ratio ($I_{475\,nm}/I_{410\,nm}$) enhanced 140-fold (0.34 to 47.62) along with fluorescence quantum yield from 5.23% to 11.27% on decreasing the pH from 9.6 to 3.2. This was mainly due to protonation of benzimidazole "N" in acid medium enhanced the ICT process, which was further confirmed by ^{1}H-NMR and TD-DFT studies. The probe was found to be reversible between pH 4.2 – 7.2 up to 6 cycles with a pK_a value of 4.86 and have good selectivity with linear response of the fluorescence intensity ratio ($I_{475\,nm}/I_{410\,nm}$) within pH 4.2 to 5.6. The

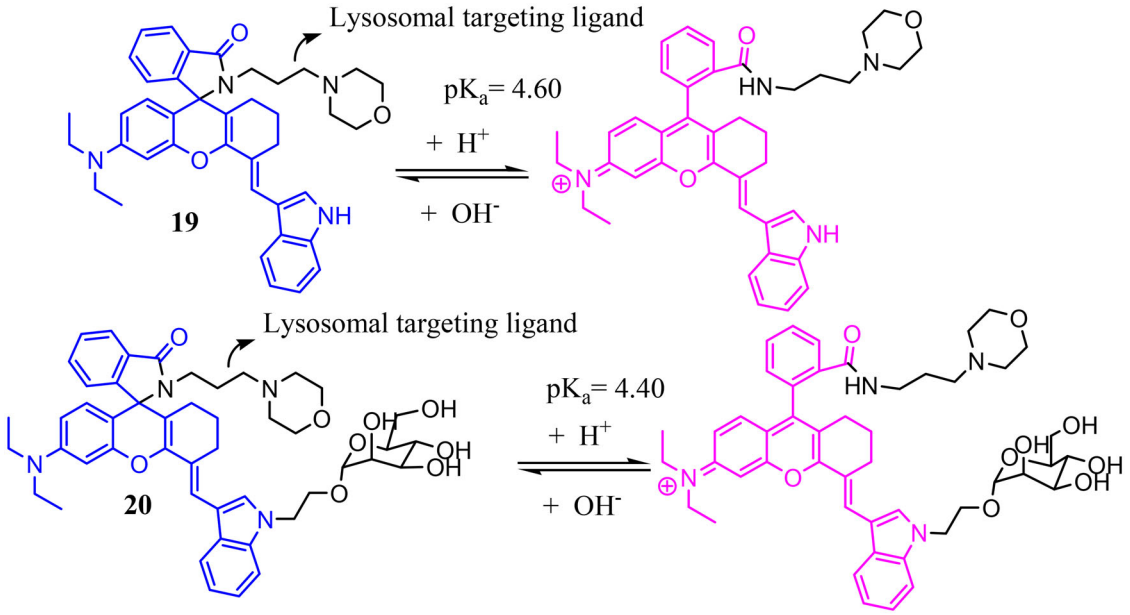

Figure 14. Chemical structures of lysosome targetable two-photon fluorescent probes **19** and **20** and their pH-dependent structural alterations.

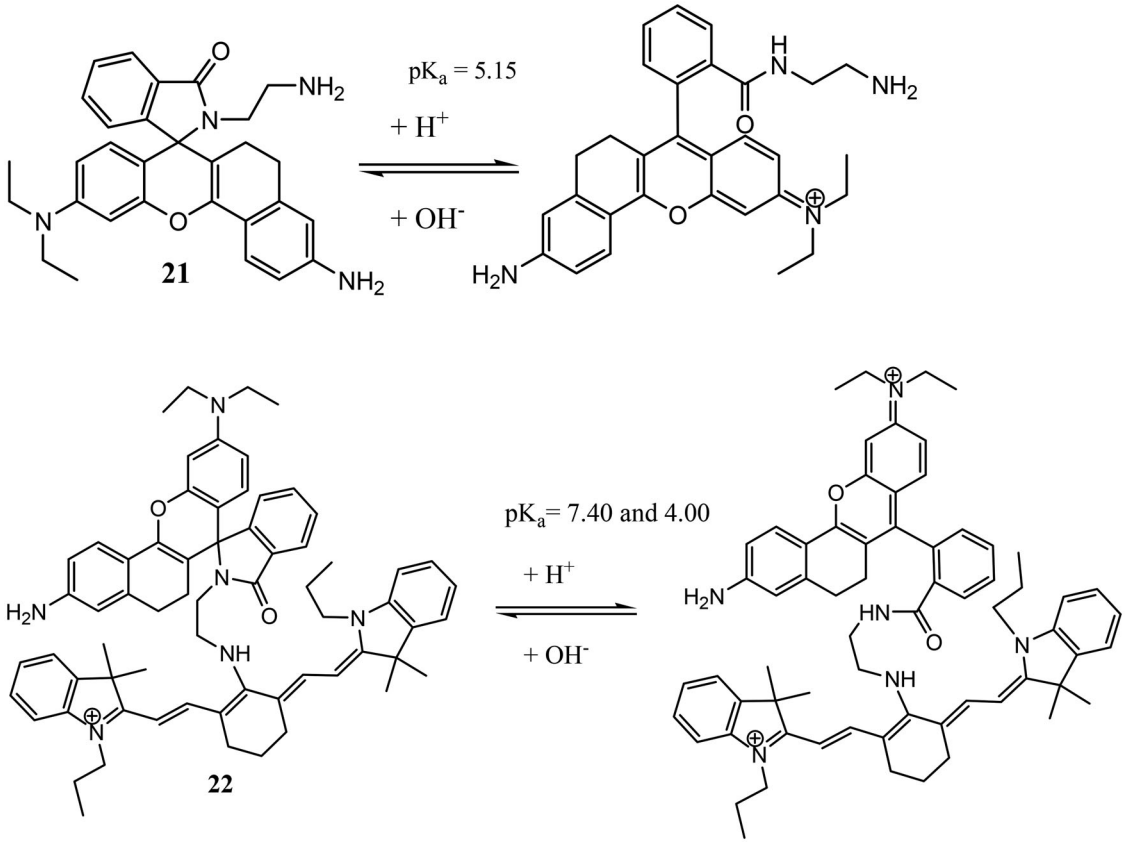

Figure 15. Chemical structures of lysosome targetable FRET-based NIR fluorescent probes **21** and **22** and their pH-dependent structural alterations.

colocalization study with LysoTracker Red revealed the probe's lysosome targeting ability. More importantly, the probe was successfully used in quantitative monitoring of intracellular pH and starvation induced autophagy through ratiometric two-photon imaging in MCF-7 cells. Overall, this probe could be very effective in real-time monitoring of autophagy conditions by using the advantages of both the ratiometric and TPM methods (Figure 17).

Based on *in situ* switching of spiropyran from its closed to open form, Li and coworkers reported four NIR pH probes **27**, **28**, **29** and **30** for ratiometric monitoring of lysosomal pH change.[69] On changing pH from 6.0 to 4.0, acid induced opening of closed spiropyran ring of all the probes led to exhibit ratiometric response with NIR emission. The pK$_a$ values of all the probes were found to be 5.40(**27**), 5.35(**28**), 5.42(**29**) and 5.26(**30**). With good selectivity and

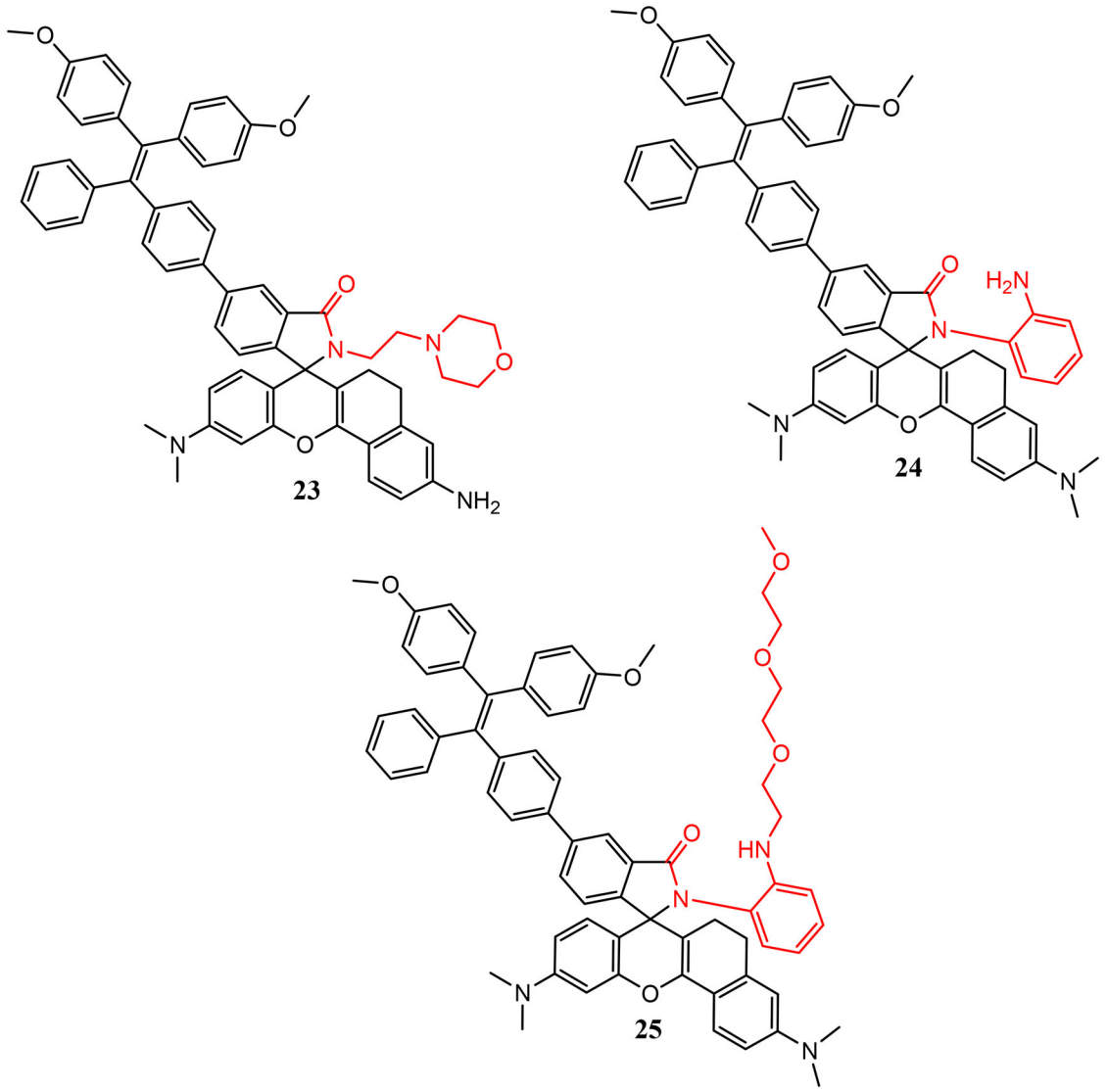

Figure 16. Chemical structures of TBET and FRET-based NIR ratiometric fluorescent pH probes **23-25**.

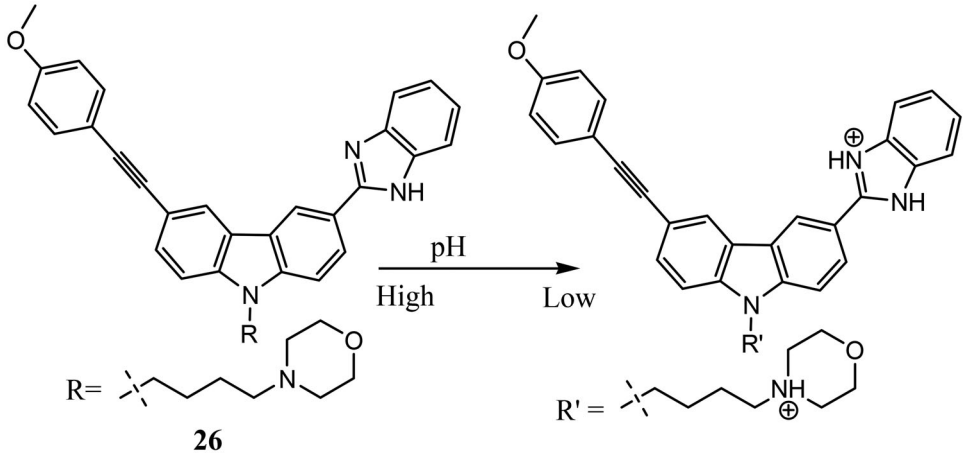

Figure 17. Chemical structure of lysosome targetable ratiometric two-photon fluorescent probe **26** and its pH-dependent structural alterations.

light stability all the probes were found to be lysosome specific where probe **28** with its best ratiometric behavior showed high PCC (Pearson's colocalization coefficients) of 0.98 when co-localized with commercial LysoTracker Green DND-26 in HepG2 cells. Moreover, probe **28** was successfully used to monitor intracellular pH change, chloroquine induced and heat shock induced lysosomal pH increase ratiometrically. Lastly, the effectiveness of these spiropyran *in situ* switching (SIS) mechanism based ratiometric NIR probes might draw the attention of new researchers (Figure 18).

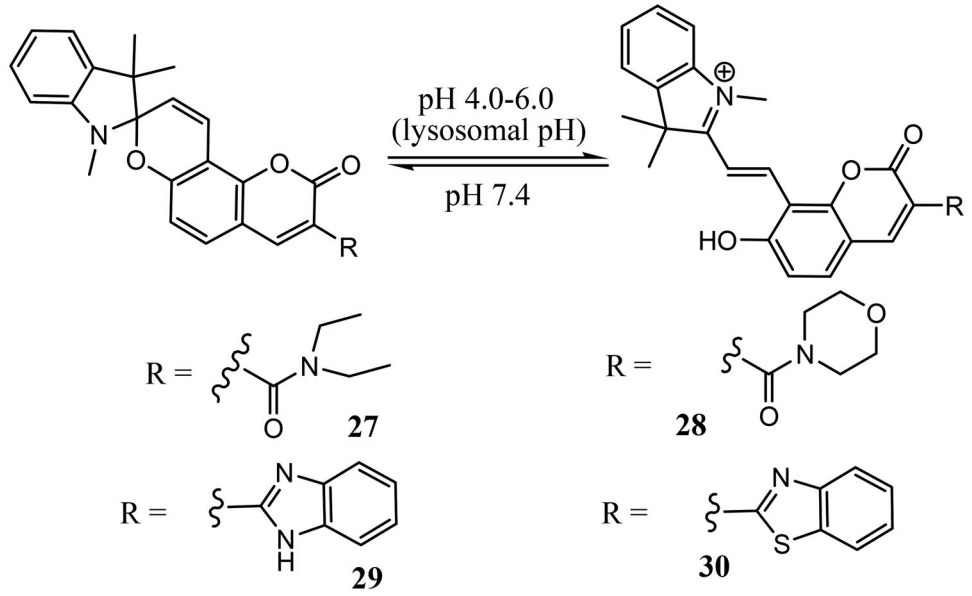

Figure 18. Chemical structures of lysosome targetable ratiometric NIR fluorescent probes **27-30** and their pH-dependent structural alterations.

Shi *et al.* Synthesized a NIR pH probe **31** by co-ordinating boron fluoride with a hemicyanine framework and this co-ordination improved the probe's photostability as well as the probe exhibited a large stoke shift of 55 nm.[70] On increasing pH from 3.29 to 9.07, the probe exhibited an obvious enhancement in emission intensity in the acidic pH range (3.29 to 6.24) whereas a slight change was observed in alkaline pH range (7.40 to 9.07). This was mainly due to protonation/deprotonation of the imine unit of the probe and that was further verified by ^{1}H-NMR study. Further, the probe showed good linear response within pH 3.29 to 6.24 with a pK_a value of 5.03 and exhibited reversible nature within the pH range of 3.5 to 9.2. Cell experiments by co-staining the probe with lysotracker displayed that the probe was lysosome targeted with good biocompatibility and high anti-interference property. Again, the probe was used to monitor intracellular pH fluctuation and chloroquine induced lysosomal pH increase in living HeLa cells. Lastly, *in vivo* imaging in living mice showed that the fluorescence intensity of the probe was higher in the saline (pH 6.9) injected side rather than the acidic side (pH 5) of mice. Finally, this novel concept of combining the boron complex with the classic hemicyanine moiety would encourage researchers to construct new kinds of fluorescent probes in the future (Figure 19).

In 2019, Liu's group designed three NIR probes **32**, **33** and **34** by connecting different donor BODIPY derivatives with acceptor rhodamine and merocyanine moieties bearing weakly basic lysosome targetable morpholine and amine residues.[71] With good selectivity and photostability, all the probes showed ratiometric fluorescence response where a decrease of donor (BODIPY derivatives) fluorescence intensity and increase of acceptor (rhodamine and merocyanine) fluorescence intensity was observed on changing pH from 7.6 to 1.6. The fluorescence enhancement of probes **32**, **33** and **34** was 138.7, 29.9, and 64.1-fold respectively and this was mainly because of acid induced opening of the acceptor's spirolactam ring which enables the energy transfer from donor to acceptor through both TBET and FRET process. Furthermore, probe **32** and **33** were found to have good lysosome targeting ability and could monitor intracellular pH ratiometrically in both visible and near-infrared channels. Again probe **33** was used to monitor N-acetyl cysteine (NAC), NH_4Cl, chloroquine and H_2O_2 induced lysosomal pH change due to its better ratiometric response (Figure 20).

Ge *et al.* reported two carbazole based pH probes **35** and **36** for monitoring lysosomal pH.[72] The probe **36** showed a red shift both in absorption spectra (397 nm to 480 nm) and emission spectra (520 nm to 608 nm), with detectable color change from colorless to pink and fluorescence change from yellow to red when the pH was reduced from 7.1 to 2.50. The fluorescence intensity ratio ($F_{520\,nm}/F_{608\,nm}$) of probe **36** also lowered with good linear response within pH 4.67–3.33. Probe **35** also displayed a 14 nm hypsochromic shift in absorption spectra (λ_{max} = 486 nm) and a 16 nm hypsochromic shift in emission spectra (λ_{em} = 592 nm) on increasing acidity of the medium. These spectral changes were attributed to enhancement of ICT from electron donating carbazole moiety to electron withdrawing benzo-indole moiety which was due to acid induced protonation of benzo-indole moiety. Both the probes showed their selective response toward pH changes over different metal ions and bio-relevant molecules with pK_a values of 4.26(**36**) and 4.51(**35**). With good photostability, excellent reversibility and low cytotoxicity, both the probes successfully targeted lysosomes in HepG2 cells with LysoTracker Green DND-26. Moreover, the probes detected intracellular pH change ratiometrically in HepG2 cells as well as H_2O_2 and NAC induced pH changes in lysosome (Figure 21).

Zhang *et al.* developed three ICT based ratiometric pH probes **37**, **38** and **39** by linking electron donor N, N-dimethylaniline and triphenylamine moieties with electron acceptor 2-(4-methoxyphenyl)imidazo [1,2-a]pyridine

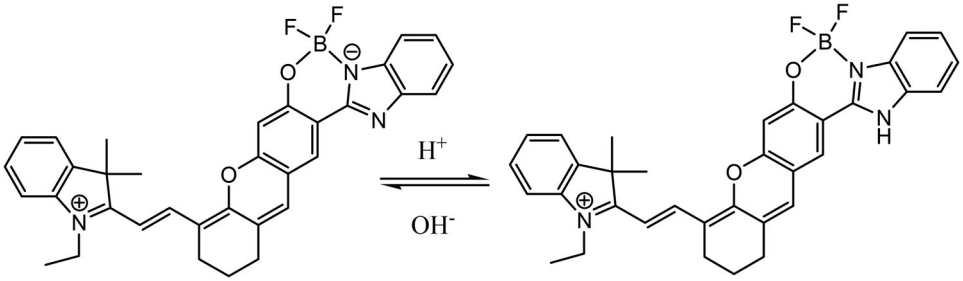

31

Figure 19. Chemical structure of lysosome targetable NIR fluorescent probe **31** and its pH-dependent structural alterations.

moiety.[73] On lowering the pH from 7.0 to 2.2, acid induced protonation of imidazopyridine N favored strong ICT and due to this reason all the probes exhibited red shift in their emission maxima. The pK_a values were determined to be 3.3 (**37**), 2.1 (**38**) and 3.1 (**39**). Probe **37** and **39** were employed in ratiometric intracellular pH monitoring in living HeLa cells with good cell permeability. Moreover, all the three probes were found to be lysosome targetable and successfully used to monitor acidic pH in Escherichia coli (E. coli) bacteria with good selectivity and reversibility (Figure 22).

Niu *et al.* reported a carbazole based NIR pH probe **40** by modifying it with a lysosome targetable methylcarbitol unit and proton responsive quinoline moiety.[74] The probe displayed a red shift (383 nm to 464 nm) in absorption spectra with an isosbestic point at 415 nm on increasing acidity (pH 7.0 to 2.5) and a distinct color change was observed from colorless to orange. Under similar conditions (pH 7.0 to 1.9), red shift was also observed in emission spectra and that enabled ratiometric response. The emission intensity ratio (I_{530}/I_{637}) exhibited more than 260-fold change with good linearity within the pH range of 3.9 to 5.3. Enhancement of the ICT process due to protonation of quinoline "N" in acid medium was the main reason behind this spectral change. With a pK_a value of 4.60, the probe showed good selectivity, photostability and reversible behavior within pH 7.0 to 2.2. Furthermore, the probe was found to be lysosome specific (PCC = 0.93) when co-localized with commercial LysoTracker Red DND-99 and could image pH change ratiometrically in B16-F10 cells. In addition, the probe was used in *in vivo* fluorescence imaging of LPS (lipopolysaccharide) induced inflamed tissues of mice (Figure 23).

Recently, Zhou's group constructed a FRET-based two-photon pH probe **41** by linking fluorophore naphthalimide as donor and rhodamine B as acceptor with lysosome targetable morpholine moiety for ratiometric monitoring of lysosomal pH in living cells and in Zebrafish.[75] On increasing acidity (pH 8.0 to 4.0), acid induced spirolactam ring opening caused FRET with a decrease of donor green emission at 510 nm and an increase of accepter red emission at 595 nm and that enabled ratiometric sensing (I_{595}/I_{510}) of pH. With good reversibility, selectivity and negligible cytotoxicity, the probe was found to be lysosome targeted when co-stained with Lysotracker Deep Red in HeLa cells. Further, the probe could track chloroquine induced lysosomal pH change by dual channel fluorescence emission in living HeLa cells and Zebrafish. These kinds of FRET-based two-photon ratiometric pH probes need to be constructed in the near future (Figure 24).

Mazi *et al.* synthesized three lysosome specifying probes **42**, **43** and **44** by incorporating bulky moiety of 2-aminophenylboronic acid pinacol ester in traditional rhodamine dye, NIR rhodamine dye and NIR hemicyanine dye.[76] On changing the medium from basic to acidic, all the probes **42**, **43** and **44** displayed enhancements in fluorescence intensity at 580 nm, 644 nm and 744 nm with pK_a values of 5.81, 5.45 and 6.97 respectively. This enhancement was mainly due to an increase in π-conjugation as a result of acid induced opening of the closed spirolactam ring. All the probes exhibited reversibility within pH 7.4 to 2.4 with good selectivity over various ions and excellent photostability. Colocalization experiments of the three probes with lysosensors Green DND-189 showed their lysosome targeting ability and probes could be used for intracellular pH imaging in MDA-MB231 and HUVEC-C cells with low toxicity (Figure 25).

Simultaneous detection of lysosomal and cytoplasmic pH is essential as it plays an important role during the autophagy process. To achieve this, Lin and coworkers designed a pH probe **45** having a dual pH sensitive site where the coumarin site responded in a neutral pH range to track cytoplasmic pH and the rhodamine site worked in an acidic pH range to monitor lysosomal pH.[77] The probe displayed a ratiometric fluorescence response where intensity ratio (I_{588}/I_{455}) declined from 1.76 to 0.04 and 0.012 to 0.004 on increasing pH from 4.5 to 5.5 and from 6.0 to 8.0 respectively. The colocalization experiments confirmed the probe's lysosome and cytoplasm targeting ability and it was employed to monitor intracellular pH variation in living HepG2 cells with low toxicity and good selectivity. However, lowering of cytoplasmic and lysosomal pH during starvation induced autophagy in living HepG2 cells and 4T1 cells was successfully monitored by using the probe in a ratiometric manner. Additionally, NH_4Cl and chloroquine induced autophagy inhibition through alkalization was also investigated (Figure 26).

A Si-rhodamine moiety was modified with morpholine unit by Zhang and coworkers to develop a NIR pH probe **46** for monitoring lysosomal pH.[78] H^+ induced protonation of morpholine "N" and ring opening of rhodamine moiety caused a turn on fluorescence with 1400-fold

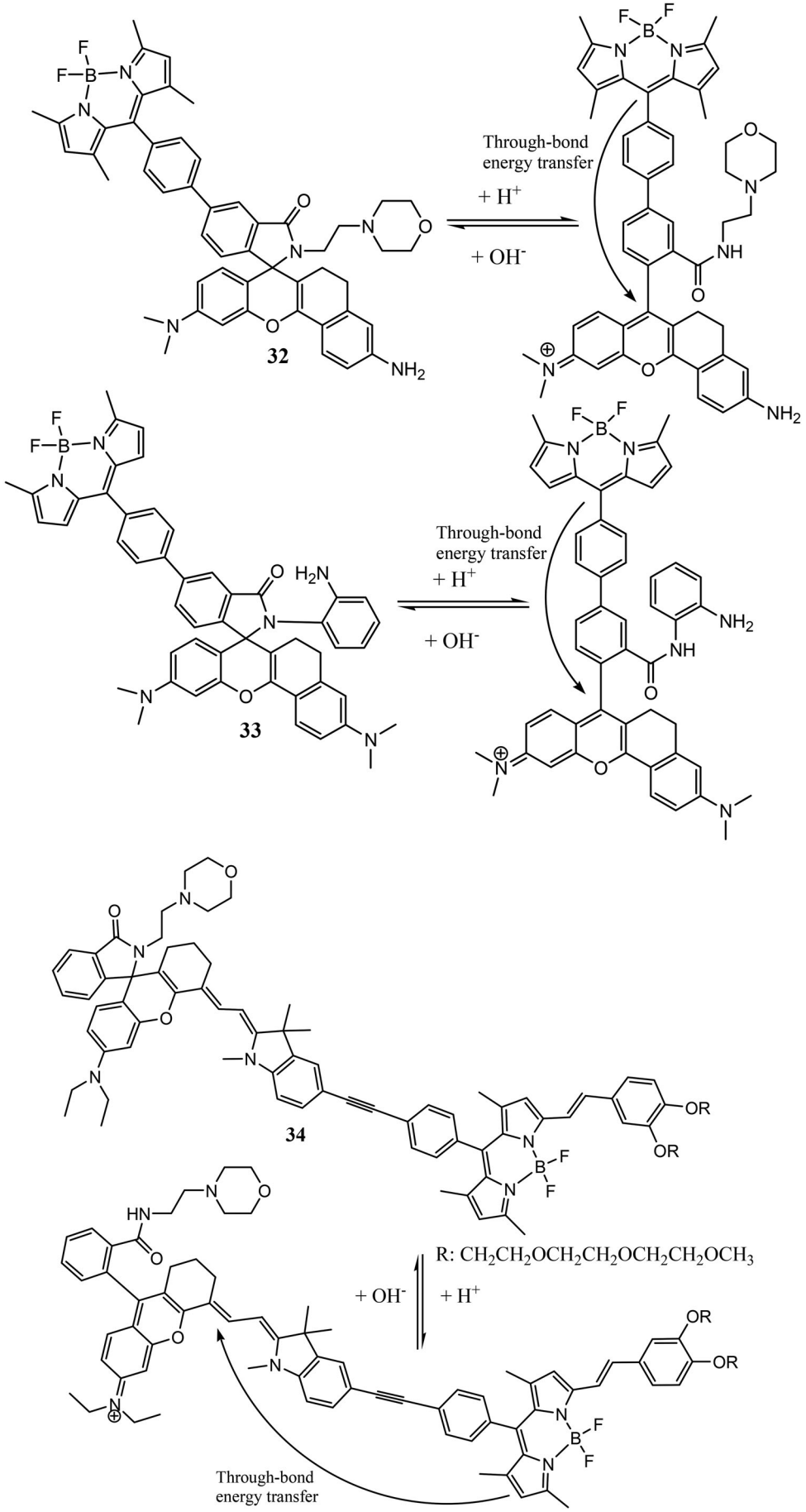

Figure 20. Chemical structures of lysosome targetable near-infrared ratiometric fluorescent probes **32-34** and their pH-dependent structural alterations.

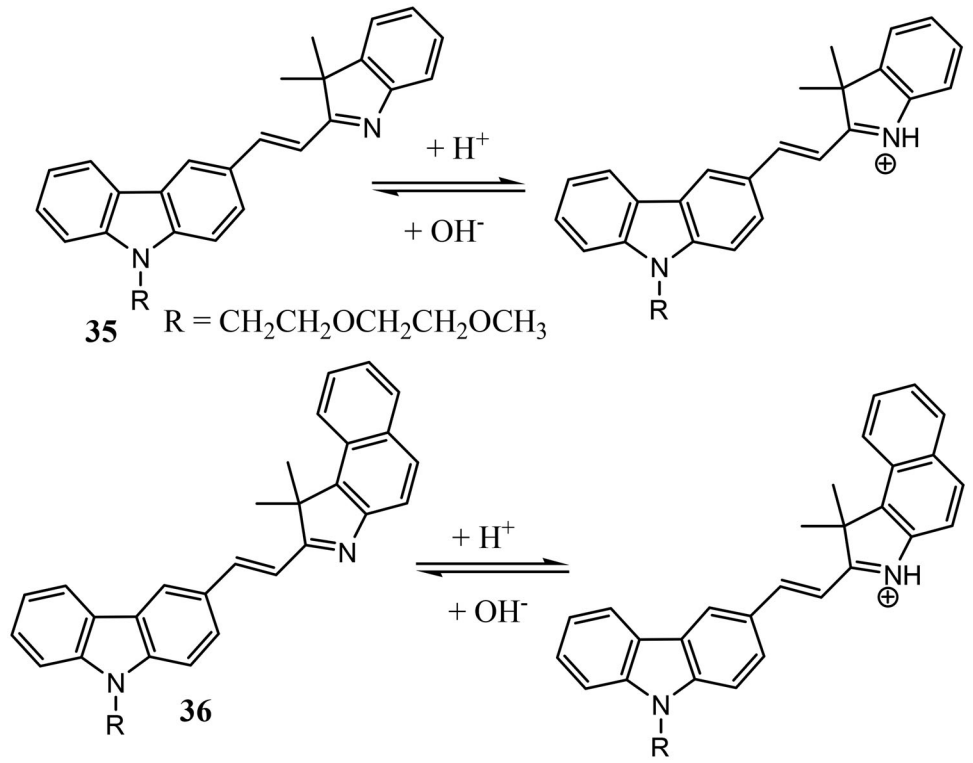

Figure 21. Chemical structures of lysosome targetable carbazole-based long-emission ratiometric fluorescent probes **35** and **36** and their pH-dependent structural alterations.

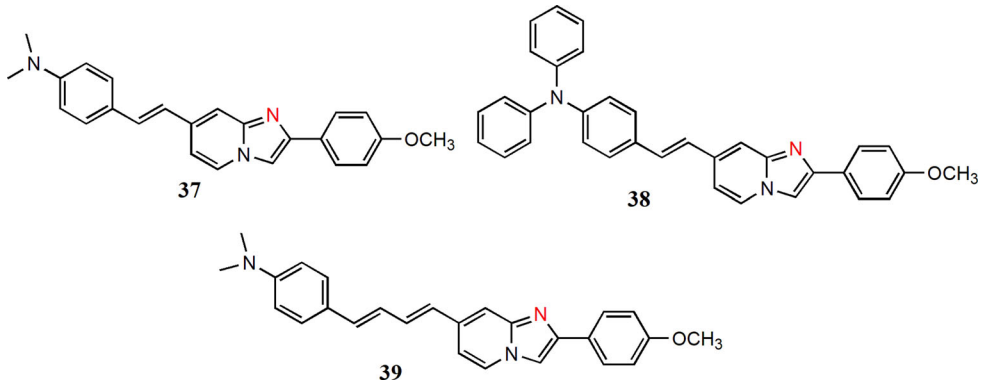

Figure 22. Chemical structures of double emissive ratiometric fluorescent pH probes **37-39**.

enhancement in fluorescence intensity at 675 nm on increasing acidity (pH 7.4 to 3). The probe was found to be highly selective over bio-relevant species with good reversible response within pH 3.5 to 7.0 and pK_a value was calculated to be 4.63. With excellent photostability and low cytotoxicity, the probe was found to be lysosome specific and was able to monitor lysosomal pH in both HeLa cells and A549 cells. Moreover, the probe was used to track dexamethasone induced apoptosis and chloroquine induced pH increase in lysosome in HeLa cells. Furthermore, heat stroke induced lysosomal pH increase was successfully imaged by the probe both in HeLa cells and A549 cells (Figure 27).

Yan *et al.* reported a FRET based pH probe **47** by connecting the BODIPY unit with rhodamine moiety.[79] On increasing the pH from 4.0 to 12, the probe showed a ratiometric fluorescence response where the emission peak at 518 nm of the BODIPY unit showed gradual decrease with an increase of rhodamine emission peak at 582 nm. The fluorescence intensity ratio (I_{582}/I_{518}) also displayed significant enhancement from 0.6 to 3.4 within pH 8.0 to 4.0 and pK_a value was calculated to be 7.1. The colocalization experiment showed that the probe was selectively stained lysosome and was used to detect lysosomal pH decrease during LPS induced inflammation in macrophages (Figure 28).

Lysosomal pH probes based on pH responsive polymers are rarely reported. To achieve this task, Lin and coworkers reported two polymer-based pH probes (**48** and **49**) for monitoring lysosomal pH by incorporating pH responsive biocompatible polymer matrix poly (N, N-dimethylaminoethyl methacrylate) into naphthalimide fluorophore.[80] On decreasing acidity (pH 3.0 to 9.0), deprotonation in the polymer chain of probe **48** displayed lowering of its emission intensity at 424 nm and the pK_a value was found to be 6.67. Due to protonated polymer chain and inhibition of

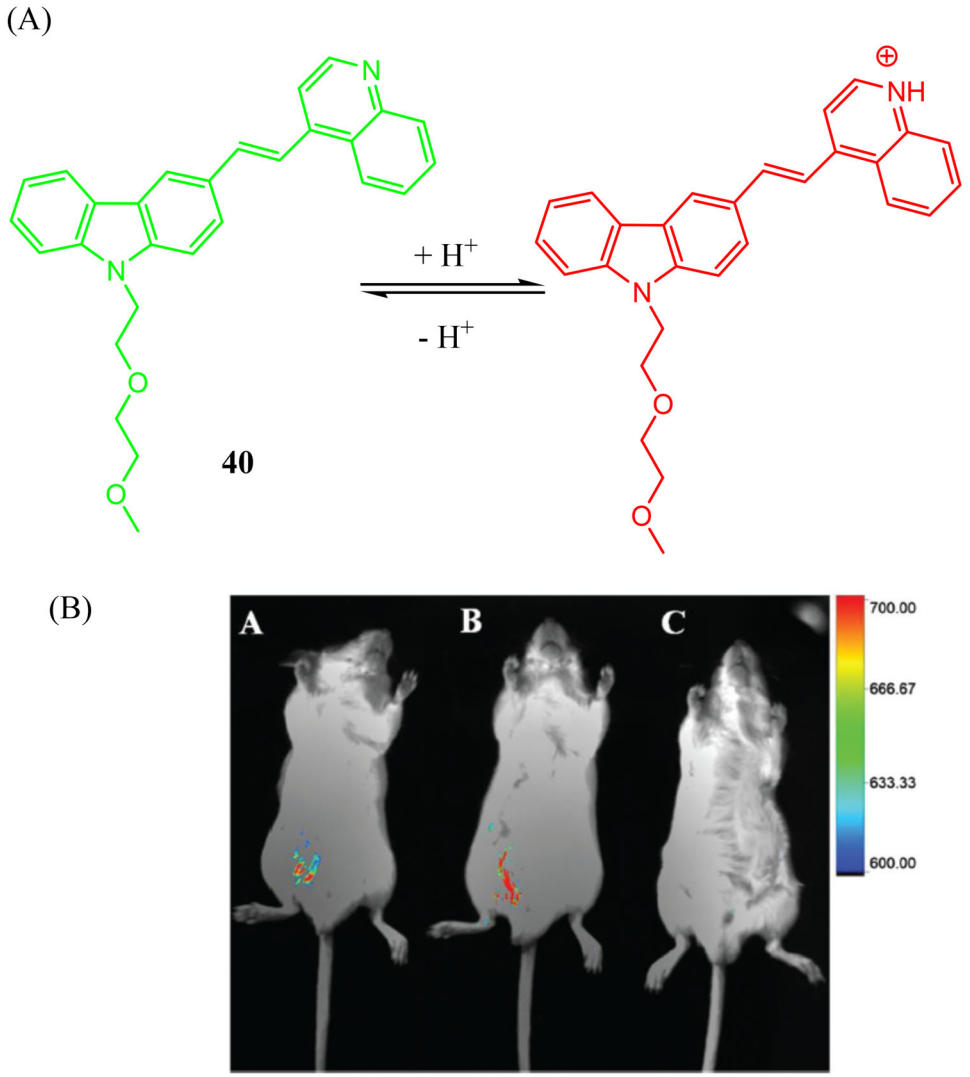

Figure 23. (A) Chemical structure of lysosome targeting NIR ratiometric fluorescent pH probe **40** and its pH-dependent structural alterations. (B) *In vivo* fluorescence images of probe **40** in mice with stimulation by LPS. (A) LPS (1.0 mg mL^{-1} in saline, 200 μL) + probe **40** (40 mM, 200 200 μL) (B) only probe **40** (40 mM, 200 200 μL) and (C) only LPS (1.0 mg mL^{-1} in saline, 200 μL) (E_x = 420 nm, E_m = 535 nm). Reproduced/Adapted from Ref. [74] with permission from the Center National de la Recherche Scientifique (CNRS) and The Royal Society of Chemistry.

PET from morpholine "N" to naphthalimide fluorophore in acid medium probe **49** showed dual emission at 467 nm and 543 nm when excited at 370 nm. But on increasing pH from 3.0 to 9.0 the emission intensity of these peaks lowered and two pK_a values were calculated to be 6.67 and 5.83. With high photostability, good selectivity and reversibility, both the probes were found to be lysosome specific with PPC (Pearson's colocalization coefficient) of 0.90 (**48**), 0.94 (**49**). Furthermore, both the probes were employed to monitor chloroquine induced lysosomal pH increase. Due to better pH sensitivity than probe **48**, probe **49** was further used to monitor the increase in lysosome pH during sucrose induced lysosomal storage disorders and during rotenone induced cell apoptosis in living HeLa cells (Figure 29).

To investigate lysosomal pH change during heat shock, Shen and coworkers reported a rhodamine based NIR pH probe **50** containing lysosome targetable morpholine moiety.[81] The probe exhibits enhancement in absorption peak at 650 nm and fluorescence intensity at 705 nm on decrease of pH from 7.40 to 2.00 and this investigation was done in B-R buffer (5% (v/v) ethanol as co-solvent). This enhancement is mainly due to structural change of the rhodamine moiety from non-fluorescent spirocyclic to fluorescent ring-open form on interaction with H^+ which was confirmed by ^{1}H-NMR. The pK_a value was found to be 4.24. The probe was also found to be highly selective toward pH over other analytes within the pH range of 7.40 to 3.00 and also found to have little response time and good reversibility. The probe could locate lysosomes in HeLa cells when co-cultured with LysoSensor Green DND-189 and explored that lysosomal pH increases with increased heat treatment (Figure 30).

Zhang *et al.* reported an ICT based hemicyanine probe **51** contained pH sensitive electron acceptor benzoindole and electron donor dimetylamino moiety.[82] On changing the pH from 7.0 to 2.0 in water/ethanol (1/9, *v/v*), the probe displayed ICT induced bathochromic shift both in absorption (421 to 555 nm) and emission spectra (534 to 622 nm) with large stoke shifts and emission intensity ratio (F_{534nm}/F_{622nm}) showed decrease from 5.60 to 0.14. Good linear response was observed within pH 3.41 to 4.82 with selective

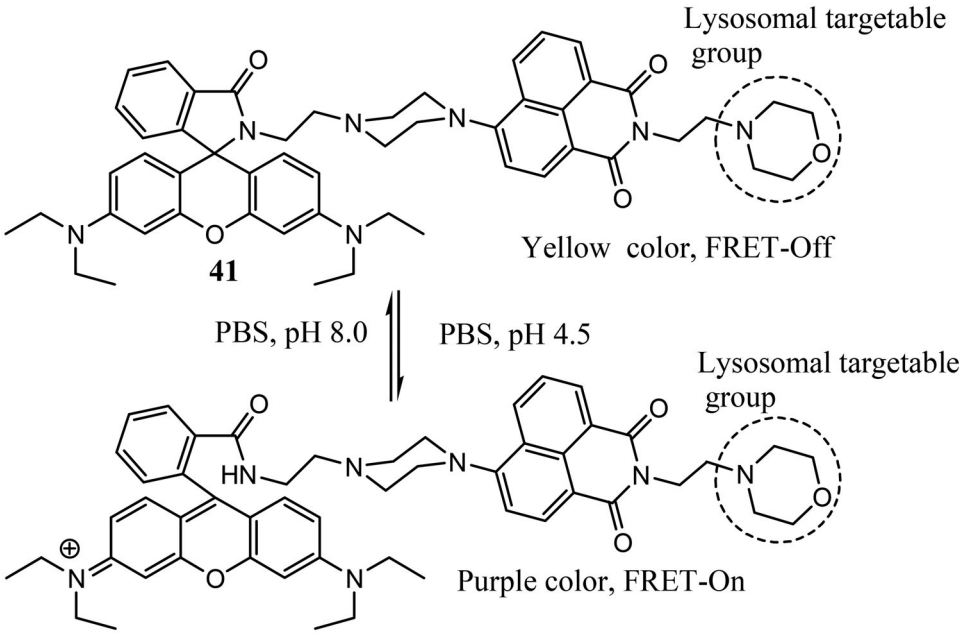

Figure 24. Chemical structure of FRET-based two-photon ratiometric fluorescent probe **41** and its pH-dependent structural alterations.

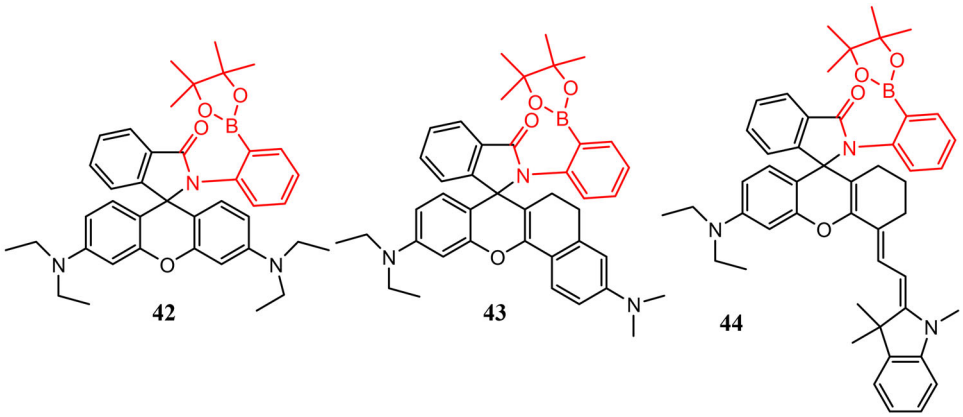

Figure 25. Chemical structures of lysosome targeteable fluorescent pH probes **42-44**.

and reversible nature of the probe and the pK_a value was found to be 4.25 from fluorometric titration. Co-localization with Lyso-Tracker Red DND-99 showed the probe's lysosome staining ability and the probe was further used to monitor intracellular pH fluctuation in living HeLa cell. H_2O_2, glucose and NH_4Cl induced pH change were also investigated ratiometrically (Figure 31).

For two photon imaging of lysosomal pH change, Dong *et al.* synthesized a pH probe **52** by modifying naphthalimide fluorophore with lysosome targetable, pH sensitive piperazine and morpholine moiety as well as additional benzyl chloride unit was incorporated for better lysosome anchoring.[83] Acid induced protonation of piperazine and morpholine "N" blocked the PET process and that caused 47-fold enhancement of emission intensity at 535 nm on decreasing pH from 10.0 to 2.0. With good selectivity, photostability and reversibility, the probe exhibited linear response within pH 5.0 to 7.3 and the pK_a value was found to be 6.24 ± 0.02. pH variation and heat shock induced lysosomal alkalization in probe loaded SMMC-7721 cells were successfully imaged by two-photon fluorescence imaging. Further the probe was applied to image lysosomal pH increase during L-buthioninesulfoximine (BSO) and cis-platinum (Cis) induced cell apoptosis. Moreover, the lysosomal pH rises during sodium selenite (SS) induced mitophagy was confirmed by dual color fluorescence imaging. Lastly, the two-photon imaging of abdominal tissues of mice pretreated with different pH buffers demonstrated the probe's *in vivo* imaging capability (Figure 32).

Zhang *et al.* reported an ICT based hemicyanine pH probe **53** which exhibited red shift in both absorption (393 to 482 nm) and emission spectra (517 to 555 nm) with large stoke shifts on lowering pH from 7.0 to 2.59. This change was due to increase in ICT on protonation of benzoindole moiety of the probe.[84] The color of the probe's solution in water/ethanol (1/1, v/v) changed from pale yellow to orange and green to red under visible and UV light respectively. The probe was found to exhibit linear response within pH 4.4 to 6.2. With low toxicity and good photostability, the probe was applied to track pH variation in living HeLa cells.

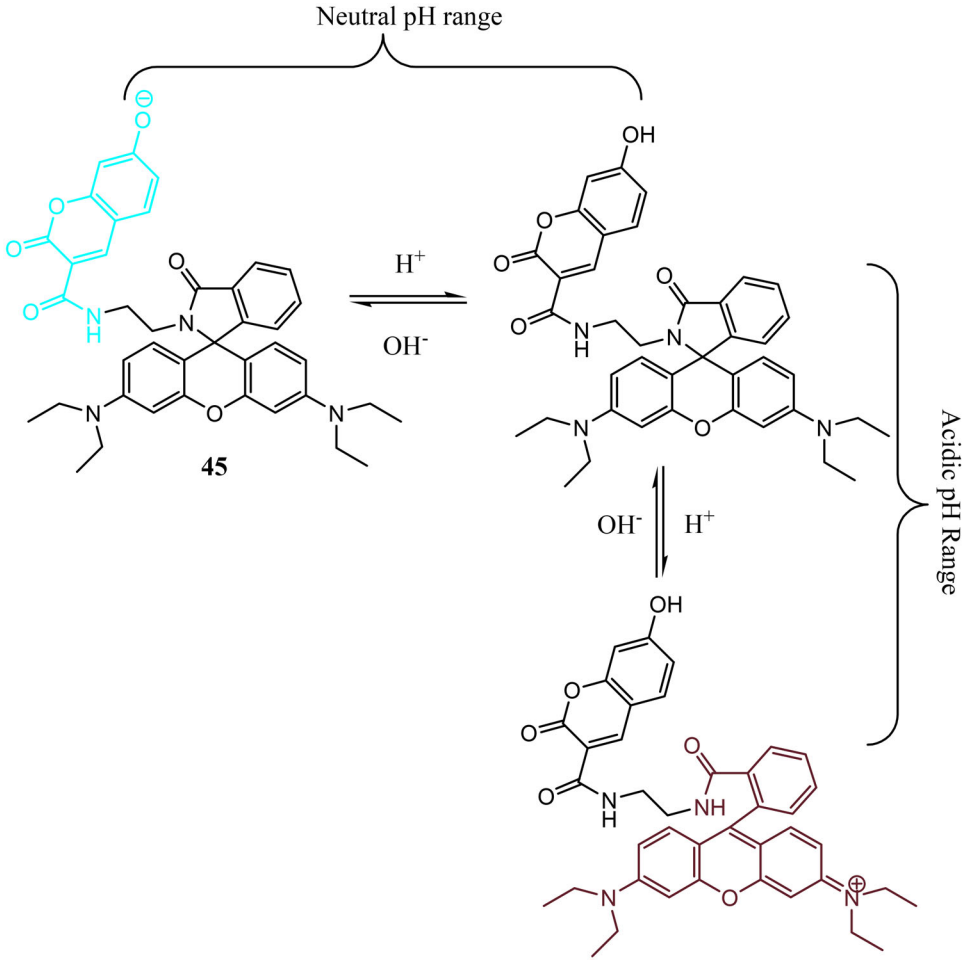

Figure 26. Chemical structure of lysosome targetable dual-site fluorescent pH probe **45** and its pH-dependent structural alterations.

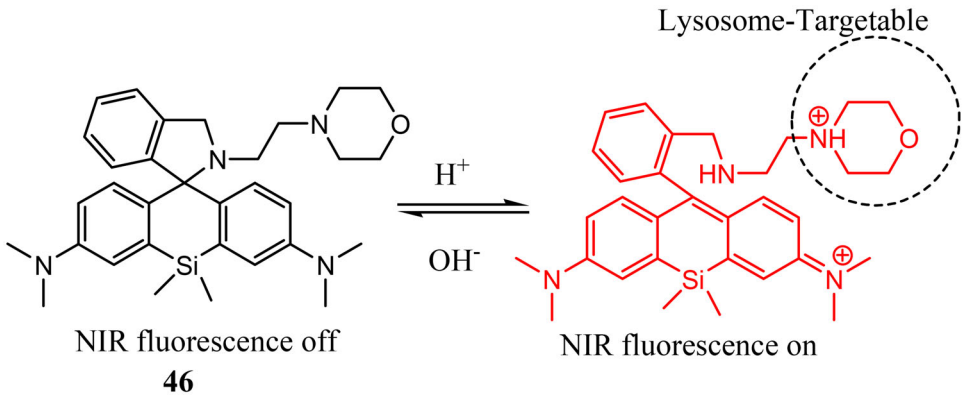

Figure 27. Chemical structure of lysosome targeting Si-rhodamine-based NIR probe **46** and its pH-dependent structural alterations.

Besides, bearing a pK_a value of 4.98, the probe was found to stain the lysosome and could monitor NAC and H_2O_2 induced pH fluctuation (Figure 33).

Another lysosome targeting pH probe **54** was designed by Wang *et al.* by incorporating a lysosome specific methylcarbitol unit in the rhodamine moiety.[85] The probe was colorless in B-R buffer solution (40 mM) containing 2.5 % DMSO at pH 7.4 but turned pink at pH 4.50 with gradual enhancement of absorption peak at 561 nm due to acid induced ring opening of the rhodamine moiety. Similarly in emission spectra, the probe displayed turn-on red fluorescence with a 148-fold increase in fluorescence intensity at 583 nm on increasing acidity (pH 7.40 to 4.40). Having good reversibility and high selectivity, the probe showed good linear response within the pH range of 4.50 to 5.70 with pK_a value of 4.96. The probe was found to be lysosome specific when co-localised with LysoTracker Green DND-26 and successfully imaged intracellular pH in HeLa cells as well as T98G and SMMC-7721 cells. Moreover, pH change in the lysosome during starvation induced autophagy condition was monitored in HeLa cells (Figure 34).

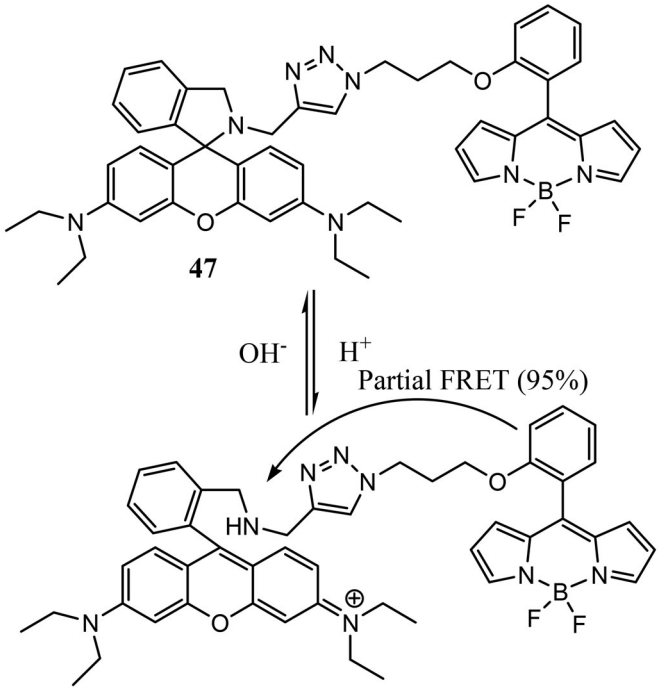

Figure 28. Chemical structure of lysosome targeting BODIPY-rhodamine ratiometric fluorescent probe **47** and its pH-dependent structural alterations.

Both water solubility and cell permeability are two essential characteristics of a good probe for its practical application in pH monitoring. To meet this need, hydrophilic pyranine and hydrophobic porphyrin units were used by Jiang and coworkers to design a FRET-based dyad **55** for ratiometric monitoring of intracellular pH.[86] Here, the pyranine unit acts as a donor and the meso-4-pyridyl substituted porphyrin unit acts as an acceptor in the FRET mechanism. On decreasing pH from 8.58 to 2.59, the probe displayed 95-fold change (1.73 to 0.018) of emission intensity ratio (I_{660}/I_{435}) in PBS buffer where the NIR band at 660 nm got dramatically quenched with a slight decrease of the blue band at 435 nm. This spectral behavior was mainly due to successive acid induced protonation of meso-pyridyl groups and inner pyrrole nitrogens of the porphyrin moiety. So, two pK_a values for two successive protonations were determined and these were 6.46 (meso-pyridyl groups) and 3.92 (inner pyrrole nitrogens). The probe was found to exhibit linear response within pH 5.4 to 7.5 and 3.3 to 4.5 as well as reversibility within pH 4.0 to 8.0. Lastly, the probe was found to have lysosome targeting ability and was used to monitor intracellular pH in living A549 cells (Figure 35).

Xu et al. synthesized a series of pH probes **56**, **57**, **58** and **59** by incorporating lysosome targetable morpholine unit in theimidazole-fused benzothiadiazole moiety.[87] By changing the substituent in the imidazole ring, photophysical properties of them were investigated in BR buffer with 10% DMAC (*N*, *N*-dimethylacetamide). All the four probes were responsive toward acidic pH and displayed enhancement in fluorescence intensity on increasing acidity (pH 8.5 to 4.0). The pK_a values of all the probes were 5.5, 5.3, 5.1, and 4.5 for **56**, **57**, **58** and **59** respectively. Further investigation showed that probe **57** showed good linear relationship (pH 4.4–5.6), selectivity over various metal ions, reactive oxygen/nitrogen species, small biomolecules and reversibility up to five cycles at pH 4.0 and 7.4. With good cell permeability, low toxicity and better photostability than LysoTracker Red, the probe **57** was found to be lysosome specific with high overlap coefficient (0.74). Moreover, the probe was found to be capable of monitoring Baf-A1 and chloroquine induced lysosomal pH increase and intracellular pH variation in MCF-7 cells (Figure 36).

By linking electron acceptor benzothiadiazole moiety with electron donor N, N-diethylamino groups, Li *et al.* synthesized an ICT based D-A-D (donor-acceptor-donor) type pH probe **60**.[88] Acid induced protonation of N, N-diethylamino groups of the probe decreased the ICT and the probe did not exhibit any distinct emission peak at acidic pH but on increasing pH value (3.0 to 7.4) it displayed a maximum emission peak at 614 nm in alkaline medium with a sharp enhancement of intensity within pH 4.5 to 5.7. Almost 25-fold enhancement in fluorescence intensity was observed with linearity within pH 4.5–5.2 and pK_a value was found to be 5.0. Additionally, the probe was found to selectively stain lysosome and used to monitor intracellular pH variation in SGC-7901 cells with good selectivity, photo-stability and negligible toxicity. Moreover, the probe was employed to track starvation induced autophagy in living cells (Figure 37).

Recently, another rhodamine-based pH probe **61** containing lysosome targeting morpholine moiety was reported by Dong's team.[89] In B-R buffer on lowering pH from 8.0 to 4.80, the probe exhibited an increase of absorption peak at 574 nm accompanied by color change from colorless to light pink. In fluorescence spectra, the peak at 590 nm showed gradual enhancement of more than 120-fold along with turn on red fluorescence. The quantum yields also increased from 0.009 to 0.12 and acid induced opening of the spirocyclic rhodamine ring was responsible for these spectral changes. Having good reversibility (pH 5.0–8.0) and linearity (pH 5.0–6.0) the probe was highly selective with pK_a value of 5.42 as cation, anions and amino acids did not induce any significant interference. Colocalization of probe with LysoTracker GreenDND-26 in HeLa cells demonstrated the lysosome labeling property and probe loaded HeLa cell with high K^+ buffers with different pH values containing nigericin showed the probe's applicability in intracellular pH monitoring. Again, lysosomal pH increases during heat shock, rapamycin induced mitophagy and dexamethasone induced apoptosis were successfully imaged by the probe in HeLa cells (Figure 38).

Mitochondria targetable pH probes

Being the "energy factory" of cells, mitochondria produce cellular energy by generating ATP (adenosine triphosphate) in respiratory cahin.[90] It also plays an important role in various cellular metabolic processes including Ca^{2+} homeostasis,[91] cellular apoptosis,[92] reactive oxygen species (ROS) production,[93] urea cycle,[94] fatty acid oxidation,[95] iron metabolism.[96] Weakly alkaline pH (~8) of mitochondria is necessary to respond properly to various subcellular

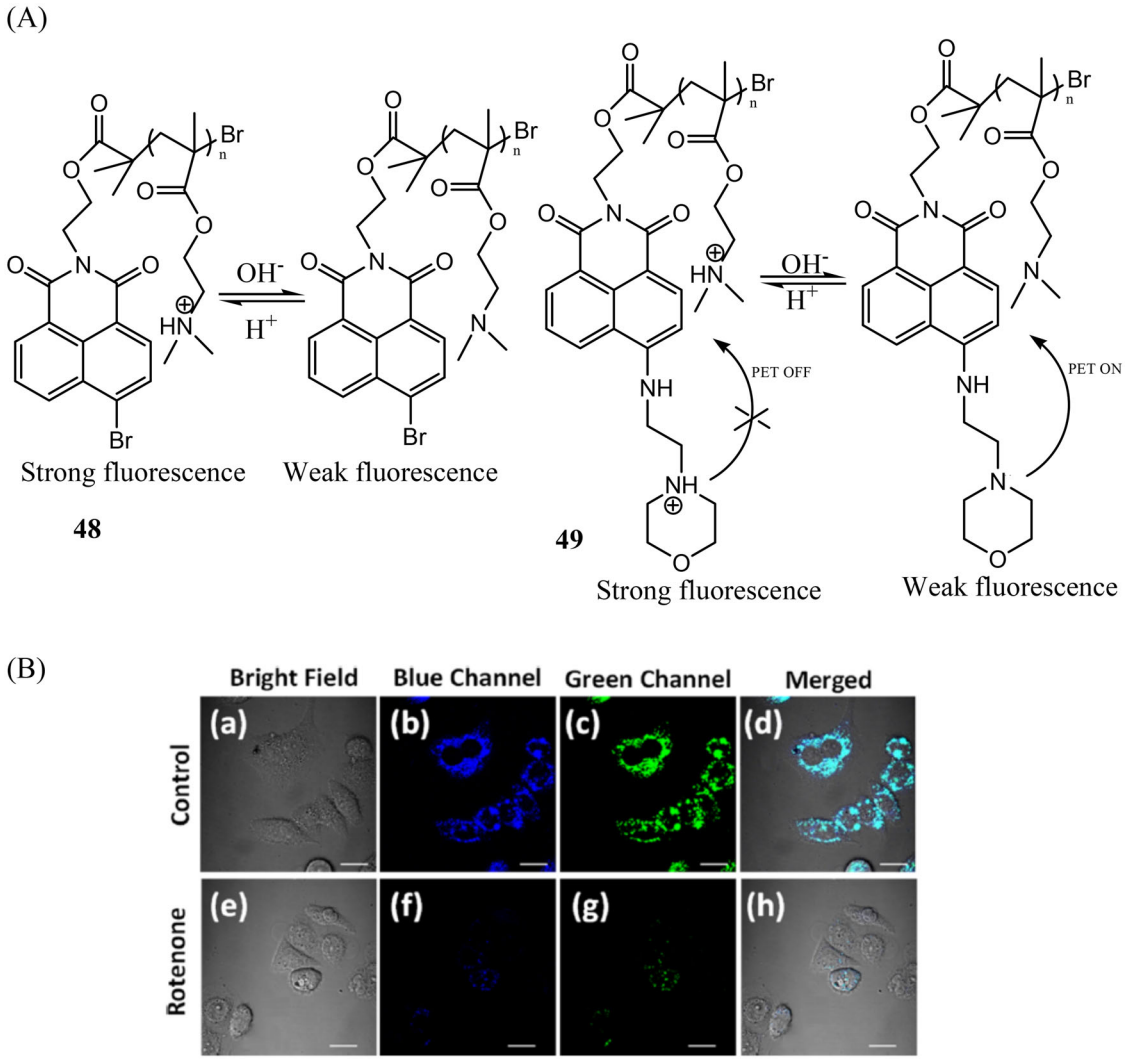

Figure 29. (A) Chemical structures of polymer-based lysosome targeting pH probes **48** and **49** and their pH-dependent structural alterations. (B) Fluorescent imaging of HeLa cells (a-d) treated with probe **49** only (60 μg/mL); and (e – h) treated with 10 μM rotenone and then with probe **49** (60 μg/mL). Scale bar: 20 μm. Reprinted (adapted) with permission from Ref. [80] Copyright (2019) American Chemical Society.

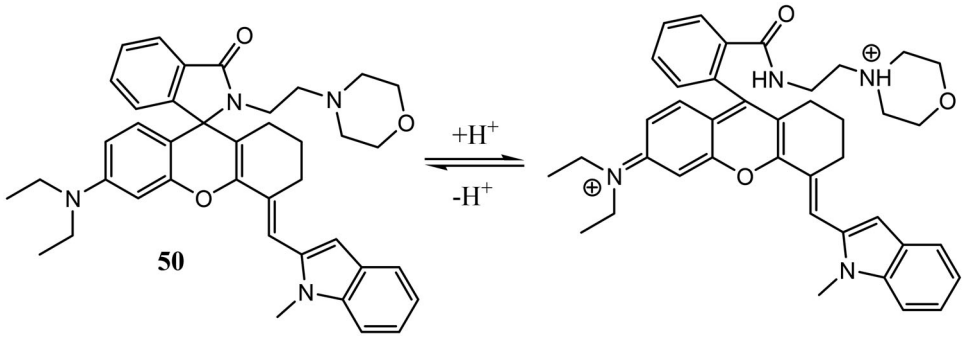

Figure 30. Chemical structure of lysosome targeting rhodamine-based NIR probe **50** and its pH-dependent structural alterations.

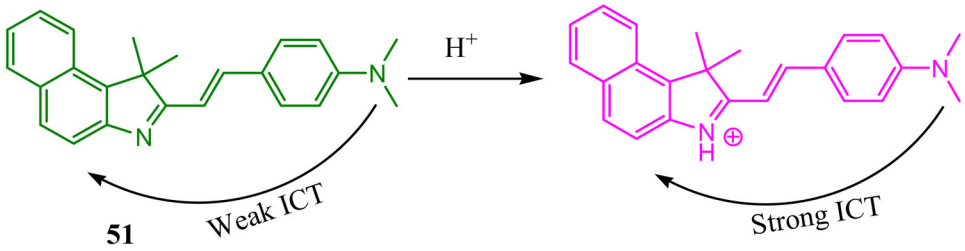

Figure 31. Chemical structure of lysosome targeting hemicyanine-based ratiometric fluorescent pH probe **51** and its sensing mechanism.

activities under normal physiological conditions. But slight fluctuation of this pH under stress or hypoxia may lead to damage of mitochondria[97] and that may further lead to mitophagy[98] or cellular apoptosis. In addition, this type of mitochondrial dysfunction is closely linked with cancer,[99] neurological and cardiovascular diseases,[100,101] metabolic disorder.[102] So, it is very essential to accurately monitor mitochondrial pH to understand its functions clearly under both physiological and pathological conditions. Negative membrane potential across the double-layered mitochondrial membrane attracts lipophilic cations (triphenylphosphonium cation, pyridinium ion etc.) through electrostatic attraction and incorporation of these cations in to probes improves their mitochondria targeting ability.[103] Furthermore, probes are generally modified with benzyl chloride to achieve high immobilization in mitochondria through nucleophilic reaction with thiol(-SH) groups of mitochondrial proteins.

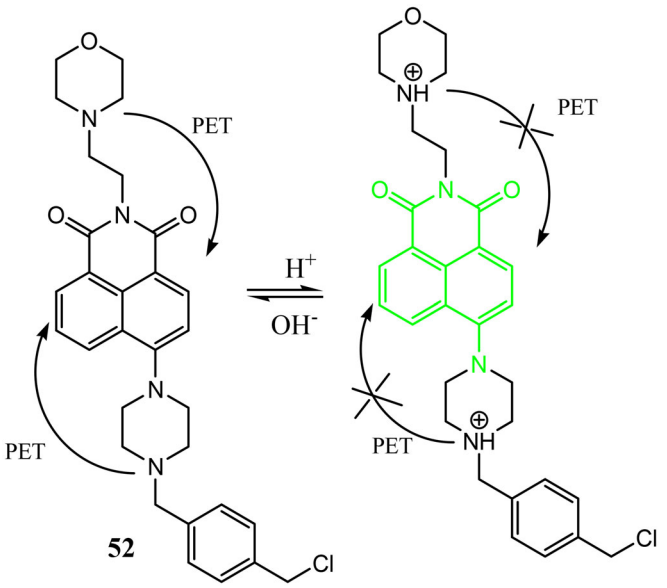

Figure 32. Chemical structure of lysosome targetable two-photon fluorscent probe **52** and its pH-dependent structural alterations.

AIE (Aggregation induced emission) has been a popular sensing mechanism in the field of chemosensors in recent years. To address this, Tang and coworkers reported a benzothaizole based ratiometric pH probe **62** that exhibited strong fluorescence emission in an aggregated state due to AIE property and that was governed by both excited-state intramolecular proton transfer (ESIPT) and RIR (restricted intramolecular rotation) processes.[104] When investigated in water/ethanol (f_w = 99%, v/v), the neutral form of the probe having low solubility in acidic pH displayed aggregated yellow emission at 551 nm whereas in alkaline medium deprotonation of phenolic –OH and carboxyl group led to cyan fluorescence at 484 nm. Distinct fluorescence change with linear response was observed within pH 6.86–8.07 and two pK_a values were calculated to be 7.3 and 8.6. In addition, the probe was found to have mitochondria targeting ability with a high Pearson correlation coefficient of 0.92 when co-localised with MitoTracker Deep-Red FM and could image intracellular pH change in living HeLa cells. Moreover, the probe was successfully employed to distinguish acid and basic vapors through probe loaded test papers (Figure 39).

In 2018, Kim and coworkers used 4-aminopyridine as a pH sensitive site to make a pH probe **63**.[105] On increasing pH from 9.5 to 3.2 with an excitation wavelength of 353 nm, the probe exhibited enhancement in fluorescence intensity at 457 nm. In contrast, when excited at 410 nm, the quenching of fluorescence was observed. With good self-calibrating nature, the similar intensity change was observed when investigated in TPM mode with excitation wavelength of 750 nm and 810 nm. The colocalization experiment showed that the probe was mitochondria targeted and could image intracellular pH in both one-photon and two-photon mode. Furthermore, the probe was used to monitor NAC and nutrient starvation induced cell acidification as well as H_2O_2 induced alkalization in RAW 264.7 cells (Figure 40).

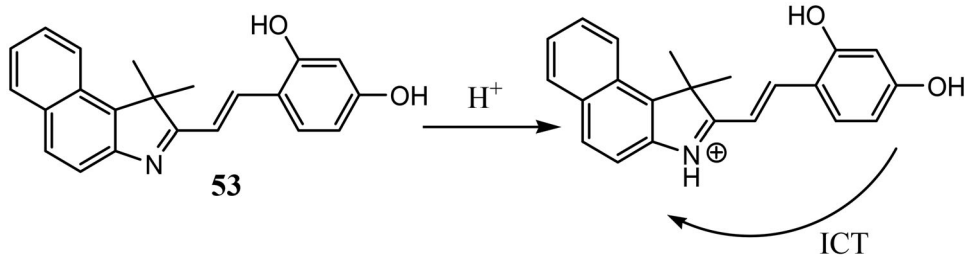

Figure 33. Chemical structure of lysosome targeting hemicyanine-based fluorescent pH probe **53** and its sensing mechanism.

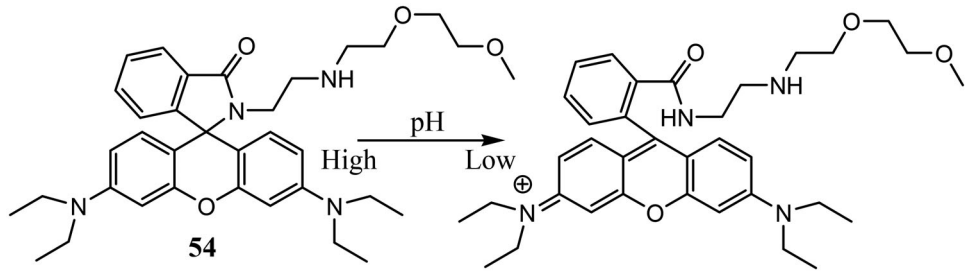

Figure 34. Chemical structures of lysosome targeting rhodamine-based fluorescent probe **54** and its pH-dependent structural alterations.

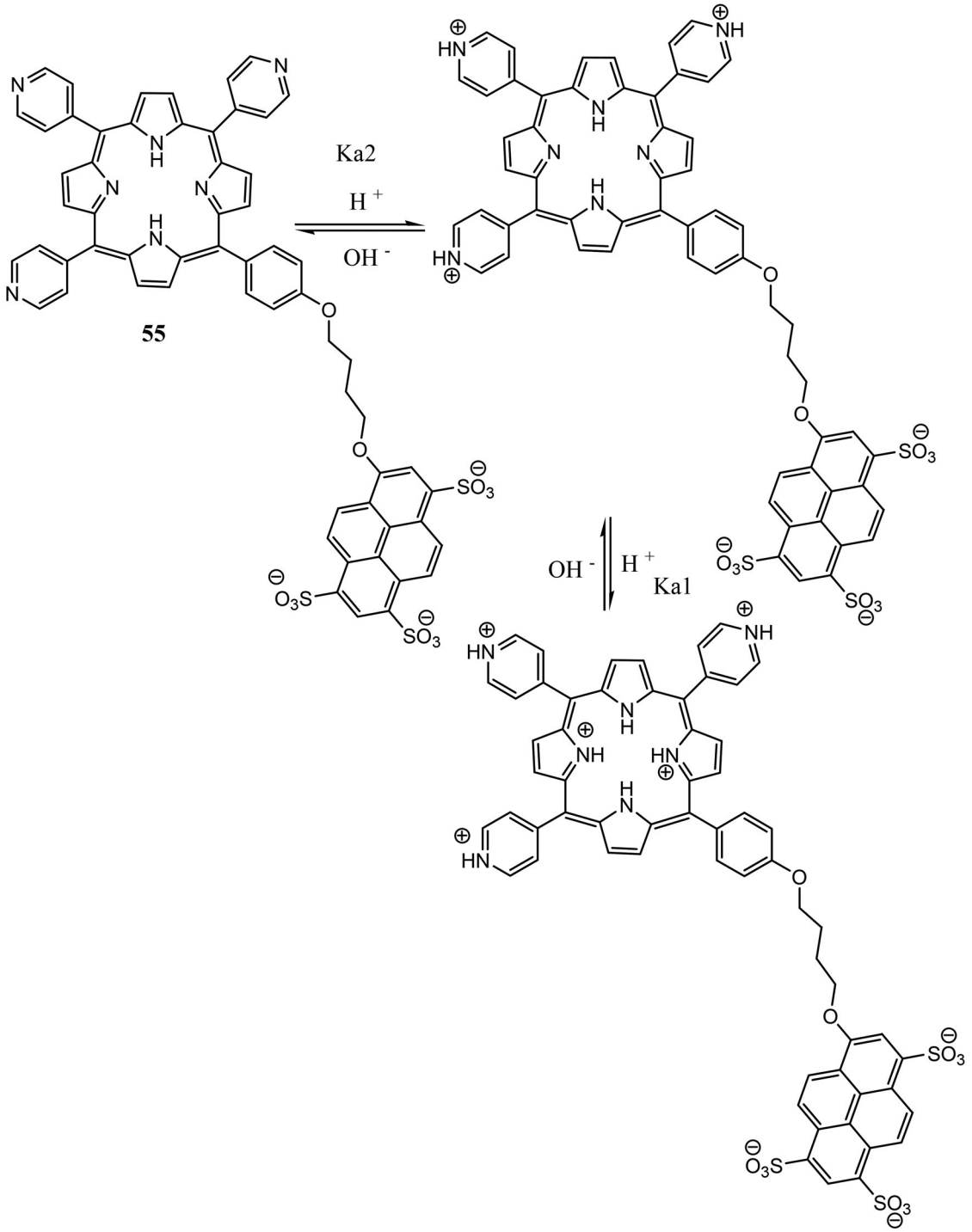

Figure 35. Chemical structure of lysosome targetable FRET-based ratiometric fluorescent probe **55** and its pH-dependent structural alterations.

In the same year, Qi *et al.* synthesized two mitochondrial pH probes **64** and **65** by fuzing fluorescein and coumarin moiety.[106] On increasing the basicity of the medium (from pH 4 to 7.4) the color of the probes in B-R buffer changed from colorless to pale yellow with the appearance of a new absorption peak at 452 nm as well as fluorescence change from colorless to yellow with enhancement of fluorescence intensity at 520 nm was observed. Both the probes showed good linear response with a fast response time of less than 1 min. The pK_a values of both the probes were calculated to be 5.84 (**64**) and 5.56 (**65**). Being a better cell permeable probe **64** was successfully located mitochondria and monitored pH change. According to the author, they successfully used probe **64** to track lactate and pyruvate induced pH changes in mitochondria (Figure 41).

A cyanine dye based NIR pH probe **66** was synthesized by Chen's group by incorporating glucosamine moiety in the probe to enhance its tumor specifying ability and solubility.[107] When investigated in sodium dodecyl sulfate (SDS) (10 mM), on decreasing pH, acid induced tautomerism in the probe caused enhancement of the peak at 710 nm with lowering of band at 420–580 nm in absorption spectra

and a red shift was observed in emission spectra. MTT (3-[4,5-dimethylthiazole-2-yl]-2,5-diphenyltetrazolium bromide) assay showed that the probe had negligible cytotoxicity and could selectively stain mitochondria and lysosome with Pearson's correlation coefficient (PCC) of 0.94 and 0.68 respectively. Importantly, staining of the lysosome after incubation of 2 hours indicated the occurrence of mitophagy and formation of autolysosome which was further confirmed by fluorescence imaging of starvation induced autophagy in probe loaded MCF-7 cells. Moreover, blocking experiment by using glucosamine in A549 and MCF-7 cells and *in vivo* fluorescence imaging of MCF-7, A549 and U87 tumor mice model proved the probe's tumor specifying ability. Lastly, the NIR nature of the probe could make it suitable for monitoring tumors and diseases related to mitophagy in the future (Figure 42).

In 2019, a hemicyanine based pH probe **67** was reported by Wang and coworkers for locating mitochondria and investigating its pH change in the mitophagy process.[108] A pH change from 6.2 to 8.0 induced a red shift in the probe's absorption maximum (422 nm to 522 nm) with a distinct color change from yellow to red. Again, in emission spectra the probe displayed green fluorescence at 530 nm at pH 6.2

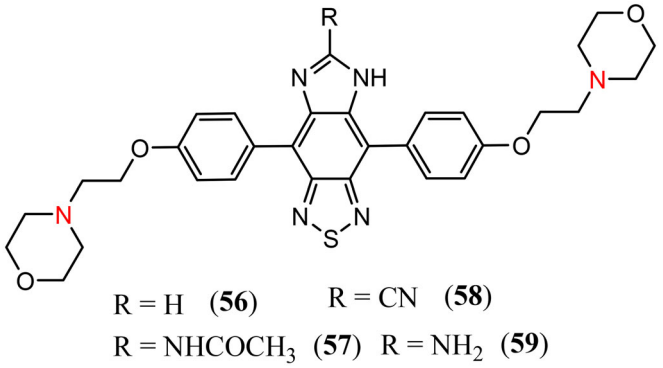

Figure 36. Chemical structures of lysosome targetable pH probes **56-59**.

with quantum yield of 0.21 and yellow fluorescence at 557 nm at pH 8.0 with quantum yield of 0.32. This change was because of protonation and deprotonation of phenolic –OH of the probe in acid and basic medium and it was further proved by ^{1}H-NMR and mass spectroscopy. Optical analysis revealed that the probe was reversible with pK_a value of 7.25 and had good selectivity over various bio-relevant anions, cations, transition metal ions. Co-culturing probe and Mito-Tracker Green FM in HeLa cells demonstrated its mitochondria labeling property due to the presence of a lipophilic cationic hemicyanine moiety. The nutrient deprivation-induced mitophagy was observed when the probe was co-cultured with a commercial autophagy tracker MDC (Dansylcadaverine) (Figure 43).

Jang and coworkers synthesized an ESIPT based pH probe **68** by conjugating hydroxythiophene with benzothaizole and it exhibited a solvent dependent dual emission character.[109] The probe was found to have a strong fluorescence response in basic pH with high quantum yield and the pK_a value was 8.03. As a result, the probe showed faster staining ability of basic organelle mitochondria when co-cultured with MitoTracker red in HeLa cells with good Pearson correlation coefficient (0.84). Moreover, the probe was applied to monitor the basic pathogen *H. pylori* (*Helicobacter pylori*) due to its urease activity both in the presence and absence of urea (Figure 44).

Based on deprotonation/protonation of amine "N" in naphthalimide moiety, Shangguan and coworkers reported a pH probe **69** by connecting pH-sensitive naphthalimide moiety with mitochondria targeted cyanine moiety.[110] Fluorescence study revealed that fluorescence intensity ratio (F_{507}/F_{720}) in presence of SDS (an anionic surfactant) and intensity ratio (F_{503}/F_{720}) in the presence of cetyltrimethylammonium bromide (CTAB, a cationic surfactant) showed gradual enhancement in PBS buffer on increasing pH from 4.33 to 8.46 with good linear response (within pH 7.10–8.46 in SDS and 5.65–8.46 in CTAB). With negligible response to

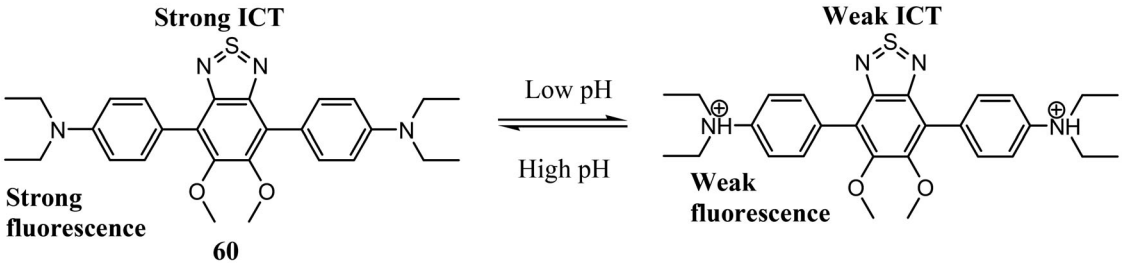

Figure 37. Chemical structure of lysosome targetable D-A-D ((donor-acceptor-donor) type fluorescent probe **60** and its pH-dependent structural alterations.

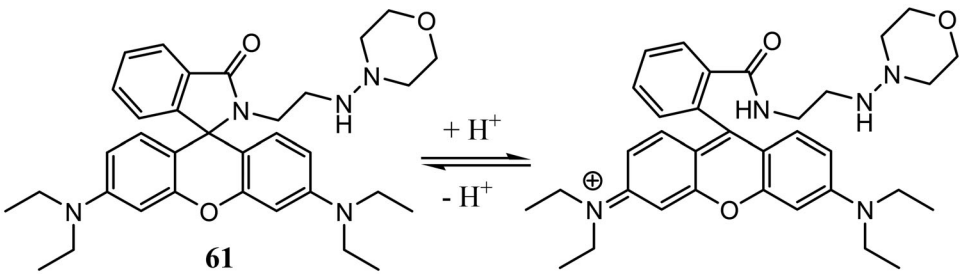

Figure 38. Chemical structures of lysosomal targeting rhodaminbe-based fluorescent pH probe **61** and its pH-dependent structural alterations.

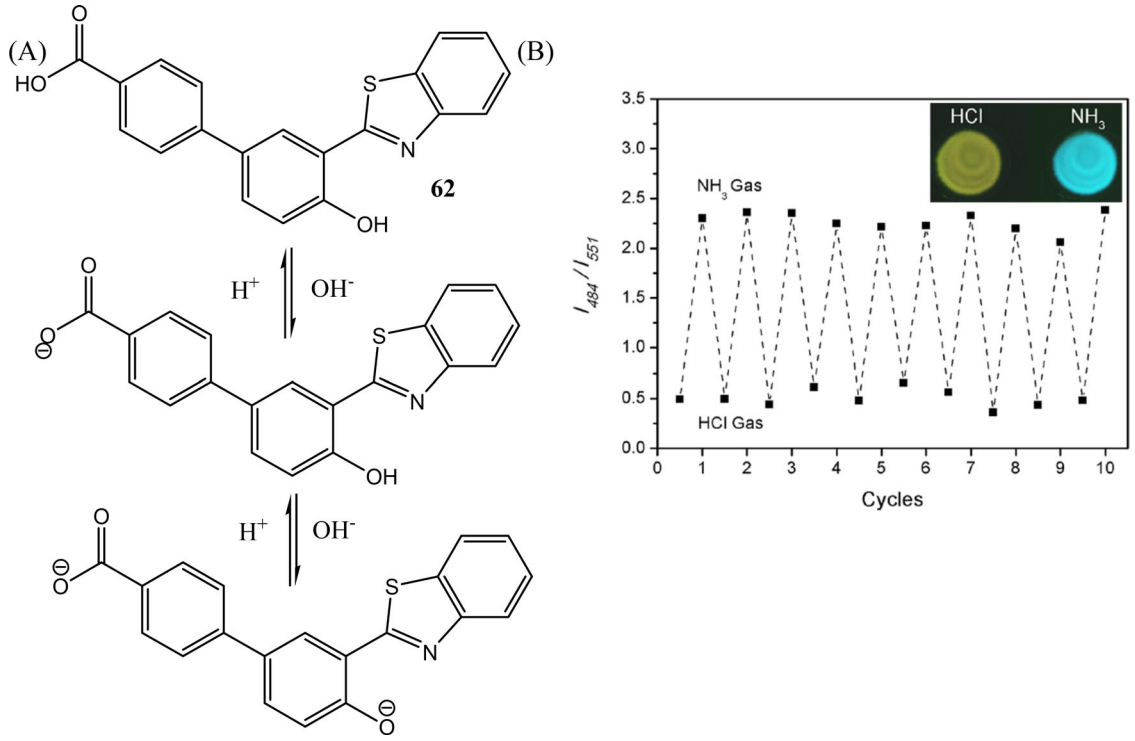

Figure 39. (A) Chemical structure of mitochondria targetable benzothiazole-baszed fluorescent probe **62** and its pH-dependent structural alterations. (B) Reversible fluorescence ratio changes of probe **62** in presence of HCl and NH_3 vapors. Inset: photographic image: **62**+HCl, **62**+NH_3. Reprinted (adapted) with permission from Ref. [104] Copyright (2018) American Chemical Society.

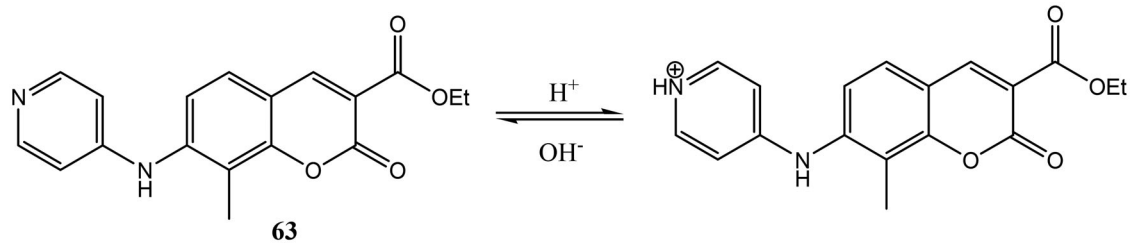

Figure 40. Chemical structure of mitochondria targetable two-photon fluorescent probe **63** and its pH-dependent structural alterations.

various metal ions (Ca^{2+}, Mg^{2+}, Hg^{2+}, Cd^{2+}, Co^{2+}, Mn^{2+}, Ni^{2+}, Ba^{2+}, Zn^{2+}, Al^{3+}, and Fe^{3+}), amino acids (Arg, Lys, and His), and redox substances (Cys, GSH, H_2O_2, and NAC), probe was successfully applied for quantitative measurement of pH changes in the mitochondria. The probe showed average pH of mitochondria 7.99 ± 0.03 in normal HeLa cells. Further investigation showed that, the probe was successfully used to image mitochondrial acidification induced by FCCP (carbonyl cyanide 4-trifluoromethoxy phenylhydrazone), NAC and H_2O_2 (Figure 45).

Wang *et al.* reported a stilbazolium based two-photon pH probe **70** which exhibited turn-off fluorescence response in SPEF (Single-photon excited fluorescence) at 590 nm and turn-on response in 2PEF (two-photon excited fluorescence) on increasing acidity with pK_a value of 4.82.[111] Acid induced protonation of the –OH group of the probe made a change in molecular stacking in SPEF and caused an increase in symmetric charge transfer in 2 PEF were responsible for this spectral behavior. With high stability, quick response time and reversible nature, the probe showed good linearity within pH 7.0–4.50. Colocalization experiment with Mito-tracker Red as well as STED (stimulated emission depletion) micrograph clearly demonstrated the probe's mitochondria staining ability. Furthermore, two-photon confocal microscopy revealed that the probe could image intracellular pH change in HeLa cells and target tumor cells in mice (Figure 46).

For ratiometric tracking of mitochondrial pH, Zhuo and coworkers utilized the merocyanine framework as a fluorophore, phenolic –OH as pH responsive site and lipophilic cationic benzyl group as mitochondria targeted unit to construct pH probe **71.**[112] On changing pH from 3 to 10, the alkali induced deprotonation of the phenolic –OH group caused enhancement of the absorption peak at 535 nm along with gradual decrease of peak at 435 nm with an isosbestic point at 480 nm and a naked eye detectable color change was observed from light yellow to pink red. In emission spectra under similar conditions a ratiometric response was observed where emission intensity ratio (I_{584}/I_{552}) increased from 0.803 to 11.5 with linear response within pH 6.0–7.8. The probe was found to be stable, biocompatible and selective over metal ions, ROS and RSS with a pK_a value of 6.87. Colocalization experiment with Mito-Tracker Deep Red revealed the probe's mitochondria targeting ability

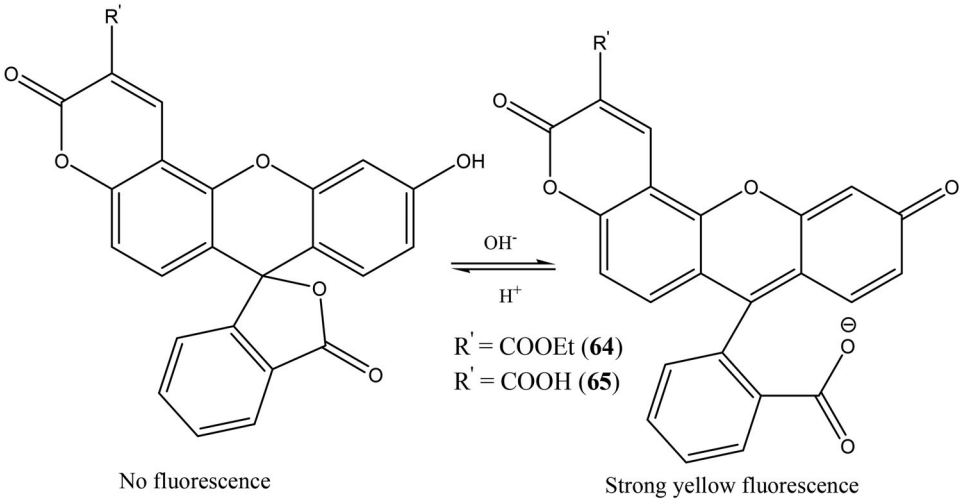

Figure 41. Chemical structures of mitochondria targetable coumarin/fluorescein-fused pH probes **64** and **65** and their pH-dependent structural alterations.

(Pearson's coefficient = 0.92) and the probe could ratiometrically detect mitochondrial pH change in living SMMC-7721 cells. Further mitochondrial acidification during sodium selenite-induced mitophagy and L-buthionine sulfoximine (BSO) induced cell apoptosis were successfully monitored by the probe. Moreover, according to the author, they did a test strip experiment by using filter paper to visualize color change on different pH in the naked eye (Figure 47).

Jiang *et al.* reported a benzimidazole-coumarin based two-photon fluorescent probe **72** for monitoring mitochondrial pH in living cells.[113] On increasing pH within 3.0–6.0, the probe displayed a decrease in fluorescence intensity with a 90 nm large stoke shift (max λ_{abs}=390 nm, max λ_{em}=480 nm) whereas within 6.0–9.0, the reverse was happened with stoke shift of 60 nm (max λ_{abs}=420 nm, max λ_{em}=480 nm). Both at pH 3.0 and 9.0, the probe exhibited blue-green fluorescence and it was mainly due to protonation of imidazole "N" in acid and deprotonation of coumarin-OH in basic medium. With little response to metal ions and amino acids, the probe showed good linear response within the pH range of 3.36–4.98 and 6.51–8.24. The pK_a values were calculated to be 4.20 for pH 2.0–6.0 and 7.20 for pH 6.0–9.0. Moreover, mitochondria targeting ability, mitochondrial pH change and nutrient deprivation-induced mitochondrial acidification were successfully imaged by probe co-culturing with MTR in HeLa cells with low toxicity and good cell permeability (Figure 48).

By modifying hydroxyl hemicyanine with benzyl chloride, Ma and coworkers synthesized a ratiometric NIR pH probe **73** for tracking mitochondrial pH change.[114] The probe was found to have good mitochondria targeting ability with negligible cytotoxicity and also had mitochondria immobilizing ability as its benzyl chloride moiety formed covalent attachment through nucleophilic reaction with mitochondrial nucleophiles. On increasing pH from 4.5 to 8.5, the probe showed a red shift (from 610 nm to 694 nm) in the absorption spectrum with a color change from blue to green. In fluorescence spectra, the probe exhibited ratiometric response where emission intensity at 678 nm showed decrease with increase at 714 nm. A good linearity and good reversibility were observed within pH 4.6–6.6 and 4.0–8.0, respectively with a pK_a value of 5.77. Again, in interference study, the probe was found to be highly selective over metal ions, anions and redox species. More interestingly, the decrease in mitochondrial pH in both rapamycin induced mitophagy and hypoxia induced mitophagy was successfully monitored by the probe through fluorescence imaging in HeLa cells. Moreover, the suitable synthetic procedure and ratiometric nature of this probe can make it an effective tool for monitoring the functions of mitochondria in various biological processes (Figure 49).

Another two interesting pH probes **74** and **75** were reported by Zhang *et al.* for ratiometric monitoring of pH changes by connecting hemicyanine dye with NIR rhodol dye.[115] On increasing acidity of the medium (pH 10.2–3.6), both the probes displayed a decrease at 535 nm with gradual enhancement of new peaks at 609 nm (**74**) and 622 nm (**75**) in absorption spectra. Similarly in emission spectra both the probes showed declining fluorescence at 558 nm with enhancement of new NIR peaks at 688 nm (**74**) and 698 nm (**75**) on excitation at 480 nm. Acid induced opening of hemiaminal ether led to the formation of indolenium having long conjugation with rhodol moiety caused this change in spectral behavior. The pK_a values were determined to be 8.26 for **74** and 7.10 for **75**. Probes showed good selectivity over metal ions, anions, amino acids, reactive oxygen and nitrogen species with good reversible response within pH 4 to 10. Mitochondria targeting ability was confirmed by co-localization experiment with IR-780 cyanine dye and Mito Tracker blue. FCCP induced mitochondrial acidification as well as nutrient starvation and rapamycin induced mitophagy was also successfully tracked by the probes. Moreover, cell experiments by culturing of probes loaded HeLa cells with K^+/H^+ buffers at different pH values containing nigericin demonstrated the applicability of probes for ratiometric monitoring of pH changes in living cells. Furthermore, according to the author, probe **74** was used for *in vivo* imaging of pH in *D. melanogaster* (*Drosophila melanogaster*) first-instar larvae (Figure 50).

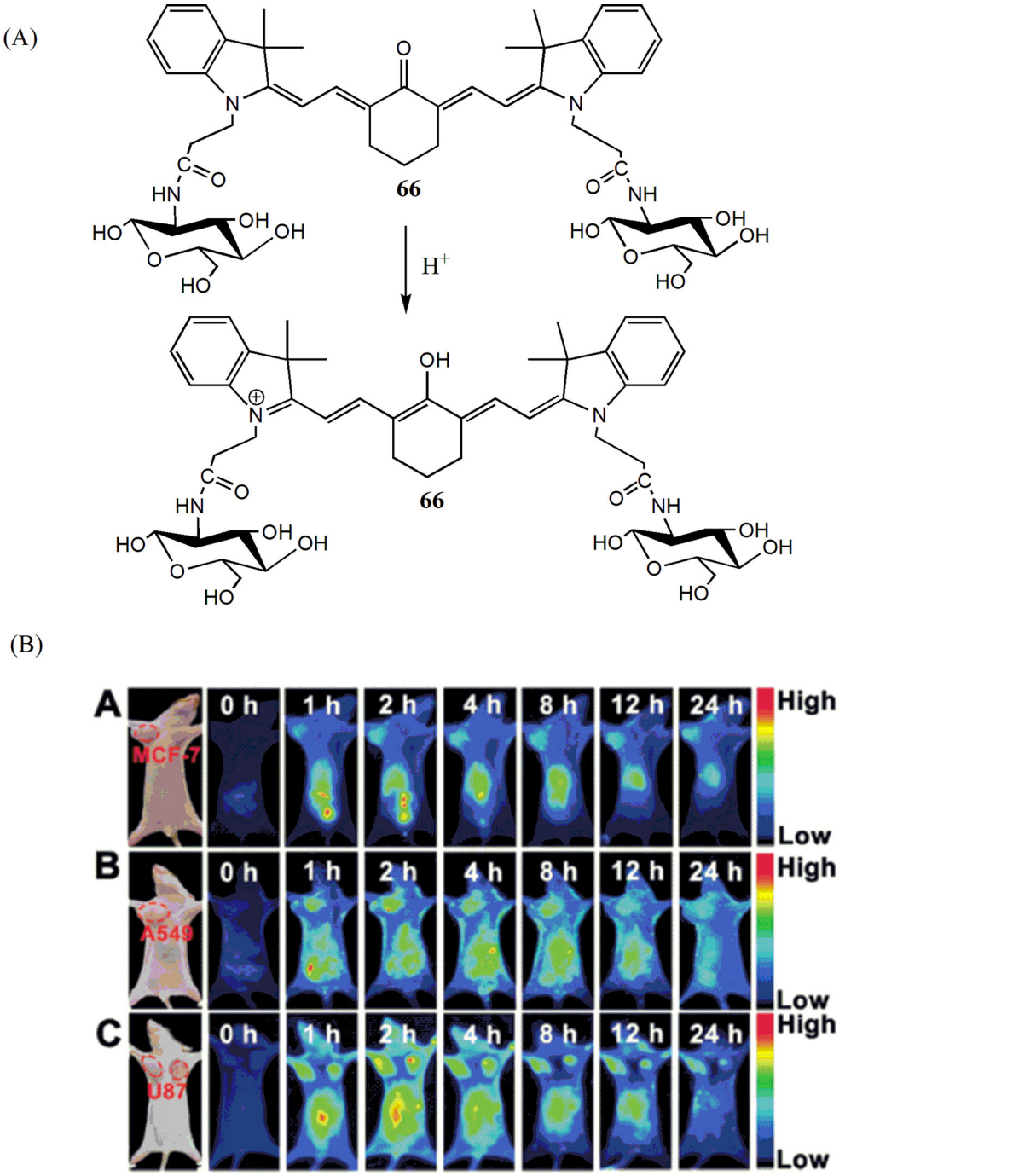

Figure 42. (A) Chemical structures of mitochondria targetable NIR fluorescent probe **66** and and its pH-dependent structural alterations. (B) Fluorescence images (*in vivo*) of probe **66** in the (A) MCF-7, (B) A549 and (C) U87 tumor-bearing mice model within 24 h. Reproduced/Adapted from Ref. [107] with permission from The Royal Society of Chemistry.

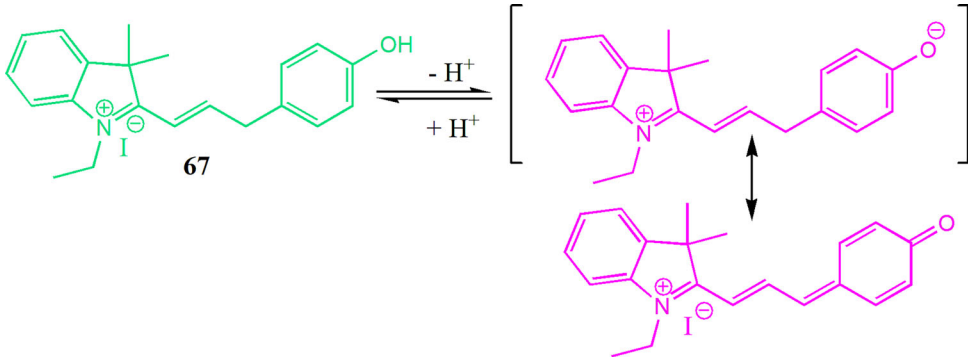

Figure 43. Chemical structures of mitochondria targetable hemicyanine-based pH probe **67** and and its pH-dependent structural alterations.

Zeng and coworkers designed a cyanine based NIR pH probe **76** with primary amine as the pH responsive moiety.[116] On increasing acidity, the probe showed gradual enhancement in emission intensity at 670 nm as protonation of the primary amine unit in acid medium caused revival of NIR fluorescence by inhibiting the ICT induced green fluorescence of the probe. With negligible cytotoxicity and a pK_a value of 3.9, the probe successfully located mitochondria and was applied to monitor rapamycin and EBS (Earle's Balanced Salt) induced autophagy in MCF-7 cells (Figure 51).

Xia *et al.* connected positively charged donor cyanine dye with acceptor hemicyanine moiety through bi-phenyl bridging to develop two NIR pH probes **77** and **78** for ratiometric monitoring of mitochondrial pH.[117] On changing the pH from 7.6 to 2.0, both the probes showed ratiometric fluorescence response where cyanine donor fluorescence (588 nm for **77** and 582 nm for **78**) got decrease with increase of hemicyanine acceptor fluorescence (740 nm for **77** and 752 nm for **78**) upon excitation at 520 nm. Acid induced spirolactam ring opening of acceptor moiety enables the TBET process to occur from donor to acceptor and was responsible for this ratiometric behavior. The pK_a values for both the probes calculated were 3.92(**77**) and 3.67(**78**) under donor excitation. Electrostatic interaction between positively charged probe and negative membrane potential of inner membrane of the mitochondria made both the probes' mitochondria targeting with good Pearson's correlation coefficient (0.92 for **77** and 0.93 for **78**) when co-cultured with MitoView blue in living HeLa cells. In addition, mitochondria staining ability of probe **77** was also confirmed by FCCP induced mitochondrial acidification. With good cell permeability, photostability and selectivity, both the probes were employed to detect intracellular pH change in living HeLa cell. More importantly, probe **77** was used to monitor nutrient starvation induced mitophagy in serum free medium and rapamycin induced mitophagy. *In vivo* imaging of pH change in *D. melanogaster* first-instar larvae was also done by using this probe (Figure 52).

Golgi body targetable pH probes

The Golgi body, one of the most important organelles found in eukaryotic cells, plays vital roles in various cellular events such as enzyme activation, processing and sorting of various secretory proteins and lipids, lysosome degradation, cell polarization and vesicular trafficking.[118–121] These cellular functions related to Golgi body is also controlled by weakly acidic Golgi pH $(6.0-6.7)$[122,123] and sometimes can be highly sensitive toward pH change like for example Protein glycosylation. So, Golgi pH misregulation can cause abnormality in the Golgi apparatus and that may lead to cancer,[124] cystic fibrosis,[125] cutis laxa,[126] and disease related to Ca^{2+}-pump.[127] Therefore, it is highly necessary to monitor Golgi pH accurately by using proper Golgi specific probes which are rarely reported. Generally, phenyl sulfonamide and sphingosine units are used in fluorescent probes to target the Golgi body.

For the first time, Dong and coworkers reported a Golgi targeted fluorescence turn-on pH probe **79** designed by connecting the Golgi targetable sphingosine unit with a pH responsive rhodamine moiety.[128] On lowering the pH value from 7.40 to 2.00, acid induced spirocyclic ring opening of rhodamine moiety of the probe caused fluorescence enhancement of more than 112-fold at 600 nm along with the appearance of pink color and red fluorescence. The fluorescence quantum yield also increased from 0.004 to 0.303 with pK_a value calculated to be 4.32. With good photo-stability, reversibility and high selectivity, the probe was found to exhibit linear response within pH 3.80–5.40. Co-localizing experiment with commercial Golgi tracker NBD C6-Ceramide in SMMC-7721, A549 and HIC cells displayed the probe's Golgi specific nature. Further quantitative

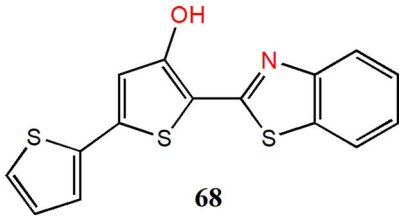

68

Figure 44. Chemical structures of mitochondria targetable ESIPT-based fluorescent pH probe **68**.

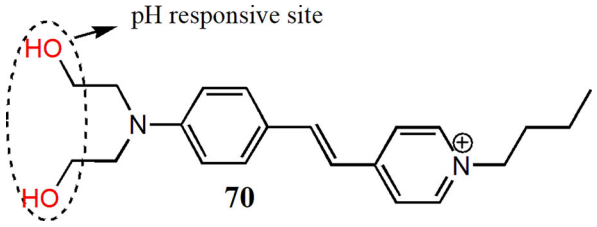

70

Figure 46. Chemical structure of mitochondria targetable stilbazolium-based two-photon fluorescent pH probe **70**.

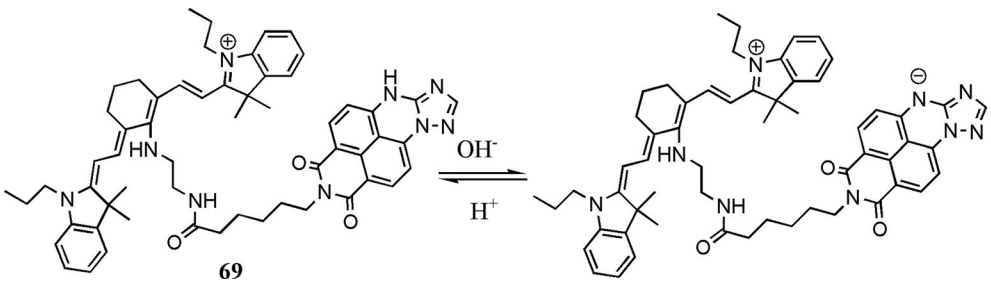

69

Figure 45. Chemical structures of mitochondria targetable ratiometric fluorescent probe **69** and its pH-dependent structural alterations.

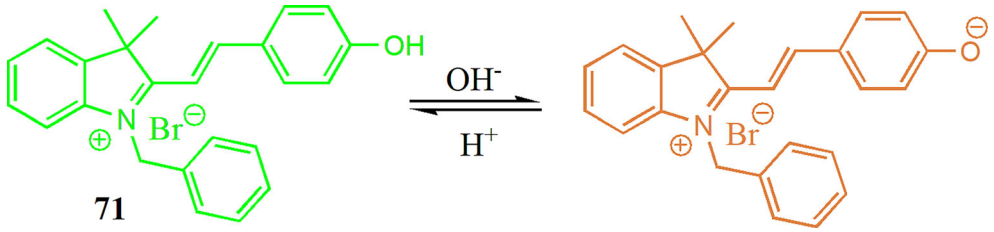

Figure 47. Chemical structure of mitochondria targetable hemicyanine-based ratiometric probe **71** and its pH-dependent structural alterations.

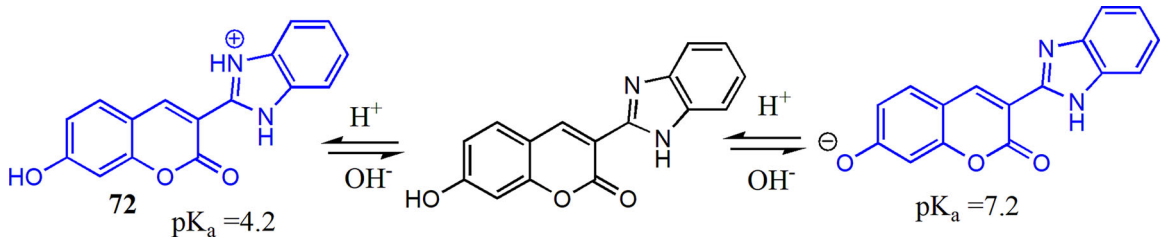

Figure 48. Chemical structure of mitochondria targetable two-photon fluorescent probe **72** and its pH-dependent structural alterations.

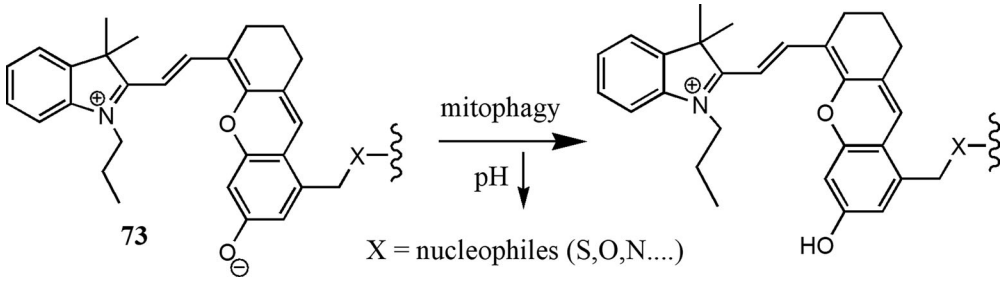

Figure 49. Chemical structure of mitochondria targetable ratiometric NIR fluorescent probe **73** and its pH-dependent structural alterations.

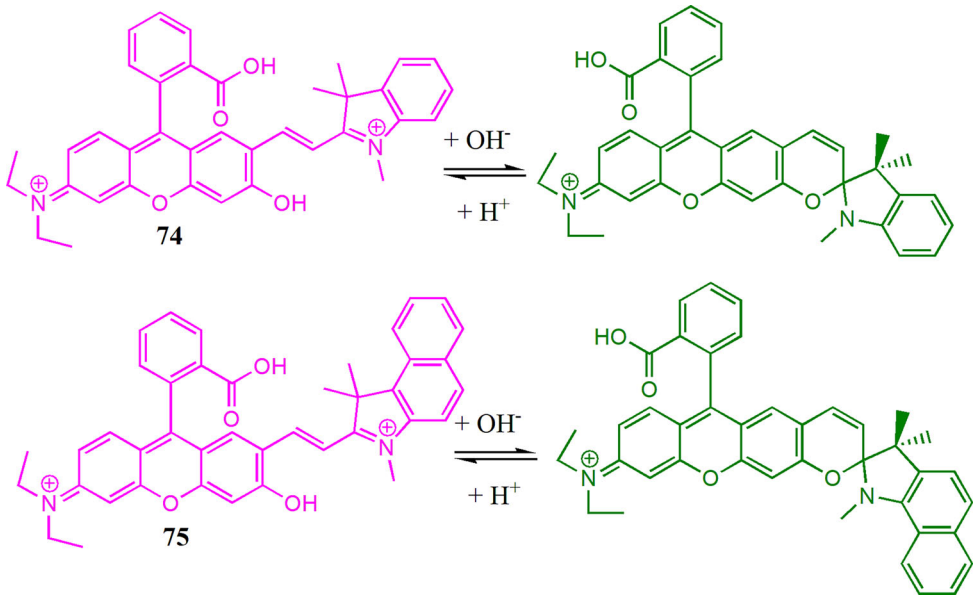

Figure 50. Chemical structures of mitochondria targetable ratiometric NIR fluorescent probes **74** and **75** and their pH-dependent structural alterations.

pH change was monitored by cell imaging study in SMMC-7721cells with low toxicity without any significant disturbance in Golgi function. Again, the treatment of bafilomycin A1 with probe loaded SMMC-7721 cells for 5 min showed a pH increase from 6.05 ± 0.10 to pH 7.12 ± 0.09 and NH_4Cl induced Golgi alkalization was also investigated. Further oxidative stress induced pH changes in Golgi were tracked where H_2O_2, N-ethylmaleimide and NaClO showed an increase in Golgi pH whereas N-acetylcysteine caused decrease in pH. Finally, acidification of tissues due to LPS induced inflammation was imaged by using an *in vivo* mouse model (Figure 53).

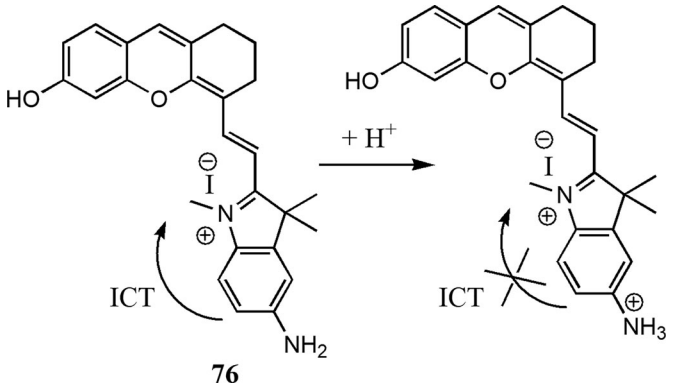

76

Figure 51. Chemical structure of mitochondria targetable NIR fluorescent pH probe **76** and its sensing process.

Wang *et al.* reported a tricarbocyanine based ratiometric pH probe **80**, modified with Golgi targeted phenyl sulfonamide moiety for monitoring Golgi pH change in both photoacoustic (PA) and fluorescence imaging methods.[129] When pH increased from 5.9 to 7.7, the fluorescence intensity of the probe displayed enhancement at 750 nm along with decrease at 810 nm whereas in PA response, the peak at 800 nm showed decrease along with negligible change of the peak at 690 nm. With good selectivity, reversibility and photo-stability, the probe was found to be Golgi targeted with a correlation coefficient of 0.97 when co-localised with Golgi-Tracker Red. Furthermore, cell experiments showed that Monensin induced Golgi oxidative stress led to increase Golgi pH. The decrease of pH due to LPS induced abdominal inflammation in mice was also monitored by both fluorescence and PA mode. Again, melanoma containing mice was used to monitor pH of tumor tissue by using PA mode. Finally, by using the probe, it was found that transmembrane protein 165 was a Golgi located H^+ transporter and its deficiency severely affected Golgi pH homeostasis (Figure 54).

Endoplasmic reticulum targetable pH probes

Being one of the important organelles of the secretory pathway, endoplasmic reticulum (ER) plays crucial roles in calcium homeostasis, synthesis and folding of lipids, sorting and targeting of proteins as well as lipids during secretion, detoxifications.[130–133] These cellular events are regulated accurately under the influence of weakly basic pH (7.2 ± 0.2) of ER and slight fluctuation can cause disturbance in enzyme activities, intracellular Ca^{2+} balance, sorting and distributing process of proteins etc.[134,135] Again, abnormal functions of ER can induce ER stress which may lead to autophagy and that condition is linked with various diseases like infectious diseases, neurodegeneration, cancer, insulin resistance, obesity and diabetes.[136–138] So, real time monitoring of ER stress is essential by investigating ER pH change in living cells for early diagnosis of ER related diseases. *p*-toluene sulfonamide is used as an ER targeting unit in fluorescent probes reported so far.

In 2018, Xiao *et al.* synthesized a pH probe **81** which contained pH responsive piperazine unit, ER (endoplasmic reticulum) targeting 4-methyl benzene sulfonamide moiety, thiol sensitive benzyl chloride unit and 1,8-naphthalimide as fluorophore for monitoring pH fluctuation of ER during stress.[139] When pH was changed from 9.5 to 2.5, the probe showed turn on fluorescence with enhancement of emission intensity at 528 nm due to protonation induced blocking of the PET process. The probe also exhibited good linear response within pH 4.0–5.0. The probe was found to be photo-stable and selective in presence of metal ions, reactive oxygen species (ROS), thiols and the pK_a value was 4.58. Colocalization experiment with ER-Tracker Red in probe loaded HeLa cell demonstrated the probe's ER targeting ability. Furthermore, tunicamycin and thapsigargin induced ER acidification under stress was successfully monitored by the probe. Again, as thapsigargin increases cytoplasmic calcium ion as well as decreases ER pH by blocking Ca^{2+}-ATPase, both the phenomenon was investigated in HepG2 cells by using the probe **81** and Fluo-3 AM, a calcium ion sensor. Moreover, they did *in vivo* imaging of pH variation in zebrafish and abdominal tissues of living mice by using two-photon fluorescence microscopy (Figure 55).

Lin and coworkers designed a two-photon pH probe **82** by modifying naphthalimide fluorophore with pH responsive piperazine unit and ER targeting 4-methylbenzenesulfonamide moiety.[140] The probe exhibited enhancement of green fluorescence at 531 nm when pH was changed from 10.0 to 4.0 and that was mainly due to inhibition of the PET effect on protonation of piperazine "N" of the probe in acid medium. With good selectivity and low toxicity, the probe was found to be ER targeted (correlation coefficient 0.90) when co-cultured with ER tracker. Furthermore, cell experiment with probe loaded HepG2 cells showed that tunicamycin induced ER stress caused ER acidification. Again, the probe was applied to monitor pH change in living tissue and zebrafish by using two-photon fluorescence imaging (Figure 56).

By connecting naphthalimide fluorophore with coumarin moiety, for the first time, Lin and coworkers synthesized a triple sensing mechanism (ICT-PET-FRET) based ER targeted pH probe **83** in which both morpholine unit and hydroxyl group of coumarin moiety acted as pH responsive sites whereas *p*-toluenesulfonamide used as an ER anchoring unit.[141] On increasing pH (from 4.09 to 8.99), the probe displayed ratiometric response where emission intensity ratio (I_{446}/I_{527}) showed about 50-fold change within pH (5.03 to 7.26) and this change was governed by ICT, PET and FRET mechanisms.With negligible cytotoxicity under 10 μM, the probe was found to be ER targeted when co-localised with ER-Tracker Red. Additionally, the probe was used for quantitative measurement of pH change in dexamethanose treated living HeLa cells as well as during Hcy (homocysteine) and tunicamycin induced ER stress. Moreover, pH probes with more than one response site and sensing mechanisms are highly desirable for quantitative measurement of small pH fluctuations in ER (Figure 57).

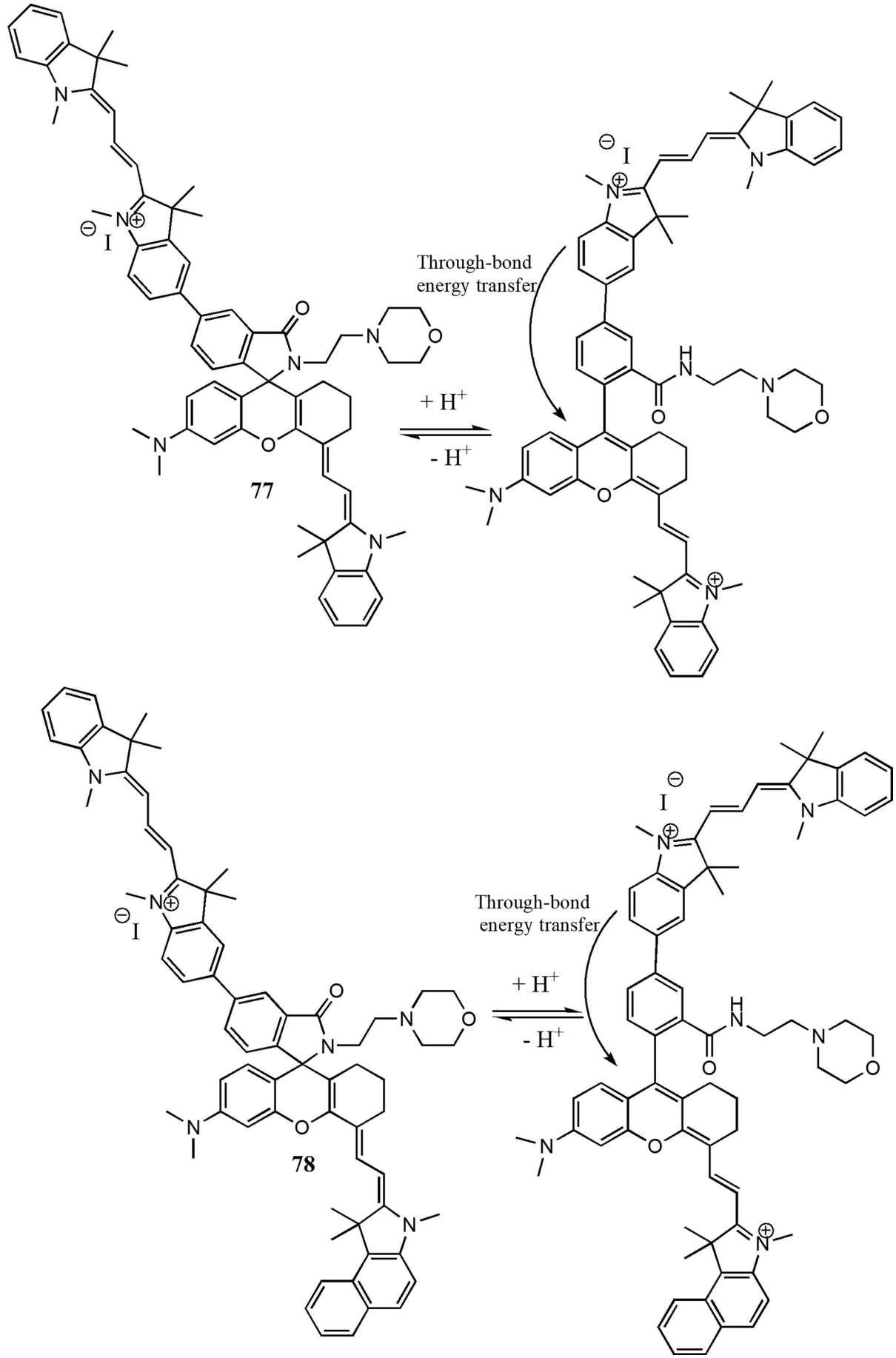

Figure 52. Chemical structures of mitochondria targetable ratiometric NIR fluorescent pH probes **77** and **78** and their pH-dependent structural alterations.

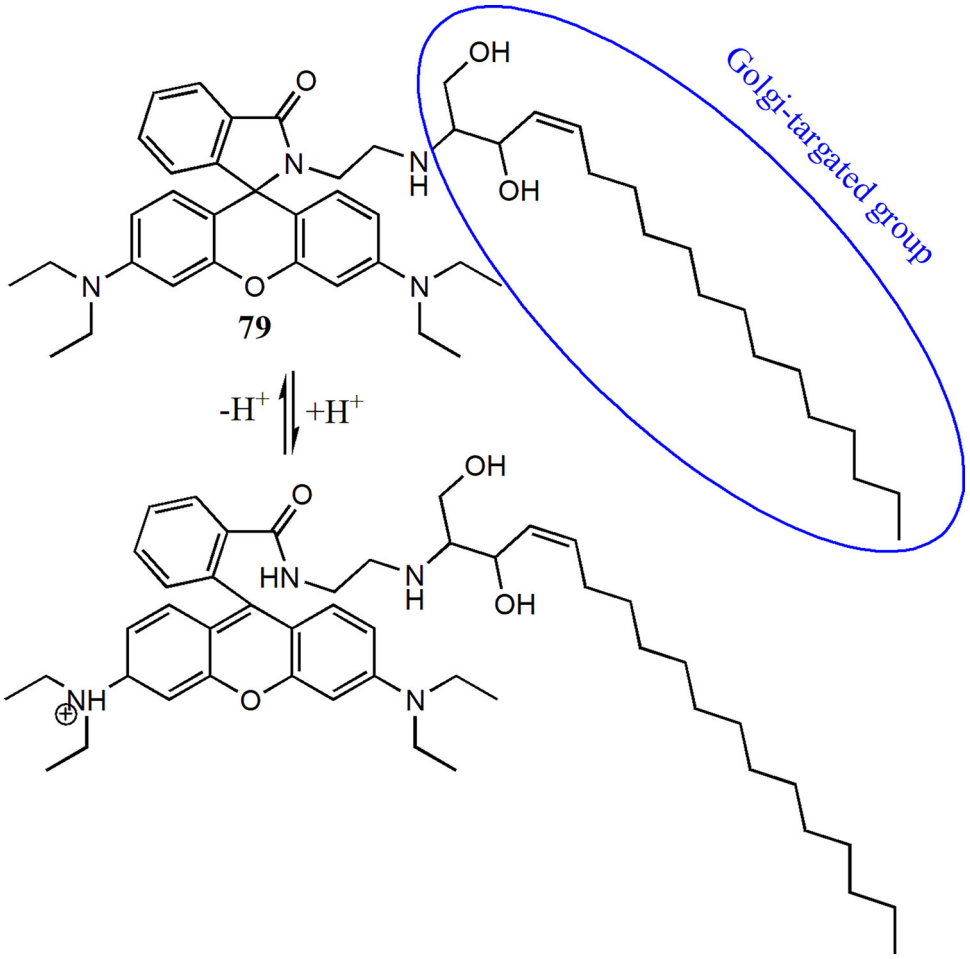

Figure 53. Chemical structure of golgi body targetable rhodamine-based pH probe **79** and its pH-dependent structural alterations.

pH probes used in nonspecific cell imaging

In this section we will discuss pH probes (**84** to **109**) which are not specific to any organelles but only used for intracellular pH monitoring and *in vivo* imaging.

By connecting the donor TPE moiety with the acceptor cyanine moiety Fang *et al.* reported a fluorescent cassette **84** which exhibited strong fluorescence response in acidic conditions (pH 5.0) due to its AIE property with 484 nm of large pseudo-Stoke's shift. TBET, operated from donor to acceptor, was responsible for this spectral response.[142] However, significant quenching of fluorescence was observed on changing pH from 5.0 to 10.7 and that was due to loss of energy for ether bond rotation between donor and acceptor as well as less aggregation of cassette due to repulsion among negatively charged phenolate ions of TPE moiety. Further, the fluorescent cassette was used to monitor oxidative stress induced intracellular pH variation in living HeLa cells caused by hydrogen peroxide and *N*-ethylmaleimide (NEM) (Figure 58).

By introducing HBT [2-(2′-hydroxyphenyl) benzothiazole] into the BODIPY moiety, Cao *et al.* synthesized a ratiometric pH probe **85** which exhibited strong solid-state emission at 607 nm.[143] On increasing the pH from 4.5 to 9.8 in PBS buffer / DMSO (v/v = 1:9), enhancement of ICT due to alkali induced deprotonation of the phenolic –OH group of the probe caused a red shift in absorption spectra (352 nm to 357 nm) with increase of new peak at 425 nm. A naked eye detectable color change was observed from lemon to orange. Under the same conditions, the fluorescence intensity ratio (I_{528}/I_{484}) showed a decrease (12.29 to 1.02) with the change of fluorescence from bright green to blackish green. With pK_a value of 7.32, the probe was found to be selective, reversible and displayed a linear relationship within pH 6.8 to 8.5. Moreover, probe **85** was applied to detect pH change in living HeLa cells with low toxicity (Figure 59).

For fluorometric monitoring of pH changes in living cells, Qiu and coworkers synthesized a probe **86** having dual pH responsive sites by connecting rhodamine and biphenylcarbonitrile moiety.[144] The probe was found to be colorless and non-fluorescent in neutral medium but on lowering pH from 7.0 to 2.0, acid induced spirolactam ring opening caused three absorption bands at 277 nm, 295 nm and 558 nm along with visible pink color as well as a strong red emission peak at 590 nm. Again, when the medium was changed from neutral to alkaline (pH 7 to 12), strong ICT due to formation of phenoxide ion caused enhancement of a new absorption peak at 358 nm with visible bright yellow color. A new emission peak at 558 nm was also evolved with yellow-green emission increased with increasing pH. In both spectra the probe displayed good linear response within pH

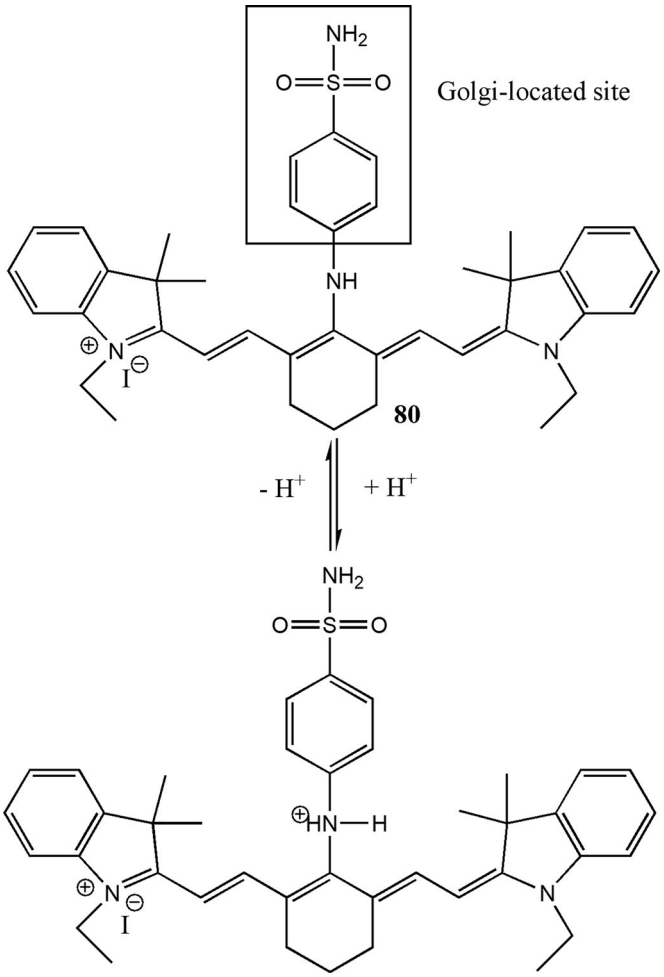

Figure 54. Chemical structure of Golgi targetable pH probe **80** and its pH-dependent structural alterations.

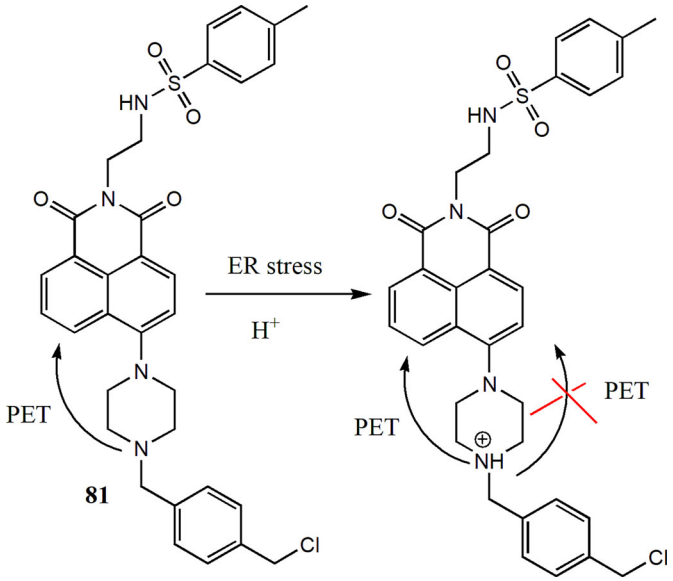

Figure 55. Chemical structure of endoplasmic reticulum targetable fluorescent probe **81** and its sensing process.

2–7 and 8–12. With good reversibility, the probe was found to be selective over various cations and anions except Cu^{2+} ion which induced a strong peak at 558 nm in absorption spectra with color change of solution but did not induce any fluorescence emission. This was mainly due to co-ordination of Cu^{2+} to form [**86**-Cu^{2+}] complex which leads to opening of the spirolactam ring. The probe was used to monitor intracellular pH change in living HepG2 cells with low cytotoxicity (Figure 60).

Zhang's group modified pyrene to synthesize probe **87** for colorimetric and fluorometric detection of pH changes in living cells and bacteria.[145] Accompanied with the pH decrease from 6.71 to 1.62, the fluorescence emission showed a decrease at 515 nm with 145 nm of large stoke shift and the pK_a value was found to be 2.98. In acid medium, N atoms of the naphthyridine group got protonated and caused this spectral change with a naked eye detectable appearance of yellow color and the yellow fluorescence got turned off. The sensing mechanism was confirmed by ^{1}H-NMR and DFT, TD-DFT studies. With good photostability, reversibility and selectivity, the probe displayed good linearity within pH 2.43–3.71. Further, the probe was applied for monitoring intracellular pH change in living A549 cells and the strong acidic environment in *E. coli* bacteria (Figure 61).

Georgiev *et al.* reported a perylenediimide based pH probe **88** having good water solubility with piperazine unit acting as an H^+ receptor.[146] Protonation of piperazine "N" of the probe in acid medium blocked the PET process and that caused enhancement of emission intensity at 550 nm with an increase in quantum yield from 0.003 to 0.11. The Interference study showed that the probe was selective over various transition metal ions and anions except Cu^{2+} and Hg^{2+} which quenched the fluorescence intensity strongly and the pK_a value was calculated to be 6.35 ± 0.02. The probe was found to be cell permeable only at a probe concentration of 1.3 μM and exhibited nontoxic nature within a wide range of concentration (330 μM to 1.3 μM) when examined in living L929 cells (Figure 62).

Liu *et al.* reported another ratiometric pH probe **89** based on quinolone by introducing a polyether chain to increase the probe's water solubility.[147] On increasing basicity (4.50 to 9.0) in Na_2HPO_4-citrate buffer, acid induced protonation-activable resonance charge transfer (PARCT) process occurred from methoxy group to quinolinic nitrogen got diminished and that caused a large hypsochromic shift of 57 nm in emission spectra with linear response within pH range of 6.35–8.00. The emission intensity ratio (I_{531}/I_{588}) increased from 0.30 to 1.36 and the pK_a value was calculated to be 7.18. The probe was found to accumulate in cytoplasm with low toxicity and was able to monitor intracellular pH change ratiometrically in NIH 3T3 cells (Figure 63).

Wang *et al.* reported a benzothio-pyrylium pentamethine cyanine **90** which exhibited stable absorption and emission peak in NIR-II region with high brightness and photostability including anti-quenching property in aqueous solution.[148] On lowering pH from 5 to 0, acid induced protonation of the diethylamino unit of the probe led to a blue shift in emission spectra (1065 nm to 980 nm) and the optimal sensitive range of pH was found to be 1–4. Moreover, with pK_a values of 0.29 and 3.81, the probe was

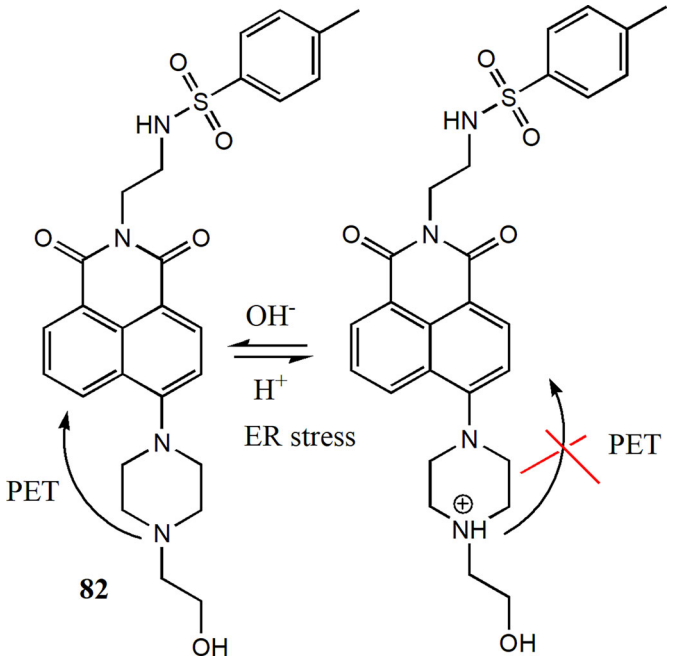

Figure 56. Chemical structure of endoplasmic reticulum targetable two-photon fluorescent probe **82** and its pH-dependent structural alterations.

successfully employed in *in vivo* imaging of gastric pH in mice with favorable imaging ability of about 4 mm deep tissue (Figure 64).

Based on the design strategy of "cycle reversible ICT," Jiang *et al.* reported a spiropyran derivative **91** as a pH probe.[149] On irradiation under UV light, the probe exhibited turn-on yellow fluorescence at 595 nm with its structural change from non-fluorescent spiropyran form to fluorescent hemicyanine form. On decreasing acidity (pH 7.53 to 8.46), deprotonation of phenolic –OH group enabled the appearance of a new red emission peak at 664 nm and on decreasing pH (7.32 to 3.87), protonation of the imide group of the probe induced a new green emission peak at 563 nm with decrease of yellow emissive peak at 595 nm in both the case. With a detection limit of 0.028 of pH change, the probe was found to be selective, photostable and could track intracellular pH change induced by UV-light during programmed cell death (Figure 65).

Lin and coworkers reported two 2-(2′-hydroxyphenyl)-benzothiazole (HBT) based ratiometric pH probes **92** and **93.**[150] Alkali induced deprotonation of phenolic –OH enabled ESIPT and that caused ratiometric fluorescence change in emission spectra of both the probes on increasing pH from 3.0 to 9.0. For better ratiometric response, probe

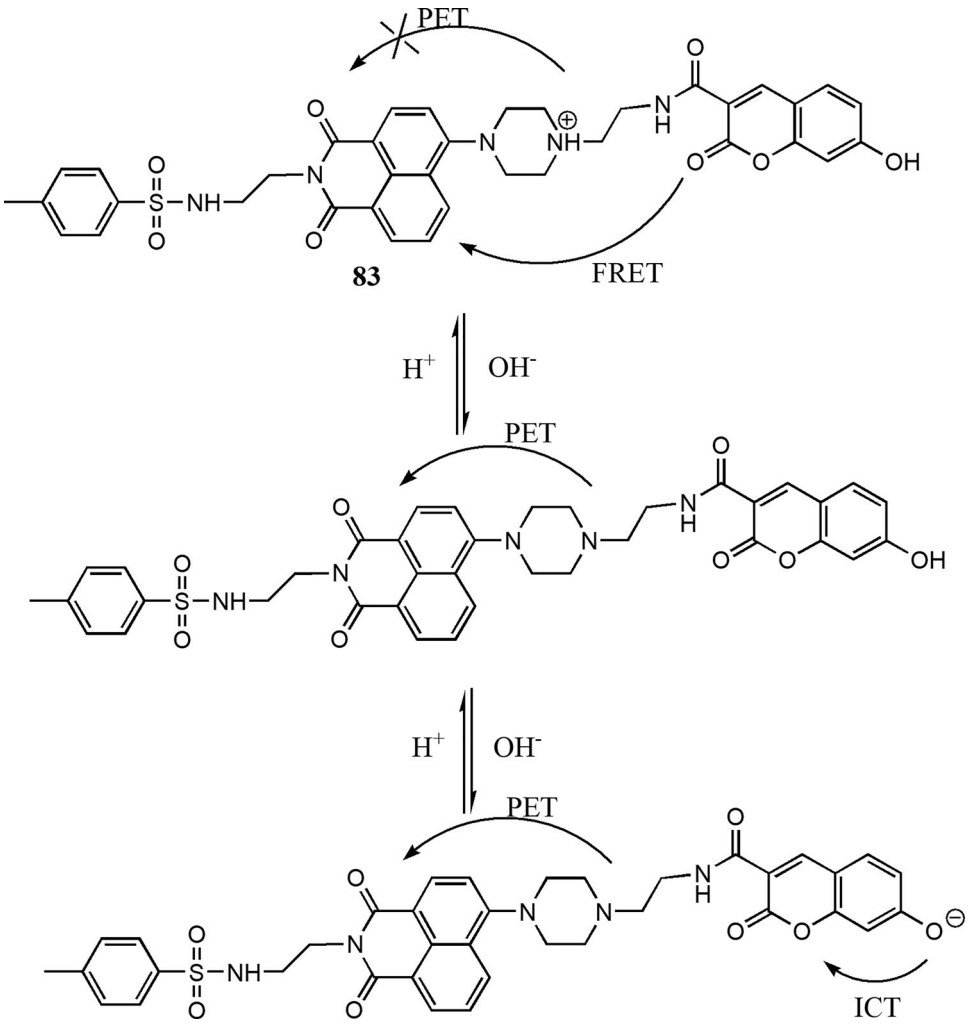

Figure 57. Chemical structure of endoplasmic reticulum targetable ratiometric fluorescent probe **83** and its pH-dependent structural alterations.

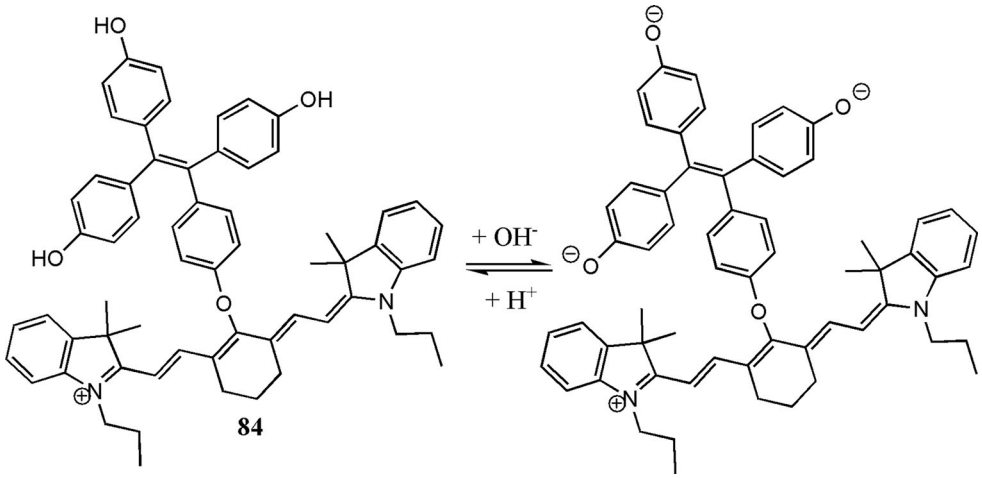

Figure 58. Chemical structure of cyanine-based fluorescent pH probe **84** and its pH-dependent structural alterations.

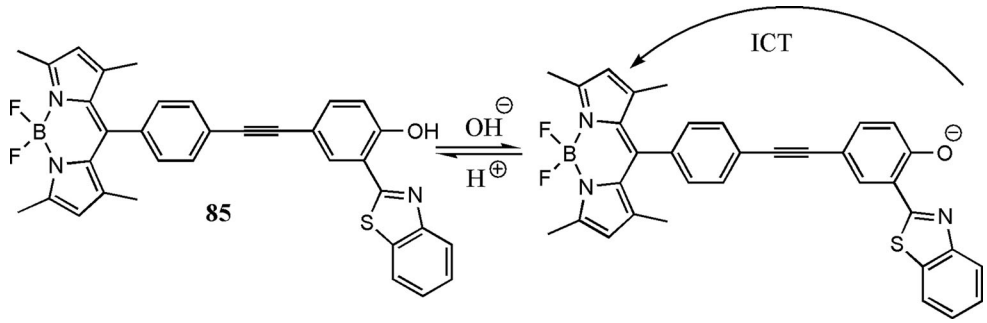

Figure 59. Chemical structures of pH probe **85** and its pH-dependent structural alterations.

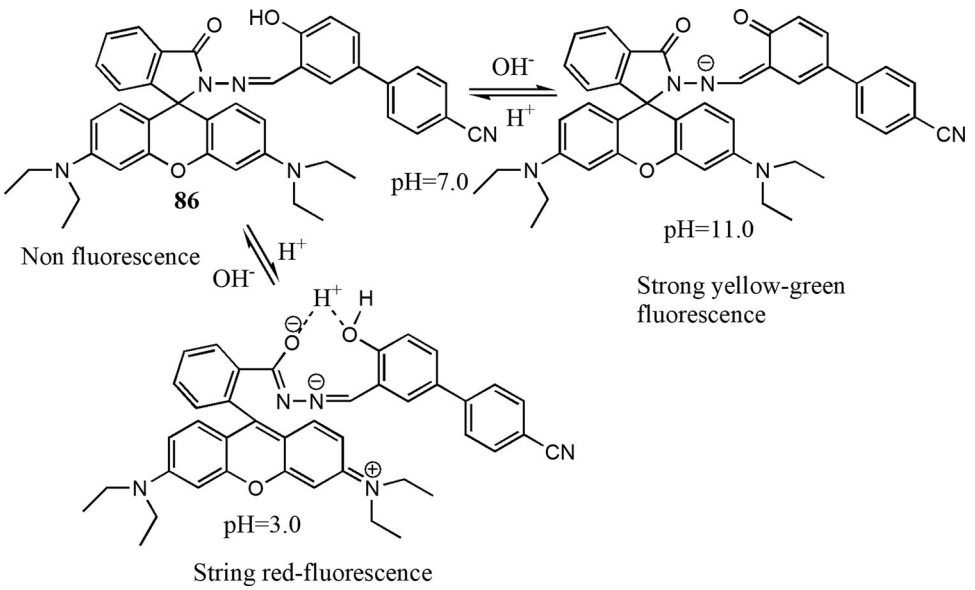

Figure 60. Chemical structure of rhodamine-based fluorescent pH probe **86** and its sensing processes.

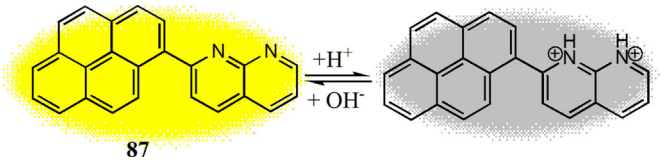

Figure 61. Chemical structures of pyrene-based fluorescent and colorimetric pH probe **87** and its pH-dependent structural alterations.

92 was applied to monitor intracellular pH change as well as NH_4Cl induced intracellular pH enhancement in living A549 cells. Further pH change in living tissues was also ratiometrically investigated by probe **92** (Figure 66).

By incorporating cationic benzoyl hydrazine with electron withdrawing bromine group in to the cyanine moiety, Mai

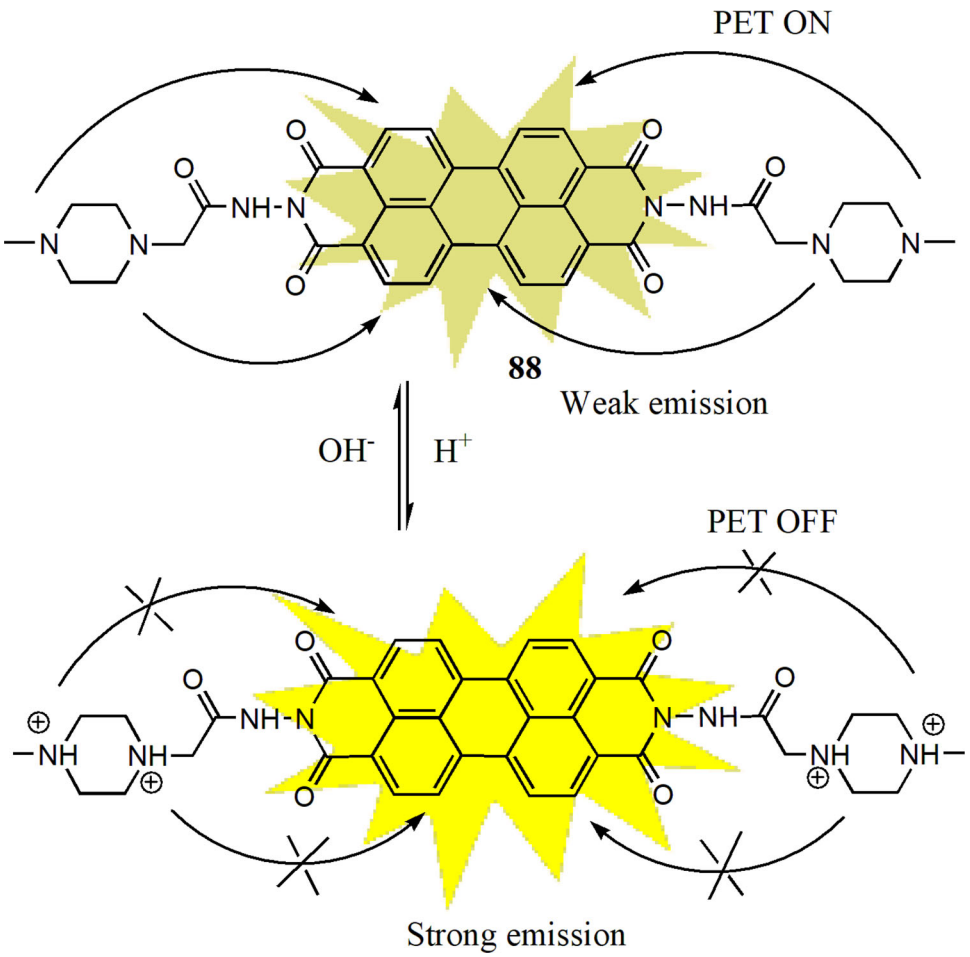

Figure 62. Chemical structure of perylene-3,4,9,10-tetracarboxylic diimide (PDI)-based fluorescent pH probe **88** and its pH-dependent structural alterations.

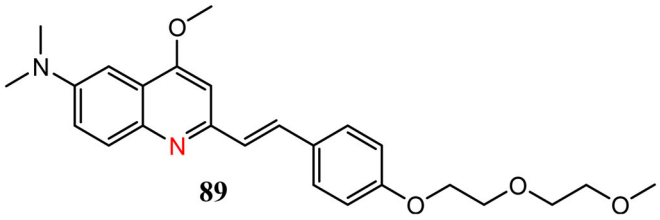

89

Figure 63. Chemical structures of quinoline-based ratiometric fluorescent pH probe **89**.

et al. developed a NIR pH probe **94** for monitoring gradual alkalization of chronic wounds during its delayed healing process.[151] With a pK_a value of 8.01, the probe exhibited about 76.9% fluorescence decrease with increasing pH from 7.0 to 9.0 in living Ewing's sarcoma cells and that was mainly due to deprotonation of acylhydrazine unit in alkaline pH. More importantly, the probe was successfully employed to visualize alkalization of chronic wounds in a diabetes-impaired mouse model and uneven pH distribution of wound areas was also observed during wound development. Thus, NIR pH probes with proper alkaline pK_a values are much more desirable for chronic wound monitoring and should be studied in the future (Figure 67).

Three cyanine based NIR pH probes **95**, **96** and **97** were designed by Chen and coworkers.[152] With increasing acidity (pH = 11.0 to 2.0), the NIR emission intensity increased gradually at 805 nm along with a naked eye notable color change of the probe's solution from pink to purple to green and that was mainly due to protonation induced enhancement of ICT process. The good linear responses were observed within 2.76–4.01(**95**), 3.65–4.70(**96**), 4.59–6.45(**97**) and the pK_a values were determined to be 3.45(**95**), 4.05(**96**), 5.52(**97**). The probes **96** and **97** were found to be distributed in cytoplasm and could monitor intracellular pH variation in SCC-7 cells (Figure 68).

Wong's group reported a pH probe **98** having an electron donor naphthol moiety and an electron acceptor benzothiazole moiety for ratiometric monitoring of intracellular pH fluctuation.[153] On lowering the pH from 11.50 to 4.00, the emission peak at 526 nm declined with enhancement of a new peak at 456 nm as well as fluorescence color changed from green to aqua-marine. With large stoke shifts (141 at pH 11.50 and 125 at pH 4.0) and high quantum yield ($\Phi = 0.88$ in DMSO and 0.61 in water), the probe displayed linear response within pH 9.50–7.00 with a pK_a value of 7.91 ± 0.03. Further, the emission intensity ratio (I_{456}/I_{526}) showed 7.6-fold enhancement with good selectivity, reversibility and photostability. Intracellular pH variation, NH_4Cl induced pH increase and H_2O_2 induced pH decrease in HeLa cells were ratiometrically monitored by the probe with good cell permeability and low cytotoxicity (Figure 69).

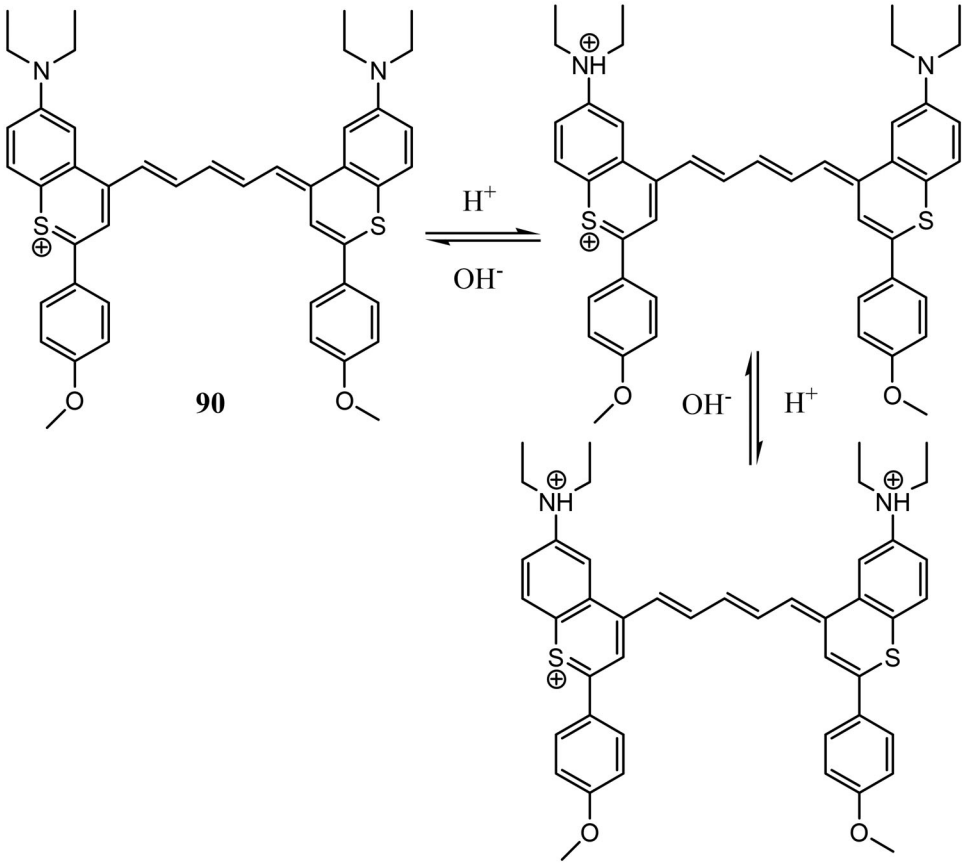

Figure 64. Chemical structures of NIR-II based fluorescent pH probe **90** and its pH-dependent structural alterations.

Zhu et al. designed three ESIPT based pH probes **99**, **100** and **101** by conjugating benzothiazole and spiropyrans.[154] Probe **99** displayed turn on fluorescence response with 36-fold fluorescence enhancement at 640 nm on decreasing the pH from 12.00 to 2.00. On a similar pH change, probe **100** and **101** exhibited ratiometric responses where fluorescence intensity at 520 nm and 525 nm decreased along with an increase at 640 nm and 675 nm respectively. This spectral change was attributed to acid induced ring opening of the spiro form of all the probes enabled ESIPT. The pK_a values of three probes **99**, **100** and **101** were 6.57, 4.90, and 3.95 respectively. In addition, probe **100** was successfully employed in intracellular pH monitoring in living HeLa cells with low toxicity (Figure 70).

Yin *et al.* reported a phenanthro [9, 10-d]imidazole-based pH probe **102** which showed weak fluorescence at 420 nm at pH 8.50 when investigated in water/EtOH solution (v/v, 1:1).[155] On lowering pH from 8.50 to 6.05 it displayed turn-on fluorescence response with an 8-fold increase in emission intensity and the quantum yield also enhanced from 0.114 to 0.818. This was mainly due to inhibition of the PET effect resulting from acid induced protonation of pyridine "N" of the probe. The pK_a value of the probe was 6.89. The probe exhibited good linear response within pH 6.24–8.56 and reversible response within pH 5.50–9.50 with good selectivity over various ions except Cu^{2+} ions. Hence, according to the author, the probe also detected Cu^{2+} ions with turn-on response and the LOD was 37.69 nM. More importantly, the probe was used for intracellular pH monitoring in living HeLa cells (Figure 71).

pH probes based on BOPYIN (Borondifluoride-3,3-dimethyl-2-[2-(2-pyrrolyl) ethenyl] indole) derivatives for monitoring strong acidic conditions are hardly available in the literature. As a result, Zhang and colleagues developed a BOPYIN-based fluorescence turn-on pH probe **103** for acidic pH determination.[156] On increasing acidity (pH = 2.47–5.01) acid induced protonation of primary amine in the probe inhibited the PET process and that caused turn-on fluorescence enhancement with naked eye detectable color change from orange to lemon and linearity was observed within pH 3.0 to 5.5. The probe was found to be reversible, selective over various metal ions (Cr^{3+}, Mg^{2+}, Na^{+}, K^{+}, Zn^{2+}, Cu^{2+}, Co^{2+}, Fe^{2+} and Al^{3+}) with a quick response time of 10 sec. With a pK_a value of 3.63, the probe was applied to visualize pH change fluorometrically with a paper strip and to monitor intracellular acidic pH variation in T24 cells (Figure 72).

Mohamed *et al.* reported a xanthene-based pH probe **104** which showed a selective colorimetric change (colorless to reddish) and turn-on fluorometric response in alkaline medium due to alkali induced opening of spirolactam ring of the probe.[157] At pH 9.7, the probe showed strong emission at 529 nm and color change was observed along with the red shift of its absorption spectra from 330 nm to 509 nm. Two pK_a values of the probe calculated by the fluorometric method were 8.72 and 10.73. Furthermore, the

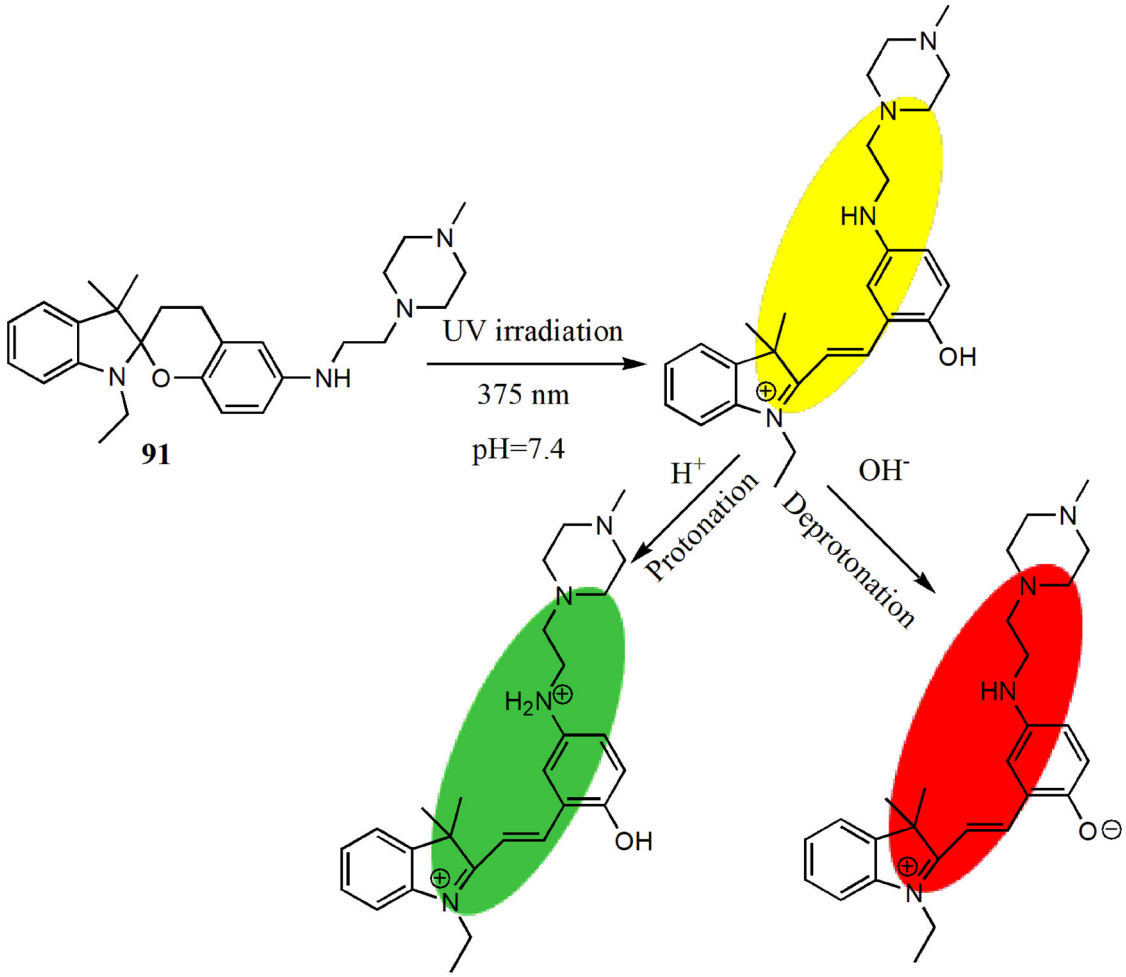

Figure 65. Chemical structure of 'cycle reversible ICT'-based pH probe **91** and its pH-dependent structural alterations.

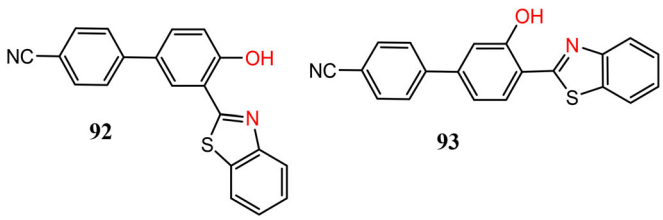

Figure 66. Chemical structures of ESIPT-based ratiometric fluorescent pH probes **92** and **93**.

probe was used to detect living E. coli bacteria through confocal fluorescence microscopy (Figure 73).

Perez-Inestrosa and coworkers reported two indolenine-based two photon pH probes **105** and **106**.[158] With pK_a values of 3.61 (**105**) and 3.65 (**106**) both the probes exhibited turn-on fluorescence response in acidic pH accompanied by red shift in both absorption and emission spectra as a result of enhanced ICT due to protonation of indole "N." Probes also showed good linear response within pH 2.50–4.50 with reversibility, photostability and good selectivity over metal ions. Furthermore, both the probes were applied to image pH fluctuation in MEF cells with lyso tracker where probe **105** was found to be cytoplasm specific and probe **106** was lysosome specific with low cytotoxicity (Figure 74).

Recently, He et al. have reported a spiropyran based ratiometric and colorimetric pH probe **107** to monitor pH change by using a FRET sensing mechanism which was due to H^+ induced structural change from closed spiropyran to open merocyanine form.[159] On decreasing the pH from 7.21 to 1.68, the probe exhibited red-shift both in absorption spectra (35 nm) and emission spectra (104 nm) with color change from green to yellow as well as fluorescence change from green to red with 10.2-fold fluorescence enhancement. The probe also showed good linearity between pH 4.0 to 6.0 and the pK_a value was found to be 4.87. The probe also exhibited good reversibility, stability and selectivity as no significant interference was observed on pH monitoring by common ions. Having good cell permeability and negligible cytotoxicity, the probe was successfully used to monitor pH changes in living cells, Zebrafish and bacteria (Figure 75).

Haldar *et al.* reported a BODIPY-based pH probe **108** which was prepared by the RAFT (reversible-addition fragmentation chain transfer) polymerization process.[160] The probe showed excellent water solubility and stability. On changing the pH from 9.0 to 1.5, this weakly emissive polymeric sensor displayed enhancement in emission intensity

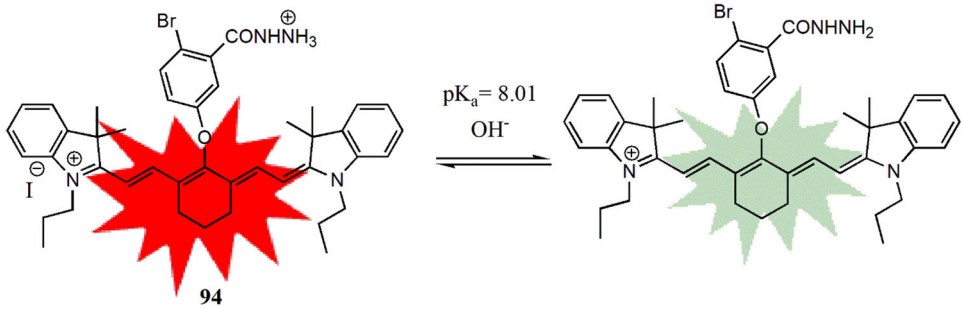

Figure 67. Chemical structure of NIR fluorescent pH probe **94** and its sensing mechanisms.

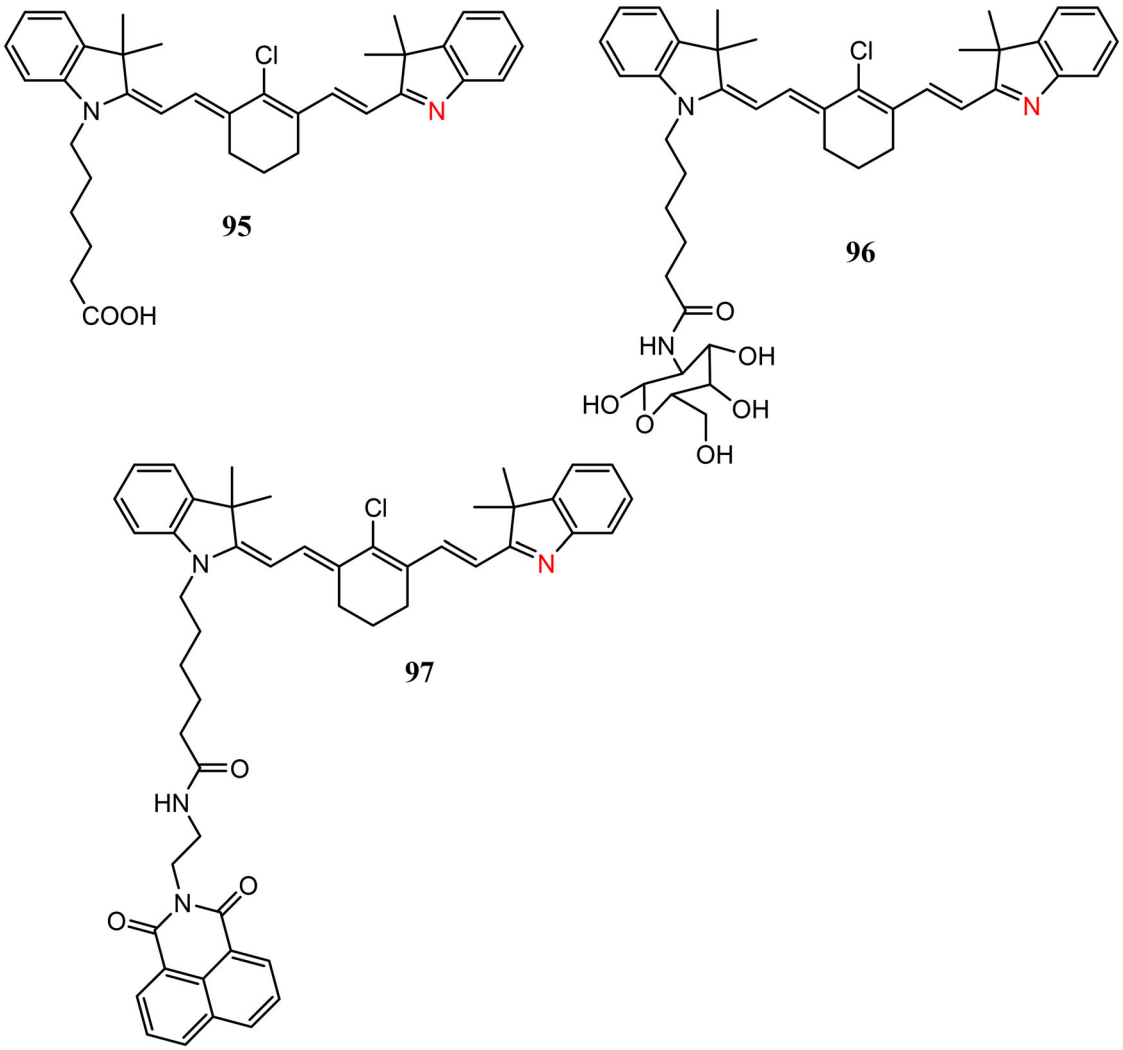

Figure 68. Chemical structures of cyanine-based NIR fluorescent pH probes **95-97**.

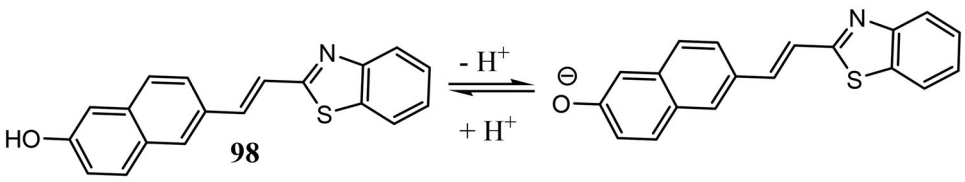

Figure 69. Chemical structure of ratiometric fluorescent pH probe **98** and its pH-dependent structural alterations.

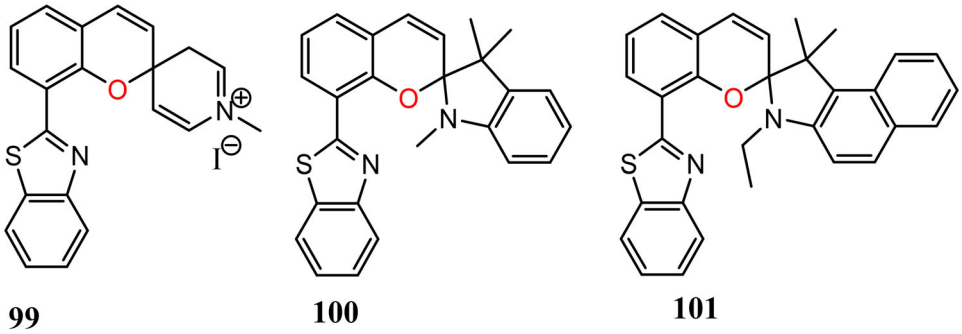

Figure 70. Chemical structure of ESPIT-based fluorescent pH probes **99-101**.

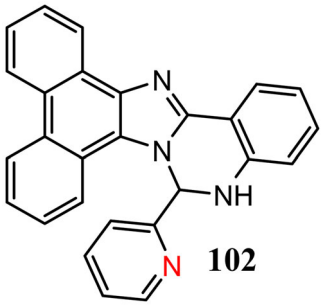

Figure 71. Chemical structure of phenanthro[9,10-*d*]imidazole-based fluorescent pH probe **102**.

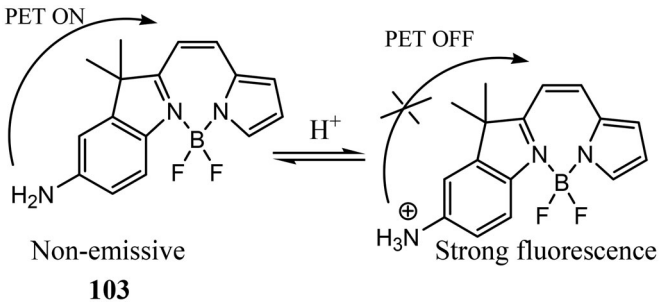

Figure 72. Chemical structure of BOPYIN-based fluorescent pH probe **103** and its sensing mechanisms.

with strong green fluorescence at 512 nm along with an increase in quantum yield from 0.017 to 0.41. This was due to inhibition of PET from amine to BODIPY moiety on protonation of amine in an acidic medium and was investigated through DFT and TDDFT studies. The probe was found to be reversible, photo-stable with pK_a value of 3.48 and showed good selectivity as various bioactive metal ions, BSA (bovine serum albumin) did not interfere in pH sensing. The probe was used to image acidic pH in breast cancer cells and *E. coli* bacteria. Furthermore, according to the author, the probe was used in paper strips to detect acid and ammonia vapor. Compared to small-molecule fluorescent probes, this kind of water-soluble polymeric pH probe selectively working in harsh acidic conditions is much more desirable for biological applications (Figure 76).

He *et al.* reported a FRET based pH probe **109** by connecting rhodamine as an electron acceptor and hydroxynaphthaldehyde as an electron donor.[161] On increasing acidity (from pH 7.5 to 2), acid induced opening of spirolactam ring caused FRET to occur in the probe and as a result, a naked eye detectable colorimetric change (green to pink) as well as ratiometric fluorescence change (green to red) was observed. The pK_a value was found to be 5.05. Furthermore, with good selectivity, reversibility and biocompatibility, the probe was applied for ratiometric imaging of pH change in living hPDLCs cells, *P. aeruginosa* bacteria and in zebrafish (Figure 77).

pH probes without cell imaging

In this section, the probes (**110** to **121**) which were not used in bioimaging will be discussed with their designing strategies, sensing mechanisms and environmental applications.

Yang et al. have reported a NIR ratiometric probe **110** containing D-π-A system dicyanomethylene-4H-pyran for monitoring pH through the ICT process.[162] On increasing the pH from 7.15 to 11.00 in C_2H_5OH–H_2O (6:4, v/v), the probe exhibited a decrease both in absorption peak at 450 nm and in emission peak at 574 nm along with an increase in absorption peak at 550 nm and in emission peak at 692 nm with naked eye detectable color change from yellow to purple. This spectral change was due to strong ICT from deprotonated phenoxide moiety on alkaline medium. The pK_a value determined from fluorometric titration was 7.21. Moreover, enhancement in fluorescence intensity ratio (I_{692}/I_{574}) made the pH monitoring ratiometric and large stoke shifts helped to reach the NIR region (Figure 78).

Fluorescent probes based on isolongifolanone, which can be synthesized from natural turpentine, are rarely reported. In order to investigate the use of natural turpentine, Wang et al. synthesized two isolongifolanone-based pH probes, **111** and **112**, by incorporating N, N-dimethylaniline as an electron donating moiety and pyrazole (**111**), and pyrimidine (**112**) as electron withdrawing moieties for monitoring acidic pH in both solid and solution states.[163] On lowering pH from 7.0 to 1.0, the fluorescence spectra of probe **111** showed quenching of the peak at 373 nm and a new peak emerged at 445 nm with the dark blue color changed to bright blue. This ratiometric response (I_{445}/I_{373}) with a large stoke shift of 120 nm displayed a good linear relationship within pH 1.5–4.0 and the pK_a value was calculated to be 2.59. Under similar conditions, the emission peak at 434 nm of probe **112** exhibited gradual quenching with stoke shift of 134 nm and a good linear response was observed within pH

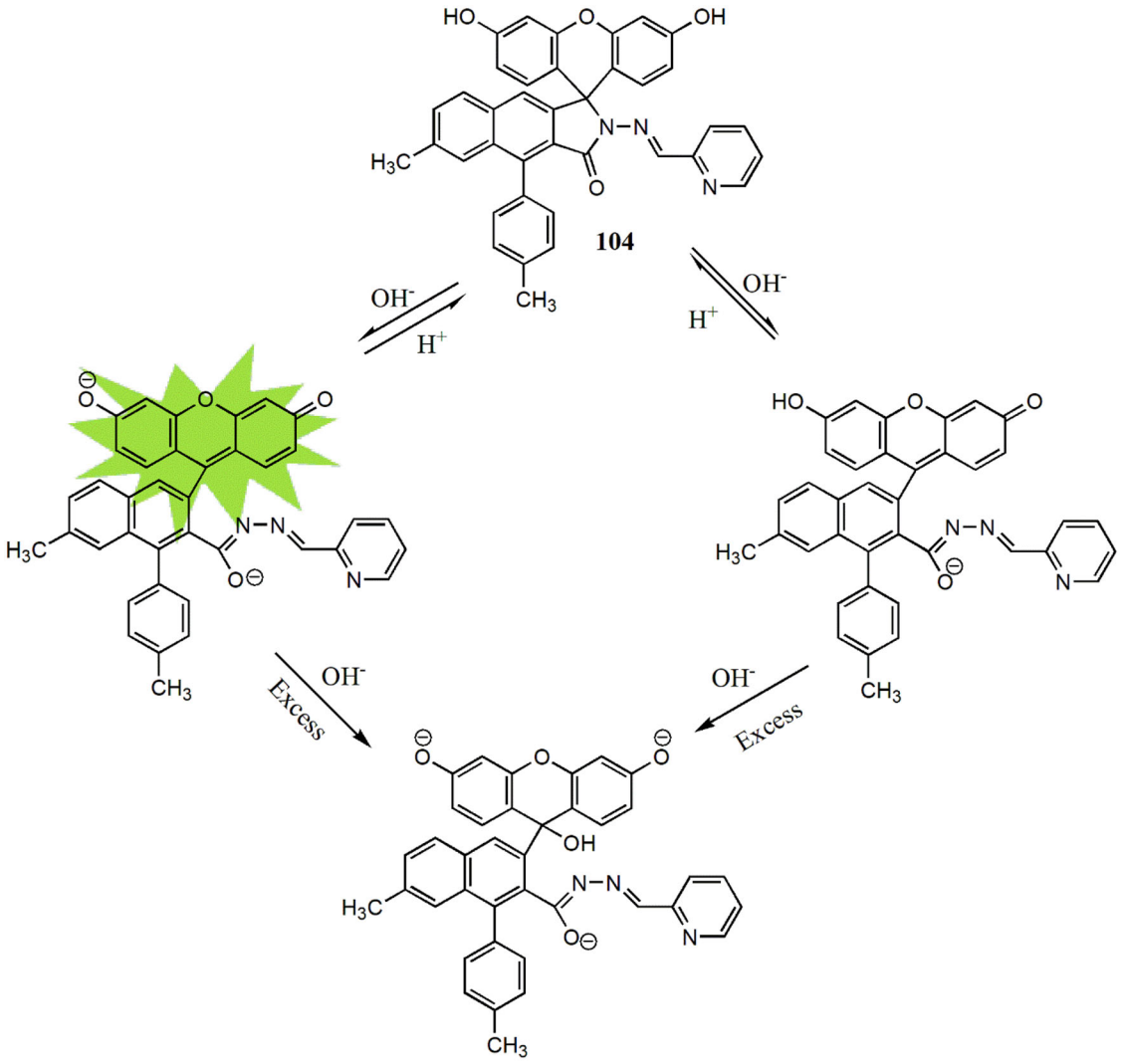

Figure 73. Chemical structure of pH probe **104** and its pH-dependent structural alterations.

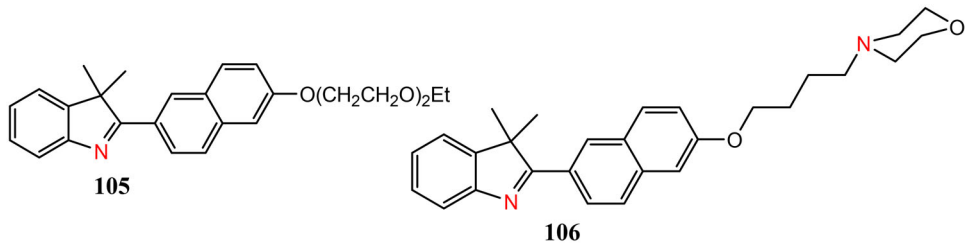

Figure 74. Chemical structure of two-photon fluorescent pH probes **105** and **106**.

3.5–7.0. The pK_a value of probe **112** was 3.69. Acid induced pyrazole "N" protonation caused ICT emission in probe **111** and protonation of pyrimidine "N" caused fluorescence quenching in probe **112**. With good reversibility, quick response time and selectivity over various transition metal ions, the probes were successfully applied to detect acidic environment fluorometrically in the presence of solid TsOH and gaseous TFA. Finally, these kinds of fluorescent probes should be more studied to explore natural resources vastly (Figure 79).

In 2018, Hwang *et al.* reported a phenanthrene derivative based probe **113** for monitoring basic pH as well as Zn^{2+} and Cu^{2+}.[164] On increasing pH in DMSO/buffer (3:2), phenolic-OH deprotonation of the probe caused quenching of blue emission at 475 nm after pH 9 with a pK_a value of 9.75. The probe also successfully detected Zn^{2+} and Cu^{2+} with LOD of 0.43 μM and 0.18 μM, respectively (Figure 80).

High sensitivity and rapid proton transfer in acid-base equilibrium are two essential criteria for pH probes. Keeping this in mind, Yuan *et al.* connected the pyridine moiety with N-heterocyclic Tröger's base by using Heck coupling to form a fluorescence turn-off pH probe **114** having a large stoke shift of 121 nm.[165] On increasing acidity, the probe's ICT induced blue emission at 460 nm gradually quenched in

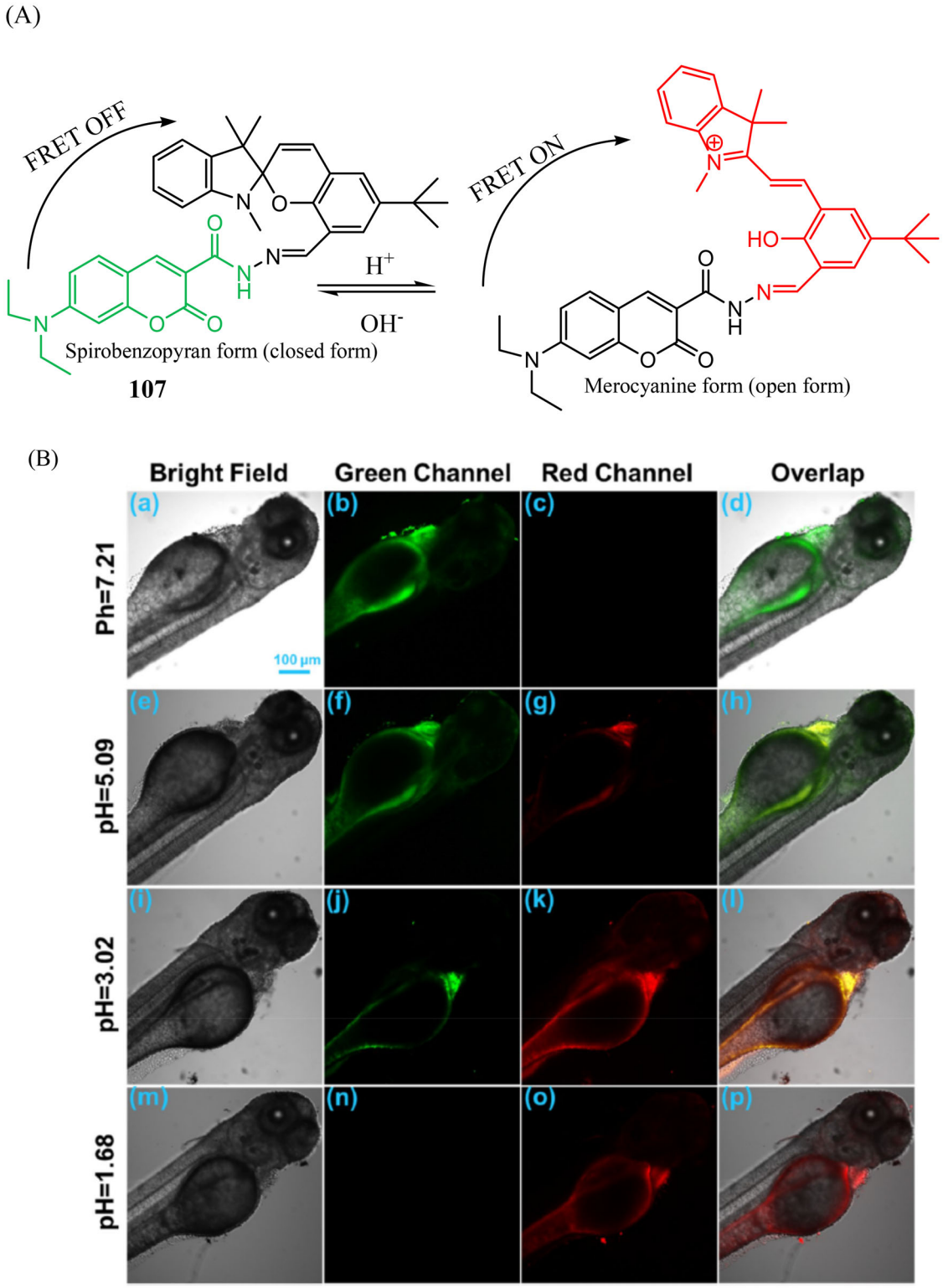

Figure 75. (A) Chemical structure of spiropyran-based fluorescent pH probe **107** and its pH-dependent structural alterations. (B) Confocal fluorescence imaging of zebrafish treated with probe **107** (5 μM) for 20 min at different pH. The wavelength of excitation was adjusted to 480 nm. Excitation wavelengths of 488 and 515 nm, as well as band-path emission filters of 500–600 nm and 600–700 nm, were used to capture the photos. Reprinted from Ref. [159] Copyright (2020), with permission from Elsevier.

the DMSO solution. Under similar conditions, a new absorption peak at 390 nm emerged with lowering of the peak at 340 nm having an isosbestic point at 356 nm and the color of the solution changed from colorless to yellow. This spectral change was due to protonation of pyridine "N" of the probe and it was confirmed by ^{1}H NMR and theoretical study. Furthermore, the probe exhibited good stability and selectivity toward pH over various metal ions (Figure 81).

Similarly, Li *et al.* synthesized two fluorescence turn-off pH probes **115** and **116** by linking indole derivatives with Tröger's base.[166] On lowering pH from 7.01 to 2.07 in

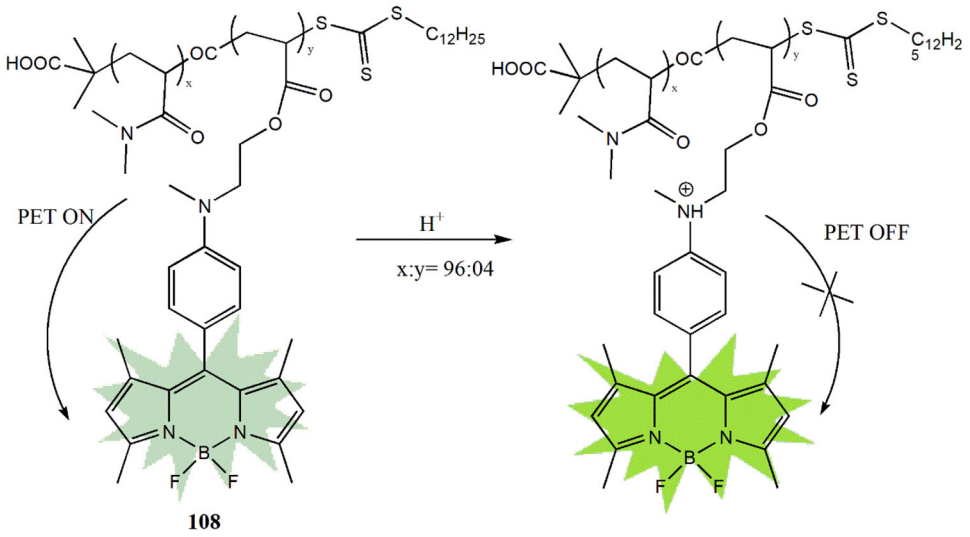

Figure 76. Chemical structure of BODIPY-based polymeric fluorescent pH probe **108** and its sensing mechanisms.

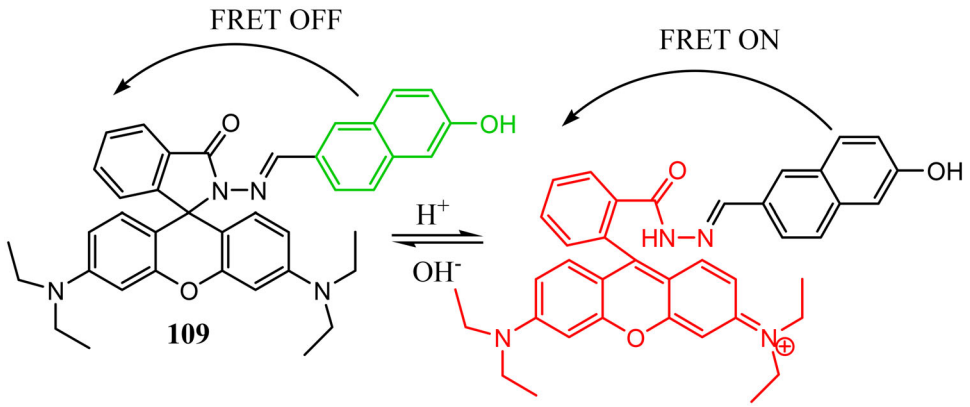

Figure 77. Chemical structure of rhodamine-based ratiometric fluorescent pH probe **109** and its pH-dependent structural alterations.

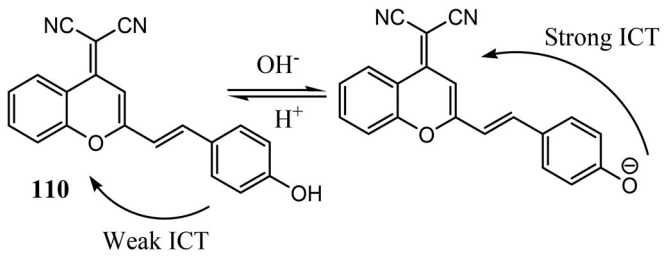

Figure 78. Chemical structure of ratiometric NIR fluorescent pH probe **110** and its pH-dependent structural alterations.

DMSO/H_2O (4/1, v/v), the probe **115** exhibited quenching of ICT based brilliant yellow fluorescence at 517 nm with a pK_a value of 2.94. In absorption spectra, the peak at 389 nm displayed a gradual decrease with the appearance of a new peak at 458 nm having an isosbestic point at 415 nm and the pale-yellow color of the probe's solution changed to saffron yellow. Similarly, on decreasing the pH from 7.01 to 1.96, the probe **116** showed quenching of ICT induced yellow-green emission at 503 nm with a pK_a value of 3.05 and the absorption peak at 370 nm gradually decreased with a new peak appeared at 430 nm having an isosbestic point at 397 nm. The colorless solution of probe **116** changed to yellow. ^{1}H NMR and theoretical study revealed that acid induced protonation of indole "N" was responsible for this spectral change. Moreover, the probe was found to be reversible, photostable and selective toward pH change (Figure 82).

Ye *et al.* synthesized a perylene based pH probe **117** by using a simple Schiff-base condensation reaction.[167] The probe exhibited gradual enhancement in fluorescence intensity at 555 nm on decreasing the pH from 4.0 to 2.6 in DMF/HEPES (v/v, 4/1) medium and showed a color change from colorless to yellow which made the probe a naked eye detector of pH. This was mainly due to the PET off mechanism on protonation of the imine N atom of the probe which was confirmed by ^{1}H NMR. The pK_a value was found to be 3.0, which made the probe responsive to an acidic environment. Moreover, the probe was found to have good reversibility, excellent photo-stability and no significant interference was observed by competitive ions (Figure 83).

In 2019, Georgeiv *et al.* synthesized a probe **118** by linking H^+ sensitive piperazine moiety with 4-amido-1, 8-

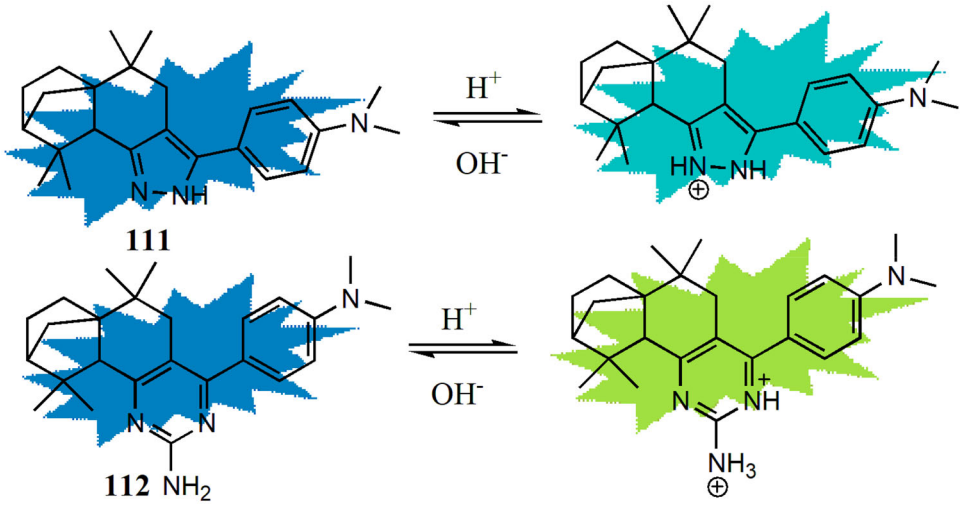

Figure 79. Chemical structures of isolongifolanone derivatives based fluorescent pH probes **111** and **112** and its pH-dependent structural alterations.

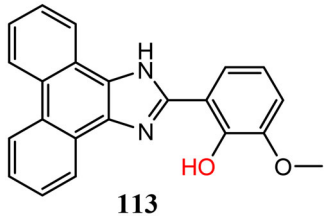

Figure 80. Chemical structure of phenanthre derivative based pH probe **113**.

naphthalimide for tracking pH change and water content through excimer-monomer emission in organic solvent.[168] When investigated in water/acetonitrile solution (1:1, v/v), absorption and emission intensity did not show any significant change on changing the pH from 12 to 9 but on further lowering of pH from 9 to 4 the piperazine "N" of the probe got protonated and caused repulsion induced destabilization of excimer complex which led to decrease of excimer emission at 560 nm accompanied with enhancement of monomer ICT emission at 460 nm. The pK_a value was found to be 6.76 ± 0.05. Again, when pH was changed from 4 to 2 the probe exhibited enhancement of monomer emission at 460 nm as protonation of both "N" of piperazine unit quenched the PET process and the pK_a value was calculated to be 2.88 ± 0.07. Furthermore, with good selectivity over various transition metal ions and anions, the probe was able to determine water content with limit of detection (LOD) of 1%. Moreover, this rarely reported excimer-monomer switching mechanism based fluorescent pH probes need to be studied more in near future (Figure 84).

For colourimetric and turn-off fluorometric monitoring of both Cu^{2+} and alkaline pH, a pyrrolinone esters hydrazone dye-based probe **119** was designed by Kamel's group in 2019.[169] On increasing pH, the absorption band at 484 nm gradually decreased and a new band started emerging at 572 nm after pH 7 with a color change from yellow to bluish. The emission intensity at 562 nm was also gradually lowered and completely quenched at pH 10 and the pK_a value calculated from emission titration was 8.58 ± 0.02. Tautomerization in the hydrazone unit with phenolic –OH deprotonation in alkali medium was the sensing mechanism of the probe. Interestingly, the probe loaded test strip was prepared for monitoring ammonia solution colourimetrically with good reversible nature. Furthermore, along with alkaline pH, the probe successfully detected Cu^{2+} ion with a detection limit of 0.63 μM (Figure 85).

To monitor wide range of pH change (1–13) in aqueous solution, a dansyl based pH probe **120** was reported by Wang *et al.* in 2019.[170] The probe exhibited weak blue fluorescence within the pH range of 1–4 due to protonation of dimethylamine group, strong yellow emission within the pH range 4–10 due to deprotonation of protonated dimethylamine group and carboxylic group as well as strong green emission within pH 11–13 due to deprotonation of sulfonamide group. In UV-Vis spectra, the probe exhibit a absorption band at 288 nm at pH 1.04 and 1.88 but it showed decrease at 288 nm with appearance of two new peak at 247 nm and 328 nm at > pH 4 up to 10.25 and after that a new peak appeared at 311 nm with disappearance of peaks at 247 nm and 328 nm. Negligible interference was observed when investigated in presence of other competitive ions and the probe also showed good reversibility (Figure 86).

Roy and coworkers synthesized a Schiff base pH probe **121** by using aminoquinoline moiety.[171] Alkali induced deprotonation of phenolic –OH caused enhancement of a new absorption peak at 435 nm with a decrease of peak at 335 nm which was finally shifted to 326 nm on increasing pH from 2.0 to 11.0. The peak at 530 nm in emission spectra also displayed enhancement with an increase in quantum yield from 0.0001 to 0.057 and the pK_a value was 7.12. A naked eye detectable color change from colorless to yellow and indigo to green were observed under visible light and UV-lamp respectively. The probe was found to be stable, selective and was successfully used to detect acidic lemon juice and alkaline river water (Figure 87 and Table 1).

Conclusion and perspective

In this review, we have discussed recent development (2018–2020) of fluorogenic chemosensors for pH detection

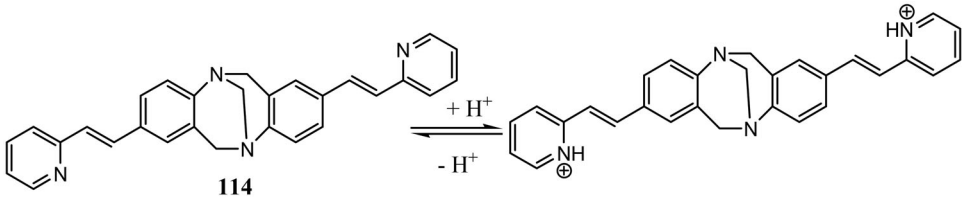

Figure 81. Chemical structure of Tröger's base derivative-based fluorescent "turn-off" pH probe **114** and its pH-dependent structural alterations.

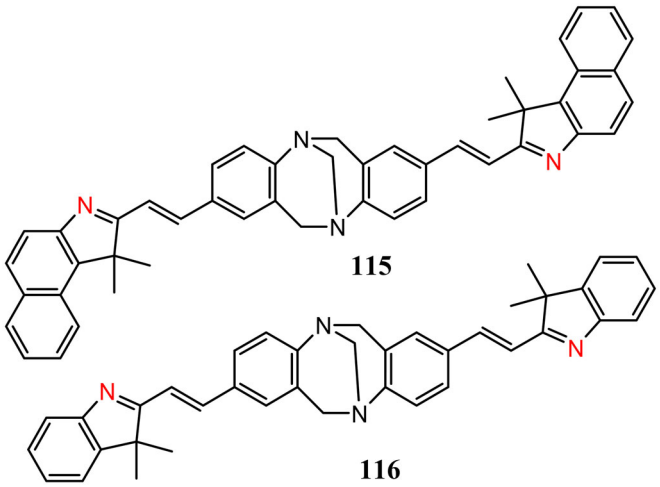

Figure 82. Chemical structures of Tröger's base derivative-based fluorescent pH probes **115** and **116**.

and monitoring. Herein, main focus was given to their designing strategies, sensing mechanisms and especially on their biological and environmental applications. We categorized these pH probes into seven types based on their applications such as 1) Accurate localization of cancer cells in the living body are essential for diagnosis and treatment of cancer. In recent years fluorogenic pH probes attract a great deal of attention to precisely locate cancer cells depending on their different pH from normal cells. Among chemosensors **1** to **6**, probe **2** showed ratiometric response and all other probes displayed turn-on responses toward pH in cancer cell discrimination process. To precise and accurate measurement of pH change in subcellular organelles researchers mainly focused on developing organelle targeted pH probes in recent times. 2) During the past decade lysosome-targetable pH sensors were the most studied pH probes and hold major attention due to their broad biological applications. Heat shock induced lysosomal pH change, various Drug (NAC, NH_4Cl, chloroquine, H_2O_2, N-ethylmaleimide, Baf-A1, dexamethasone and artesunate) induced lysosomal pH change, starvation induced autophagy, LPS induced inflammation, drug induced mitophagy condition, drug (L-buthioninesulfoximine, dexamethasone, cis-platinum) induced cell apoptosis, pH of cancerous tissues and cells, *in vivo* imaging and bacterial pH monitoring were studied by using lysosome specific pH probes. 3) Mitochondria specific pH probes are the most reported probes after lysosome among organelle targeted pH probes. These are applied in various cellular events like drug (NAC, H_2O_2, FCCP, lactate and pyruvate) induced mitochondrial pH change, Mitophagy induced by nutrient deprivation as well as sodium selenite, rapamycin and hypoxia, BSO induced cell apoptosis, urease activity in basic pathogen H. pylori, *in vivo* imaging in D. melanogaster first-instar larvae as well as in tumor mice. 4) Golgi and ER targeted pH probes were rarely reported and we discussed two Golgi probes (**79** and **80**) and three ER probes (**81**, **82** and **83**) in this review. Probe **79** showed turn-on response and probe **80** showed ratiometric response toward pH change with their various applications such as Monensin induced Golgi oxidative stress, bafilomycin A1 and NH_4Cl induced Golgi alkalization, LPS induced abdominal inflammation in mice, function of transmembrane protein 165 including *in vivo* imaging. 5) ER pH probes were mainly applied to track ER acidification under stress (induced by tunicamycin and thapsigargin) and *in vivo* imaging in Zebrafish and mice where probes **81**and **82** exhibited turn-on response and probe **83** exhibited ratiometric response toward pH change. 6) In the next section, we discussed various pH probes used in non-specific intracellular pH monitoring including pH change in tissues, bacteria and Zebrafish. Among these probes, probe **94** was used to monitor alkalization of chronic wounds in diabetic mice, probe **90** was used in *in vivo* imaging of gastric pH in mice tissues and probe **91** was utilized in intracellular pH determination during UV-light induced programmed cell death. 7) pH probes which were only applied in environmental applications like to check the pH of alkaline river water, detect acid-base solution and vapors by using test strips are discussed in this section. Although these probes do not possess wide applications but we introduce it to explore the scope of their designing strategies and sensing mechanisms.

Almost all of these reported pH probes determine pH by acid-base neutralization process (protonation-deprotonation) of phenolic –OH and amine containing groups with various sensing mechanisms like ICT, PET, TBET, FRET, AIE, ESIPT, RIR, PARCT and excimer-monomer complex. A wide range of fluorophores like tetraphenylethene (TPE), coumarin, naphthalimide, cyanine- and hemicyanine, boron dipyrromethene (BODIPY), rhodamine, fluorescein, spiropyran were used to design main framework of these probes.

To achieve more precise sensing of pH a good probe must contain following properties and these are the main challenges for researchers- 1) Development of NIR probe as well as implementation of two-photon fluorescence microscopy (TPM) enables deep tissue penetration strength with

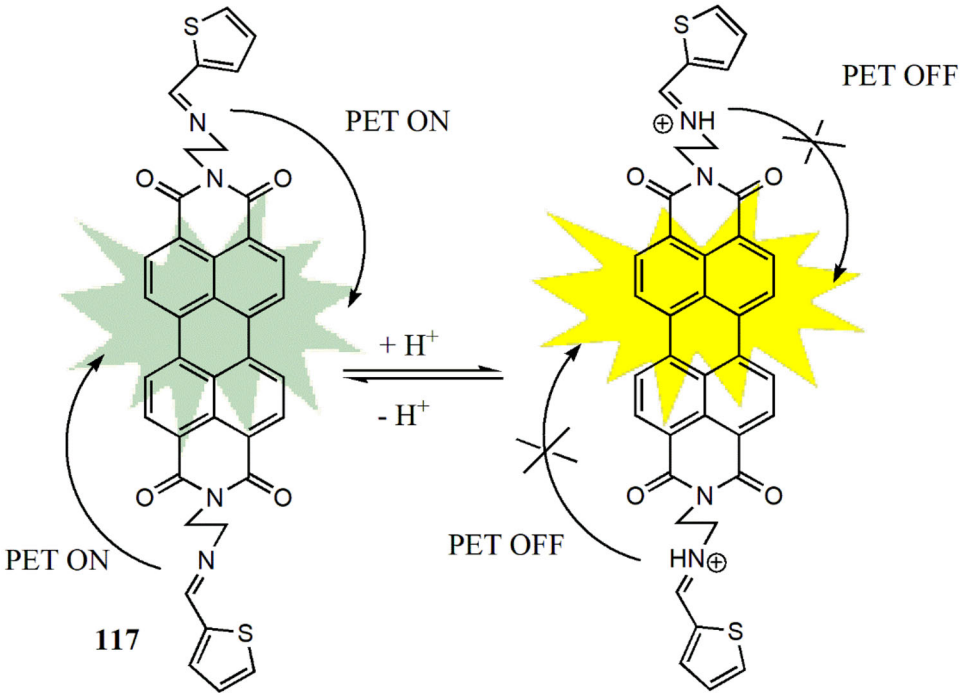

Figure 83. Chemical structure of perylene-based fluorescent pH probes **117** and its sensing mechanisms.

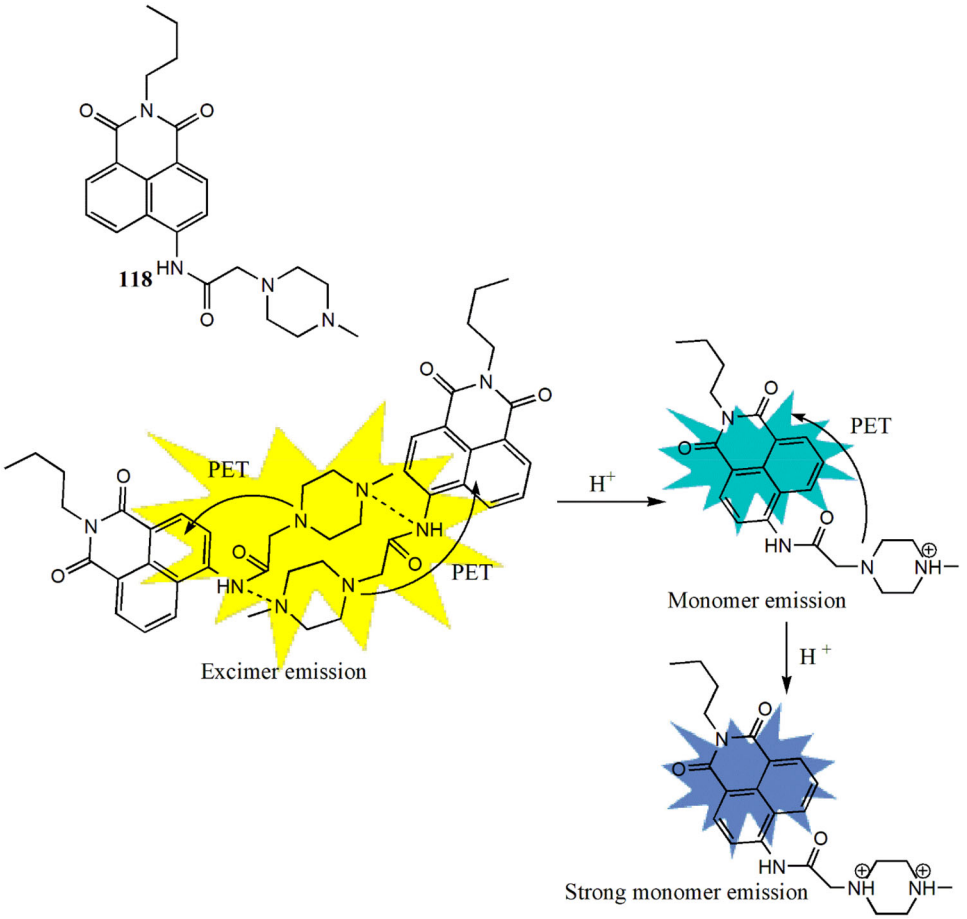

Figure 84. Chemical structure of 4-amido-1,8-naphthalimide-based ratiometric fluorescent pH probe **118** and its sensing mechanisms.

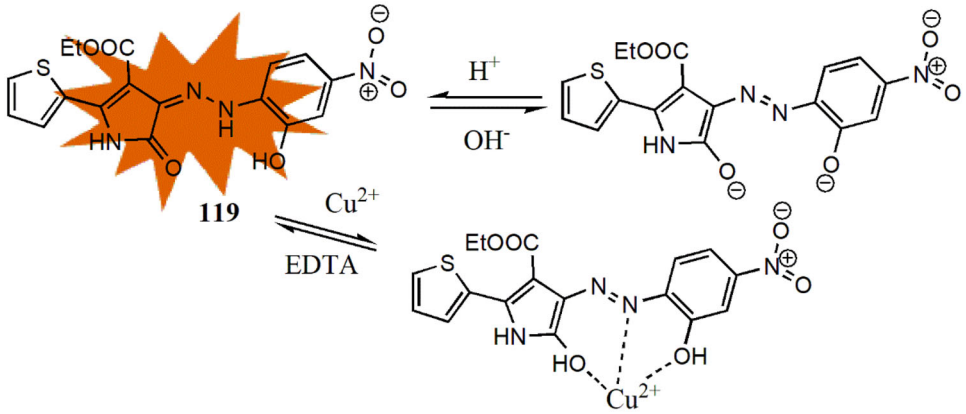

Figure 85. Chemical structure of pyrrolinone ester hydrazone dye derivative-based probe **119** and its sensing mechanisms.

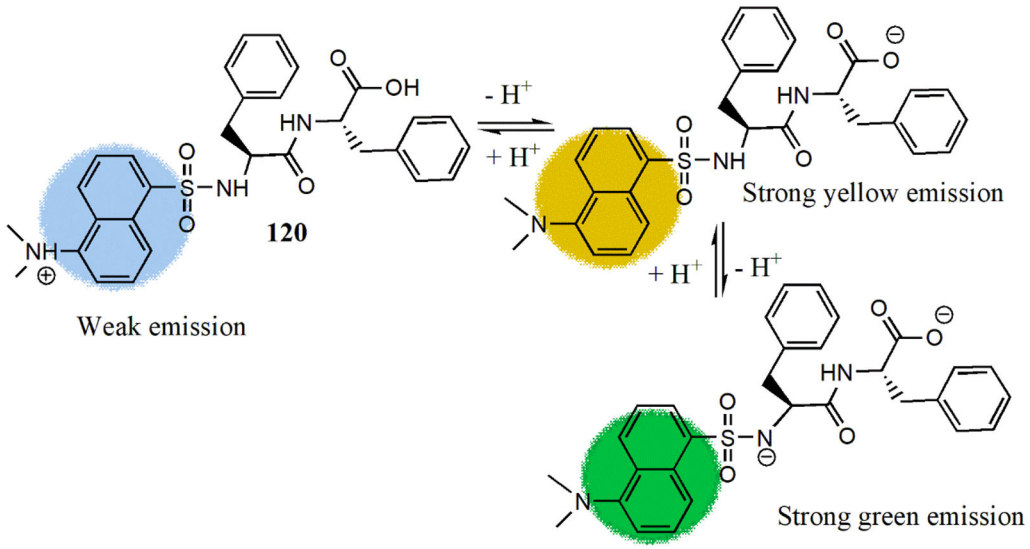

Figure 86. Chemical structure of pH probe **120** and its pH-dependent structural alterations.

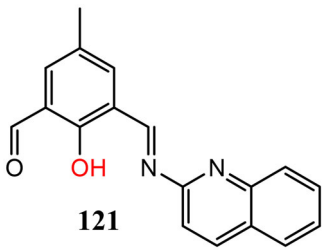

Figure 87. Chemical structure quinoline derivative based fluorescent pH probe **121**.

low photo damage of the sample, least interference from background auto-fluorescence and high spatial resolution. 2) Ratiometric fluorescent probes permit the measurement of emission intensities at two distinct wavelengths and eliminate environmental factors, fluctuation of probe concentration and instrumental errors. 3) Probes with large stoke shifts are also desirable as they reduce excitation interference as well as are able to overcome auto-fluorescence of bio-samples. 4) Moreover, probes should be fully biocompatible for biological applications, i.e., probes should have good water solubility, photostability and cell permeability with low cytotoxicity. 5) In spite of higher sensitivity toward pH, some reported probes suffer from interference from other analytes. Therefore, research and development on interference free fluorescent probes is still of great interest. 6) In addition, some probes show "turn-off" fluorescence response toward pH monitoring. However, "turn-on" probes will be more effective for accurate determination of pH in environmental and biological applications. It will be another significant direction of research. 7) In order to design organelle targeted pH probes, it is necessary to keep the pK_a value within the pH range of the target organelle so that it helps to monitor pH change of that organelle accurately. 8) It is essential to focus on continuous development of Golgi and ER pH probes as they are rarely reported till now. 9) In recent years, AIE (Aggregation induced emission) and AIEE (Aggregation-induced emission enhance) are two emerging

Table 1. Overview and comparison of the photophysical characteristics of pH chemosensors (**1**–**121**).

Probe	Medium	Linear response	Probe type/ Sensing mechanism	λ_{Ex}(nm)	λ_{Em}(nm)	Response time	pK_a	Application	Two photon fluorescence imaging	Reference
1	DMSO buffer solution	2.40-4.00	Turn-on or off/-	354	475	–	3.22	Cancer cell discrimination	yes	[41]
2	PBS-CH_3CN (10: 1)	7.0-8.0	Ratiometric/ICT	550	572 to 623	–	7.45	Cancer cell discrimination & intracellular pH monitoring	no	[42]
3	Britton–Robinson buffer	–	Turn-on or off/PET	400	460	–	5.7	Cancer cell discrimination	no	[43]
4	In SDS (5 mM) at different pH	5.0-7.4	Turn-on or off/-	720	780	$<$ 3 min.	6.14	Discriminating cancerous cell, tissue & living animal	no	[44]
5 & 6	Britton–Robinson buffer	–	Turn-on or off/-	378(**5**) 430(**6**)	530	–	7.15(**5**) and 6.57(**6**)	Cancer cell discrimination	no	[45]
7	H_2O/DMSO (4/1, v/v)	5.0-3.82	Ratiometric/ICT	360	454 to 514	–	4.46	Intracellular pH monitoring in HeLa cell and liver tissues of cancerous mouse, tracking of lysosomal pH change induced by NH_4Cl, H_2O_2 and NAC.	yes	[57]
8 & 9	10 mM citrate buffer containing 40% EtOH	–	Ratiometric/-	680 nm	528 to 755(**8**) 515 to 740(**9**)	–	4.2 (**8**) 4.8 (**9**)	Intracellular pH monitoring in living HeLa cell	no	[58]
10,11 & 12	10 mM citrate buffer containing 30% ethanol	–	Ratiometric/ TBET	420(10) 390(11 &12)	510 to 737(**10**) 505 to 754(**11**) 540 to 747(**12**)	–	–	Intracellular pH monitoring in living HeLa cell	no	[59]
13	Britton-Robinson (BR) buffers containing 1 % MeCN	4.2-6.0	Turn-on or off/-	550	588	–	4.10	Chloroquine, dexamethasone and artesunate induced lysosomal pH change.	no	[60]
14	Different pH in solutions containing 0.1% DMSO as co-solvent	–	Ratiometric/-	473	522 to 557	–	5.96	Lysosomal pH increase during heat stroke	no	[61]
15	Buffer containing 10% ethanol	–	Turn-on or off/-	550	655	–	5.4	1) H_2O_2 , N-ethylmaleimide, NH_4Cl and chloroquine induced lysosomal pH change 2) Intracellular pH monitoring	no	[62]
16 & 17	THF/H_2O (1:1. v/v)	–	Ratiometric/ICT	470(**16**) 480(**17**)	665 to 515 (**16**) 730 to 520 (**17**)	–	2.0(**16**) 3.3 and 1.5(**17**)	Intracellular pH monitoring in A549 cells.	no	[63]

(*continued*)

Table 1. Continued.

Probe	Medium	Linear response	Probe type/ Sensing mechanism	λ_{Ex}(nm)	λ_{Em}(nm)	Response time	pK_a	Application	Two photon fluorescence imaging	Reference
18	B-R buffer (5% EtOH)	–	Turn-on or off/PET	450	531	–	–	Chloroquine induced lysosomal pH change	yes	[64]
19 & 20	Citrate-phosphate buffers with 1% ethanol	–	Turn-on or off/-	645(**19**) 640(**20**) 800(**19,20**)	699(**19,20**) 693(**19,20**)	–	4.80(**19**) and 4.40(**20**)	Lysosomal pH monitoring in living cells (HeLa cell, KB cells, HUVEC-C and MDA-MB231 breast cancer cells)	no	[65]
21 & 22	pH buffers containing 1% DMSO	–	Turn-on or off/-	550(21) 450(22)	623 (**21**) 616 & 743 (**22**)	–	5.15(**21**) 4.0 & 7.4(**22**)	Intracellular pH monitoring in living HeLa cell	no	[66]
23,24 & 25	10 mM citrate buffers containing 30% acetonitrile	–	Ratiometric/ TBET & FRET	405	497 to 630(**23**) 489 to 642(**24**) 481 to 641(**25**)	–	4.4(**23**),4.6(**24**) and 4.8(**25**)	Monitoring Intracellular pH in living HeLa cell and chloroquine induced lysosomal pH change	no	[67]
26	Britton–Robinson buffers (10 μM, 30% DMSO, v/v)	4.2 to 5.6	Ratiometric/ICT	370	410 to 475	–	4.86	Monitoring of intracellular pH and starvation induced autophagy in MCF-7 cells	yes	[68]
27,28,29 & 30	Phosphate buffer solution	–	Ratiometric/-	375(**27, 28**) 405(**29,30**)	460 to 662 (**28**) -/660(**27**) -/692(**29**) -/693(**30**)	–	5.40(**27**), 5.35(**28**), 5.42(**29**),5.26(**30**)	Monitoring intracellular pH change, chloroquine and heat shock induced pH change	no	[69]
31	PBS buffer (1% DMSO)	3.29-6.24	Turn-on or off/-	635	730	–	5.03	Monitoring intracellular pH change, chloroquine induced lysosomal pH change, *in vivo* imaging in living mice.	no	[70]
32,33,34	10mM citrate buffers with 10% ethanol	–	Ratiometric/ TBET & FRET	470(**32 & 33**) 550(**34**)	518 to 633(**32**) 512 to 639(**33**) 595 to 755(**34**)	–	3.4(**32**) 3.96(**33**) 3.3(**34**)	1) Intracellular pH monitoring in living HeLa cell 2) Lysosomal pH change induced by NAC, NH_4Cl, chloroquine and H_2O_2	no	[71]
35 & 36	H_2O/EtOH (4/1, v/v)	4.67-3.33 (**36**)	Ratiometric/ICT	420(**36**)	520 to 608(**36**)	–	4.26(**36**) 4.51(**35**)	1) Intracellular pH monitoring in living HepG2 cells. 2) Lysosomal pH change induced by NAC and H_2O_2	no	[72]
37,38 & 39	DMSO/water (1/5, v/v)	2.5-4.1 (**37 & 39**)	Ratiometric/ICT	402(37), 413(38) and 429(39)	500 to 580(**37**) 511 to 600(**38**)	–	3.3(**37**) 2.1(**38**) and 3.1(**39**)	Intracellular pH monitoring in living HeLa cells and acidic	no	[73]

					560 to 650(**39**)			pH monitoring in *E. coli* bacteria.		
40	DMSO/H_2O (1/1, v/v)	3.9-5.3	Ratiometric/ICT	415	530 to 637	–	4.60	Intracellular pH monitoring in living B16-F10 cells and *in vivo* imaging in living mice.	no	[74]
41	PBS buffer (10 mM)	–	Ratiometric/ FRET	400	510 to 595	–	–	Monitoring of chloroquine induced lysosomal pH change.	yes	[75]
42,43 & 44	0.1 M Citrate-phosphate Buffer (pH 2.0–7.0) and phosphate buffer (pH 7.0–10.8) containing 1% ethanol	–	Turn-on or off/-	530(**42**), 560(**43**), and 660(**44**)	580(**42**), 644(**43**) and 744(**44**)	–	5.81(**42**), 5.45(**43**) and 6.97(**44**)	Intracellular pH imaging in MDA-MB231 and HUVEC-C cells	no	[76]
45	PBS buffer	–	Ratiometric/-	405 500	455 588	–	3.5 and 6.2	Monitoring of Intracellular pH, starvation induced autophagy, NH_4Cl and chloroquine induced autophagy inhibition	no	[77]
46	–	–	Turn-on or off/-	635	675	–	4.63	1) lysosomal pH monitoring in HeLa cells and A549 cells 2) dexamethasone induced apoptosis, chloroquine and heat stroke induced lysosomal pH change	no	[78]
47	–	–	Ratiometric/ FRET	480 nm	582 to 518	–	7.1	Monitoring lysosomal pH during LPS induced inflammation in macrophages.	no	[79]
48,49	PBS solution containing 1% DMSO	–	Turn-on or off/PET	345(48) 370 and 440(49)	424(48) 467,543 and 553(49)	–	6.67(48) 6.67 and 5.83(49)	Chloroquine induced lysosomal pH change, pH change during sucrose induced lysosomal storage disorder and rotenone induced cell apoptosis.	no	[80]
50	B-R buffer (5% (v/v) ethanol as co-solvent).	–	Turn-on or off/-	650	705	–	4.24	Heat shock induced lysosomal pH increase	no	[81]
51	Water/EtOH (*v/v* = 1:9)	3.41-4.82	Ratiometric/ICT	421	534 to 622	–	4.25	1)Intracellular pH monitoring in living HeLa cell 2)Monitoring of H_2O_2, glucose and NH_4Cl	no	[82]

(*continued*)

Table 1. Continued.

Probe	Medium	Linear response	Probe type/ Sensing mechanism	λ_{Ex}(nm)	λ_{Em}(nm)	Response time	pK_a	Application	Two photon fluorescence imaging	Reference
								induced pH change		
52	PBS buffer solutions (10 % DMSO)	5.0-7.3	Turn-on or off/PET	400	535	–	6.24 ± 0.02	1) L-buthioninesulfoximine (BSO) and cis-platinum (Cis) induced cell apoptosis, sodium selenite (SS) induced mitophagy and heat shock induced lysosome alkalization 2) *in vivo* imaging of abdominal tissues of mice	yes	[83]
53	Water/ethanol (1/1, v/v)	4.4-6.2	Ratiometric/ICT	393	517/555	–	4.98	1) Intracellular pH monitoring in living HeLa cell 2) monitoring of NAC and H_2O_2 induced pH fluctuation	no	[84]
54	B-R buffer solution (40 mM) containing 2.5 % DMSO	4.50-5.70	Turn-on or off/-	560	583	–	4.96	Intracellular pH variation and starvation induced autophagy	no	[85]
55	PBS buffer	5.4-7.5 and 3.3–4.5	Ratiometric/ FRET	370	660 to 435	–	6.46 and 3.92	Monitoring of intracellular pH in living A549 cells	no	[86]
56,57,58 & 59	BR buffer with 10% DMAC	4.4-5.6	Turn-on or off/-	453(**56**) 441(**57**) 475(**58**) 402(**59**)	590(**56**) 590(**57**) 610(**58**) 552 to 590(**59**)	–	5.5(**56**)5.3(**57**)5.1(**58**) and 4.5(**59**)	1)Monitoring Baf-A1 and chloroquine induced lysosomal pH increase 2) Intracellular pH variation in MCF-7 cells	no	[87]
60	BR buffer solution (with 10% DMAC)	4.5-5.2	Turn-on or off/ICT	465	614	–	5.0	Monitoring Intracellular pH variation and starvation induced autophagy	no	[88]
61	B-R buffer	5.0-6.0	Turn-on or off/-	574	590	–	5.42	1) Intracellular pH monitoring in living HeLa cell 2) Heat shock induced lysosomal pH increase, rapamycin induced mitophagy and dexamethasone induced apoptosis monitoring	no	[89]
62		6.86-8.07		–	551 to 484	–	7.3 & 8.6		no	[104]

	water/ethanol (f_w = 99%, v/v)		Ratiometric/ AIE,ESIPT, RIR					Intracellular pH change in living HeLa cells and detection of acid and basic vapors through probe loaded test papers		
63	PBS-buffer (1.0% DMSO)	–	Turn-on or off/-	353 410	457	–	6.58 ± 0.02(at λ_{abs} 353 nm) and 6.53 ± 0.02(at λ_{abs} 410 nm)	Monitoring of NAC and nutrient starvation induced cell acidification as well as H_2O_2 induced alkalization.	yes	[105]
64 & 65	BR buffer solution (40 mM)	5.2-6.2(**64**) 5.0-6.0(**65**)	Turn on or off/-	450	520	<1 min	5.84(64) & 5.56(65)	Monitoring of lactate and pyruvate induced mitochondrial acidification	no	[106]
66	10 mM SDS (1% DMSO in PBS)	–	Ratiometric/-	710	–	–	–	Autophagy lysosome detection and fluorescence imaging of tumor in tumor containing mice model.	no	[107]
67	disodium hydrogen phosphate-citric acid buffers containing 1% DMSO	–	Ratiometric/-	452	530 to 557	–	7.25	Monitoring of nutrient deprivation-induced mitophagy	no	[108]
68	10mM PBS buffer solution containing 1% DMSO, 150 mM NaCl (ph =1.0-13.0)	–	Turn- on or off/ESIPT	388	–	–	8.03	Monitor urease activity both in presence and absence of urea in basic pathogen H. pylori	no	[109]
69	PBS buffer (containing SDS and CTAB)	7.10-8.46 in SDS & 5.65-8.46 in CTAB	Ratiometric/-	635 & 488	720 to 507 (in SDS) 720 to 503 (in CTAB)	–	–	Monitoring mitochondrial pH change in living HeLa cell and mitochondrial acidification induced by FCCP, NAC and H_2O_2	no	[110]
70	PBS buffer	7.0-4.50	Turn-on or off/-	–	590	–	4.82	Monitoring intracellular pH change in HeLa cell and target tumor cell in mice	yes	[111]
71	–	6.0-7.8	Ratiometric/-	480	552 to 584	–	6.87	Mitochondrial pH change in living SMMC-7721 cells, sodium selenite-induced mitophagy, BSO induced cell apoptosis and test strip experiment.	no	[112]

(*continued*)

Table 1. Continued.

Probe	Medium	Linear response	Probe type/ Sensing mechanism	λ_{Ex}(nm)	λ_{Em}(nm)	Response time	pK_a	Application	Two photon fluorescence imaging	Reference
72	BR buffer solutions	3.36-4.98 & 6.51-8.24	Turn-on or off /ICT	390 (pH 2-6) & 420 (pH 6-9)	480	–	4.20(pH 2-6) & 7.20(pH 6-9)	Monitoring mitochondrial pH change and nutrient deprivation-induced mitochondrial acidification	yes	[113]
73	phosphate buffer (20 mM)	4.6-6.6	Ratiometric/-	635	678 to 714	–	5.77	Monitoring of rapamycin and hypoxia induced mitophagy	no	[114]
74 & 75	Buffers containing 30% ethanol	–	Ratiometric/-	480	558 to 688 (**74**) 558 to 698 (**75**)	–	8.26(**74**)and 7.10 (**75**)	Intracellular pH change, *in vivo* imaging of pH in D. melanogaster first-instar larvae, FCCP induced mitochondrial acidification, nutrient starvation and rapamycin induced mitophagy	no	[115]
76	PBS buffer containing 1% DMSO	–	-/ICT	640	670	–	3.9	rapamycin and EBS induced autophagy in MCF-7 cells	no	[116]
77 & 78	Buffer with 10% ethanol	–	Ratiometric/ TBET	520	588 to 740(**77**) & 582 to 752(**78**)	–	3.92(**77**) and 3.67(**78**)	FCCP induced mitochondrial acidification, intracellular pH change in living HeLa cell, nutrient starvation induced mitophagy and rapamycin induced mitophagy, *in vivo* imaging of pH change in *D. melanogaster* first-instar larvae.	no	[117]
79	B–R buffer solution (40 mM)	3.80-5.40	Turn-on or off/-	570	600	–	4.32	bafilomycin A1 and NH_4Cl induced Golgi alkalization, oxidative stress induced Golgi pH change, *in vivo* imaging of LPS induced acidification of tissues in mouse.	no	[128]
80	Phosphate-buffered saline (0.1 M) with DMSO (v/v = 150:1)	5.9-7.7	Ratiometric/-	675	810 to 750	–	6.74 ± 0.02	Monensin induced Golgi oxidative stress, LPS induced abdominal inflammation in mice, monitor pH of tumor tissue in melanoma containing mice,	no	[129]

								function of transmembrane protein 165.		
81	PBS buffer(20 mM, containing 10% DMSO)	4.0-5.0	Turn-on or off/PET	400	528	–	4.58	Tunicamycin and thapsigargin induced ER acidification under stress, *in vivo* imaging of pH variation in zebrafish and abdominal tissues of living mice.	yes	[139]
82	PBS buffer (20 mM, 10% MeOH)	5.5-8.0	Turn-on or off/PET	400	531	–	–	Tunicamycin induced ER stress, pH change in living tissue and zebrafish	yes	[140]
83	B-R buffers (5% EtOH).	5.03-7.26	Ratiometric/ ICT-PET-FRET	405	527 to 446	–	–	Quantitative measurement of pH change in dexamethasone treated living HeLa cell, pH change during Hcy and tunicamycin induced ER stress	no	[141]
84	Buffer containing 30% ethanol	–	Turn on or off/ AIE &TBET	350 & 720	–	–	–	Oxidative stress induced intracellular pH variation	no	[142]
85	PBS buffer / DMSO (v/v = 1:9)	6.8-8.5	ratiometric/ICT	350	528 to 484	–	7.32	Intracellular pH change in living HeLa cell.	no	[143]
86	Britton-Robinson buffer solutions (1% EtOH)	2-7 and 8-12	Turn-on or off/ICT	470 & 500	590 & 558	–	–	Intracellular pH change in living HepG2 cells	no	[144]
87	DMSO/water (1/4 v/v)	2.43-3.71	Turn-on or off/-	370	515	–	2.98	Intracellular pH change in living A549 cell and strong acidic environment in *E. coli* bacteria.	no	[145]
88	Aqueous solutions	–	Turn-on or off/PET	–	550	–	6.35 ± 0.02	–	no	[146]
89	Na_2HPO_4-citrate buffer	6.35-8.00	Ratiometric/ PARCT	405	588 to 531	Within 10 sec	7.18	Intracellular pH change in NIH 3T3 cells	no	[147]
90	–	–	Ratiometric/ICT	808	1065 to 980	–	0.29 and 3.81	*In vivo* imaging of gastric pH in mice	no	[148]
91	PBS buffer solutions	7.53–8.46 7.32–3.87	Ratiometric/ICT	487	595 to 563 595 to 664	–	–	Intracellular pH change induced by UV-light during programmed cell death.	no	[149]
92 & 93	PBS buffers (5% MeOH)	6.5-8.5	Ratiometric/ ESIPT	405	546 to 473 (**92**) 539 to 473 (**93**)	–	–	NH_4Cl induced intracellular pH change and pH change in tissues.	no	[150]
94	Citrate-phosphate buffer and carbonate-bicarbonate	–	Turn-on or off/-	715	–	–	8.01	Monitoring gradual alkalization of chronic wounds in diabetes-	no	[151]

(*continued*)

Table 1. Continued.

Probe	Medium	Linear response	Probe type/ Sensing mechanism	λ_{Ex}(nm)	λ_{Em}(nm)	Response time	pK_a	Application	Two photon fluorescence imaging	Reference
	buffer containing 10 % DMSO							impaired mouse model		
95,96 & 97	Ethanol-water (3/7, V/V)	2.76-4.01(**95**) 3.65-4.70(**96**) 4.59-6.45(**97**)	Turn-on or off/ICT	680	805	–	3.45(**95**), 4.05(**96**), 5.52(**97**).	Intracellular pH variation in SCC-7 cells	no	[152]
98	–	9.50-7.00	Ratiometric/ICT	349	526 to 456	–	7.91 ± 0.03	Intracellular pH variation, NH_4Cl induced pH increase and H_2O_2 induced pH decrease in HeLa cells	no	[153]
99,100 & 101	DMSO: PBS = 1: 9, v/v	–	Turn on or off , ratiometric/ ESIPT	–	640(**99**) 520 to 640(**100**) 525 to 675(**101**)	–	6.57(**99**), 4.90(**100**), and 3.95(**101**)	Intracellular pH monitoring in living HeLa cell	no	[154]
102	Water/EtOH solution (v/v, 1:1, HEPES 0.01 M)	6.24-8.56	Turn-on or off/PET	310	420	–	6.89	Intracellular pH monitoring in living HeLa cell	no	[155]
103	0.01 mol/L PBS buffer (PBS/ CH_3CN 6: 1, v/v)	3.0-5.5	Turn-on or off/PET	478	520	< 10 sec	3.63	Paper strip experiment and intracellular acidic pH variation in T24 cells	no	[156]
104	B-R buffer (0.004 M)	–	Turn-on or off/-	485	529	–	8.72 and 10.73	detection of living *E. coli* bacteria	no	[157]
105 & 106	HCl aqueous solution	2.50-4.50	Turn-on or off/ICT	402(**105**) 401(**106**)	500	–	3.61(**105**) and 3.65(**106**)	Intracellular pH variation in MEF cells	yes	[158]
107	PBS buffer (1% EtOH)	4.0-6.0	Ratiometric/ FRET	420	525 to 629	–	4.87	Imaging pH change in living cell, bacteria and Zebrafish.	no	[159]
108	Aqueous solution	–	Turn-on or off/PET	485	512	Within 10 sec. (vapor phase)	3.48	1)Acidic pH imaging in cancer cell and bacteria 2) used in paper strip for vapor (acid &ammonia) detection	no	[160]
109	BR buffer solution containing 1% DMSO (v/v)	3.8-6.4	Ratiometric/ FRET	430	526 to 592	–	5.05	pH change in living hPDLCs cells, *P. aeruginosa* bacteria and in zebrafish.	no	[161]
110	C_2H_5OH–H_2O (6:4, v/v)	–	Ratiometric/ICT	483	574 to 692	–	7.21	–	no	[162]
111 & 112	EtOH/H_2O(v/v = 8/2) & DMF/H_2O (v/v = 8/2)	1.5-4.0 (**111**) 3.5-7.0 (**112**)	Ratiometric/ICT	325(111) 300(112)	373 to 445(**111**) 434(**112**)	–	2.59 (**111**) 3.69 (**112**)	Acidic pH determination in presence of solid TsOH and gaseous TFA.	no	[163]

113	DMSO/buffer (3:2)	–	Turn off /-	330	475	–	9.75	–	no	[164]
114	DMSO	–	Turn-on or off/ICT	340	460	–	–	–	no	[165]
115 & 116	DMSO/H_2O (4/1, v/v)	2.50-4.00	Turn off/ICT	370	517(**115**) 503(**116**)	–	2.94(**115**) 3.05(**116**)	–	no	[166]
117	DMF/HEPES (v/v, 4/1)	–	Turn-on or off/PET	500	555	–	3.00	–	no	[167]
118	water/acetonitrile solution (1:1, v/v)	–	Ratiometric/ PET and excimer-monomer	360	560 to 460 (pH 12-4) 460 (pH 4 to 2)	–	6.76 ± 0.05(within pH 9-4) 2.88 ± 0.07(within pH 4-2)	–	no	[168]
119	R–B buffer	–	Turn off/-	–	562	–	8.58 ± 0.02	test strip experiment for monitoring ammonia solution colourimetrically	no	[169]
120	Aqueous solution	–	Ratiometric/-	337	436(<pH 4) 550(5< pH< 10) 517(pH > 11)	–	–	–	no	[170]
121	Britton Robinson buffer	–	Turn on or off/-	435	530	–	7.12	Detection of acidic lemon juice and alkaline river water	no	[171]

research topics in the field of chemosensors. So, molecules with AIE and AIEE effects should be designed and studied in the near future. Although many of the discussed probes fulfill some of the above qualities, it still requires more effort to overcome these challenges.

Overall, we believe that this review will encourage researchers to explore novel fluorescent pH probes along with innovative applications.

Acknowledgements

DB and AM are grateful to the CSIR, New Delhi, India [File No.: 08/003(0143)/2020-EMR-I and 08/ 003(0139)/2019-EMR-I for DB and AM, respectively] for providing a fellowship.

Conflicts of interest

The authors declare no conflict of interest for this manuscript.

ORCID

Dipanjan Banik http://orcid.org/0000-0002-7654-4456
Saikat Kumar Manna http://orcid.org/0000-0001-6059-5083
Anwesha Maiti http://orcid.org/0000-0003-3159-9792
Ajit Kumar Mahapatra http://orcid.org/0000-0002-7197-0579

References

[1] Ma, J.; Li, W.; Li, J.; Shi, R.; Yin, G.; Wang, R. A Small Molecular pH-Dependent Fluorescent Probe for Cancer Cell Imaging in Living Cell. *Talanta* **2018**, *182*, 464–469. DOI: 10.1016/j.talanta.2018.01.088.

[2] Lagadic-Gossmann, D.; Huc, L.; Lecureur, V. Alterations of Intracellular pH Homeostasis in Apoptosis: Origins and Roles. *Cell Death Differ.* **2004**, *11*, 953–961. DOI: 10.1038/sj.cdd.4401466.

[3] Barott, K. L.; Barron, M. E.; Tresguerres, M. Identification of a Molecular pH Sensor in Coral. *Proc. R Soc. B.* **2017**, *284*, 20171769. DOI: 10.1098/rspb.2017.1769.

[4] Nogueira, L.; Shiah, A. A.; Gandra, P. G.; Hogan, M. C. Ca^{2+}-Pumping Impairment during Repetitive Fatiguing Contractions in Single Myofibers: Role of Cross-Bridge Cycling. *Am. J. Physiol. Regul. Integr. Comp. Physiol.* **2013**, *305*, R118–R125. DOI: 10.1152/ajpregu.00178.2013.

[5] Ramírez, P.; Mafé, S.; Alcaraz, A.; Cervera, J. Modeling of pH-Switchable Ion Transport and Selectivity in Nanopore Membranes with Fixed Charges. *J. Phys. Chem. B.* **2003**, *107*, 13178–13187. DOI: 10.1021/jp035778w.

[6] Yao, H.; Haddad, G. G. Calcium and pH Homeostasis in Neurons during Hypoxia and Ischemia. *Cell Calcium.* **2004**, *36*, 247–255. DOI: 10.1016/j.ceca.2004.02.013.

[7] Shen, Y.; Rosendale, M.; Campbell, R. E.; Perrais, D. pHuji, a pH-Sensitive Red Fluorescent Protein for Imaging of Exo- and Endocytosis. *J. Cell Biol.* **2014**, *207*, 419–432. DOI: 10.1083/jcb.201404107.

[8] Simon, S.; Roy, D.; Schindler, M. Intracellular pH and the Control of Multidrug Resistance. *Proc. Natl. Acad. Sci. USA.* **1994**, *91*, 1128–1132. DOI: 10.1073/pnas.91.3.1128.

[9] Liang, J.; Wu, Y. L.; Chen, B. J.; Zhang, W.; Tanaka, Y.; Sugiyama, H. The C-Kit Receptor-Mediated Signal Transduction and Tumor-Related Diseases. *Int. J. Biol. Sci.* **2013**, *9*, 435–443. DOI: 10.7150/ijbs.6087.

[10] Johnson, D. E.; Ostrowski, P.; Jaumouille, V.; Grinstein, S. The Position of Lysosomes within the Cell Determines Their Luminal pH. *J. Cell Biol.* **2016**, *212*, 677–692. DOI: 0.1083/jcb.201507112. DOI: 10.1083/jcb.201507112.

[11] Rivinoja, A.; Pujol, F. M.; Hassinen, A.; Kellokumpu, S. Golgi pH, Its Regulation and Roles in Human Disease. *Ann. Med.* **2012**, *44*, 542–554. DOI: 10.3109/07853890.2011.579150.

[12] Bao, Y. Y.; Keersmaecker, H.; De.; Corneillie, S.; Yu, F.; Mizuno, H.; Zhang, G. F.; Hofkens, J.; Mendrek, B.; Kowalczuk, A.; Smet, M. Tunableratiometric Fluorescence Sensing of Intracellular pH by Aggregation-Induced Emission-Active Hyperbranched Polymer Nanoparticles. *Chem. Mater.* **2015**, *27*, 3450–3455. DOI: 10.1021/acs.chemmater.5b00858.

[13] Liu, X.; Wang, L.; Bing, T.; Zhang, N.; Shangguan, D. A Mitochondria-Targeted Ratiometric Fluorescent pH Probe. *ACS Appl. Bio Mater.* **2019**, *2*, 1368–1375. DOI: 10.1021/acsabm.9b00061.

[14] Hou, J. T.; Ren, W. X.; Li, K.; Seo, J.; Sharma, A.; Yu, X. Q.; Kim, J. S. Fluorescent Bioimaging of pH: From Design to Applications. *Chem. Soc. Rev.* **2017**, *46*, 2076–2090. DOI: 10.1039/C6CS00719H.

[15] Chen, J. H.; Xu, W.; Sheppard, D. N. Altering Intracellular pH Reveals the Kinetic Basis of Intraburst Gating in the CFTR Cl-Channel. *J. Physiol.* **2017**, *595*, 1059–1076. DOI: 10.1113/JP273205.

[16] Fang, B.; Wang, D.; Huang, M.; Yu, G.; Li, H. Hypothesis on the Relationship between the Change in Intracellular PH and Incidence of Sporadic Alzheimer's Disease or Vascular Dementia. *Int. J. Neurosci.* **2010**, *120*, 591–595. DOI: 10.3109/00207454.2010.505353.

[17] Swietach, P.; Wigfield, S.; Cobden, P.; Supuran, C. T.; Harris, A. L.; Vaughan-Jones, R. D. Tumor-Associated Carbonic Anhydrase 9 Spatially Coordinates Intracellular PH in Three-Dimensional Multicellular Growths. *J. Biol. Chem.* **2008**, *283*, 20473–20483. DOI: 10.1074/jbc.M801330200.

[18] Fukuda, T.; Ewan, L.; Bauer, M.; Mattaliano, R. J.; Zaal, K.; Ralston, E.; Plotz, P. H.; Raben, N. Dysfunction of Endocytic and Autophagic Pathways in a Lysosomal Storage Disease. *Ann. Neurol.* **2006**, *59*, 700–708. DOI: 10.1002/ana.20807.

[19] He, X.; Xu, W.; Xu, C.; Ding, F.; Chen, H.; Shen, J. Reversible Spiropyran-Based Chemosensor with pH-Switches and Application for Bioimaging in Living Cells Pseudomonas aeruginosa and Zebrafish. *Dyes Pigm.* **2020**, *180*, 108497. DOI: 10.1016/j.dyepig.2020.108497.

[20] Wang, C.; Telpoukhovskaia, M. A.; Bahr, B.; Chen, X.; Gan, L. Endo-Lysosomal Dysfunction: A Converging Mechanism in Neurodegenerative Diseases. *Curr. Opin. Neurobiol.* **2018**, *48*, 52–58. DOI: 10.1016/j.conb.2017.09.005.

[21] Deutsch, C.; Taylor, J. S.; Wilson, D. F. Regulation of Intracellular pH by Human Peripheral Blood Lymphocytes as Measured by 19F NMR. *Proc. Natl. Acad. Sci. USA.* **1982**, *79*, 7944–7948. DOI: 10.1073/pnas.79.24.7944.

[22] Anemone, A.; Consolino, L.; Arena, F.; Capozza, M.; Longo, D. L. Imaging Tumor Acidosis: A Survey of the Available Techniques for Mapping in Vivo Tumor pH. *Cancer Metastasis Rev.* **2019**, *38*, 25–49. DOI: 10.1007/s10555-019-09782-9.

[23] Kiani, M. J.; Razak, M. A. A.; Harun, F. K. C.; Ahmadi, M. T.; Rahmani, M. SWCNT-Based Biosensor Modelling for pH Detection. *J. Nanomater.* **2015**, *16*, 721251–721257. DOI: 10.1155/2015/721251.

[24] He, S.; Mason, R. P.; Hunjan, S.; Mehta, V. D.; Arora, V.; Katipally, R.; Kulkarni, P. V.; Antich, P. P. Development of Novel 19F NMR pH Indicators: Synthesis and Evaluation of a Series of Fluorinated Vitamin B6 Analogues. *Bioorg. Med. Chem.* **1998**, *6*, 1631–1639. DOI: 10.1016/S0968-0896(98)00104-7.

[25] Zhang, R. G.; Kelsen, S. G.; Lamanna, J. C. Measurement of Intracellular pH in Hamster Diaphragm by Absorption Spectrophotometry. *J. Appl. Physiol.* **1990**, *68*, 1101–1106. DOI: 10.1152/jappl.1990.68.3.1101.

[26] Balazs, N.; Sipos, P. Limitations of pH-Potentiometric Titration for the Determination of the Degree of Deacetylation of Chitosan. *Carbohydr. Res.* **2007**, *342*, 124–130. DOI: 10.1016/j.carres.2006.11.016.

[27] Kim, T. H.; Kim, S. H.; Tan, L. V.; Dong, Y.; Kim, H.; Kim, J. S. Diazo-Coupled Calix[4]Arenes for Qualitative Analytical Screening of Metal Ions. *Talanta* **2008**, *74*, 1654–1658. DOI: 10.1016/j.talanta.2007.10.033.

[28] Wang, J.; Liu, H.; Wu, M.; Liu, X. L.; Sun, H. Y.; Zheng, A. X. Water-Soluble Organic Probe for pH Sensing and Imaging. *Talanta* **2019**, *205*, 120095. DOI: 10.1016/j.talanta.2019.06.095.

[29] Yang, Y. M.; Zhao, Q.; Feng, W.; Li, F. Y. Luminescent Chemodosimeters for Bioimaging. *Chem. Rev.* **2013**, *113*, 192–270. DOI: 10.1021/cr2004103.

[30] Banik, D.; Manna, S. K.; Mahapatra, A. K. Recent Development of Chromogenic and Fluorogenic Chemosensors for the Detection of Arsenic Species: Environmental and Biological Applications. *Spectrochim. Acta A Mol. Biomol. Spectrosc.* **2021**, *246*, 119047. DOI: 10.1016/j.saa.2020.119047.

[31] Mondal, S.; Manna, S. K.; Pathak, S.; Masum, A. A.; Mukhopadhyay, S. A Colorimetric and "Off–On" Fluorescent Pd^{2+} Chemosensor Based on a Rhodamine-Ampyrone Conjugate: Synthesis, Experimental and Theoretical Studies along with *in Vitro* Applications. *New J. Chem.* **2019**, *43*, 3513–3519. DOI: 10.1039/C8NJ05194A.

[32] Mondal, S.; Manna, S. K.; Pathak, S.; Ghosh, A.; Datta, P.; Mandal, D.; Mukhopadhyay, S. A. "Turn-On" Fluorescent and Colorimetric Chemodosimeter for Selective Detection of Au^{3+} Ions in Solution and in Live Cells via Au^{3+}-Induced Hydrolysis of a Rhodamine-Derived Schiff Base. *New J. Chem.* **2020**, *44*, 7954–7961. DOI: 10.1039/D0NJ01273D.

[33] Yin, J.; Huang, L.; Wu, L.; Li, J.; James, T. D.; Lin, W. Small Molecule Based Fluorescent Chemosensors for Imaging the Microenvironment within Specific Cellular Regions. *Chem. Soc. Rev.* **2021**, ***50***, 12098–12150. DOI: 10.1039/D1CS00645B.

[34] Han, H.-H.; Tian, H.; Jr., Zang, Y.; Sedgwick, A. C.; Li, J.; Sessler, J. L.; He, X.-P.; James, T. D. Small-Molecule Fluorescence-Based Probes for Interrogating Major Organ Diseases. *Chem. Soc. Rev.* **2021**, ***50***, 9391–9429. DOI: 10.1039/D0CS01183E.

[35] Benčina, M. Illumination of the Spatial Order of Intracellular pH by Genetically Encoded pH-Sensitive Sensors. *Sensors* **2013**, *13*, 16736–16758. DOI: 10.3390/s131216736.

[36] Shi, W.; Li, X.; Ma, H. Fluorescent Probes and Nanoparticles for Intracellular Sensing of pH Values. *Methods Appl. Fluoresc.* **2014**, *2*, 042001–042014. DOI: 10.1088/2050-6120/2/4/042001.

[37] Schäferling, M. Nanoparticle-Based Luminescent Probes for Intracellular Sensing and Imaging of pH. *Wiley Interdiscip. Rev. Nanomed. Nanobiotechnol.* **2016**, *8*, 378–413. DOI: 10.1002/wnan.1366.

[38] Yue, Y.; Huo, F.; Lee, S.; Yin, C.; Yoon, J. A Review: The Trend of Progress about pH Probes in Cell Application in Recent Years. *Analyst* **2016**, *142*, 30–41. DOI: 10.1039/C6AN01942K.

[39] Hou, J. T.; Ren, W. X.; Li, K.; Seo, J.; Sharma, A.; Yu, X. Q.; Kim, J. S. Fluorescent Bioimaging of pH: From Design to Applications. *Chem. Soc. Rev.* **2017**, *46*, 2076–2090. DOI: 10.1039/C6CS00719H.

[40] Chen, W.; Ma, X.; Chen, H.; Liu, S. H.; Yin, J. Fluorescent Probes for pH and Alkali Metal Ions. *Coord. Chem. Rev.* **2021**, *427*, 213584. DOI: 10.1016/j.ccr.2020.213584.

[41] Ma, J.; Li, W.; Li, J.; Shi, R.; Yin, G.; Wang, R. A Small Molecular pH-Dependent Fluorescent Probe for Cancer Cell Imaging in Living Cell. *Talanta* **2018**, *182*, 464–469. DOI: 10.1016/j.talanta.2018.01.088.

[42] Liu, M.; Lv, Y.; Jie, X.; Meng, Z.; Wang, X.; Huang, J.; Peng, A.; Tian, Z. A Super-Sensitive Ratiometric Fluorescent Probe for Monitoring Intracellular Subtle pH Fluctuation. *Sens. Actuators B* **2018**, *273*, 167–175. DOI: 10.1016/j.snb.2018.06.048.

[43] Mandal, J.; Ghorai, P.; Brandão, P.; Pal, K.; Karmakar, P.; Saha, A. An Aminoquinoline Based Biocompatible Fluorescent and Colourimetric pH Sensor Designed for Cancer Cell Discrimination. *New J. Chem.* **2018**, *42*, 19818–19826. DOI: 10.1039/C8NJ04753G.

[44] She, Z. P.; Tian, Y.; Xia, Y. S.; Jie, J.; Li, Y.; Li, C. Y. A Facile pH near-Infrared Fluorescence Probe for the Diagnosis of Cancer in Vivo. *Dyes Pigm.* **2020**, *179*, 108402. DOI: 10.1016/j.dyepig.2020.108402.

[45] Dhawa, T.; Hazra, A.; Barma, A.; Pal, K.; Karmakar, P.; Roy, P. 4-Methyl-2, 6-Diformylphenol Based Biocompatible Chemosensors for pH: Discrimination between Normal Cells and Cancer Cells. *RSC Adv.* **2020**, *10*, 15501–15513. DOI: 10.1039/D0RA00754D.

[46] Ohkuma, S.; Poole, B. Fluorescence Probe Measurement of the Intralysosomal pH in Living Cells and the Perturbation of pH by Various Agents. *Proc. Natl. Acad. Sci. USA.* **1978**, *75*, 3327–3331. DOI: 10.1073/pnas.75.7.3327.

[47] Nishi, T.; Forgac, M. The Vacuolar (H^+)-ATPases-Nature's Most Versatile Proton Pumps. *Nat. Rev. Mol. Cell. Biol.* **2002**, *3*, 94–103. DOI: 10.1038/nrm729.

[48] Settembre, C.; Fraldi, A.; Medina, D. L.; Ballabio, A. Signals from the Lysosome: A Control Centre for Cellular Clearance and Energy Metabolism. *Nat. Rev. Mol. Cell. Biol.* **2013**, *14*, 283–296. DOI: 10.1038/nrm3565.

[49] Xu, H.; Ren, D. Lysosomal Physiology. *Annu. Rev. Physiol.* **2015**, *77*, 57–80. DOI: 10.1146/annurev-physiol-021014-071649.

[50] Maxfield, F. R.; Willard, J. M.; Lu, S. Lysosomes: Biology, Diseases, and Therapeutics. John Wiley & Sons: New York, **2016**.

[51] Kroemer, G.; Jäättelä, M. Lysosomes and Autophagy in Cell Death Control. *Nat. Rev. Cancer.* **2005**, *5*, 886–897. DOI: 10.1038/nrc1738.

[52] Futerman, A. H.; Meer, G. V. The Cell Biology of Lysosomal Storage Disorders. *Nat. Rev. Mol. Cell Biol.* **2004**, *5*, 554–565. DOI: 10.1038/nrm1423.

[53] Fehrenbacher, N.; Jäättelä, M. Lysosomes as Targets for Cancer Therapy. *Cancer Res.* **2005**, *65*, 2993–2995. DOI: 10.1158/0008-5472.can-05-0476.

[54] Saftig, P.; Sandhoff, K. Cancer: Killing from the inside. *Nature* **2013**, *502*, 312–313. DOI: 10.1038/nature12692.

[55] Li, S. S.; Zhang, M.; Wang, J. H.; Yang, F.; Kang, B.; Xu, J. J.; Chen, H. Y. Monitoring the Changes of pH in Lysosomes during Autophagy and Apoptosis by Plasmon Enhanced Raman Imaging. *Anal. Chem.* **2019**, *91*, 8398–8405. DOI: 10.1021/acs.analchem.9b01250.

[56] Nylandsted, J.; Hansen, M. G.; Danielewicz, A.; Fehrenbacher, N.; Lademann, U.; Høyer-Hansen, M.; Weber, E.; Multhoff, G.; Rohde, M.; Jäättelä, M. Heat Shock Protein 70 Promotes Cell Survival by Inhibiting Lysosomal Membrane Permeabilization. *J. Exp. Med.* **2004**, *200*, 425–435. DOI: 10.1084/jem.20040531.

[57] Ge, J.; Fan, L.; Zhang, K.; Ou, T.; Li, Y.; Zhang, C.; Dong, C.; Shuang, S.; Wong, M. S. A Two-Photon Ratiometric Fluorescent Probe for Effective Monitoring of Lysosomal pH in Live Cells and Cancer Tissues. *Sens. Actuators B, Chem.* **2018**, *262*, 913–921. DOI: 10.1016/j.snb.2018.02.082.

[58] Xia, S.; Wang, J.; Bi, J.; Wang, X.; Fang, M.; Phillips, T.; May, A.; Conner, N.; Tanasova, M.; Luo, F. T.; Liu, H. Fluorescent Probes Based on π-Conjugation Modulation between Hemicyanine and Coumarin Moieties for Ratiometric Detection of pH Changes in Live Cells with Visible and Near-Infrared Channels. *Sens. Actuators B Chem.* **2018**, *265*, 699–708. DOI: 10.1016/j.snb.2018.02.168.

[59] Liu, H.; Wang, J.; Xia, S.; Bi, J.; Fang, M.; Mazi, W.; Zhang, Y.; Conner, N.; Luo, F. T.; Lu, H. P. Ratiometric near-Infrared Fluorescent Probes Based on through-Bond Energy Transfer and π-Conjugation Modulation between Tetraphenylethene and Hemicyanine Moieties for Sensitive Detection of pH

Changes in Live Cells. *Bioconjugate Chem.* **2018**, *29*, 1406–1418. DOI: 10.1021/acs.bioconjchem.8b00111.

[60] Lee, D.; Swamy, K. M. K.; Hong, J.; Lee, S.; Yoon, J. A Rhodamine-Based Fluorescent Probe for the Detection of Lysosomal pH Changes in Living Cells. *Sens. Actuators B Chem.* **2018**, *266*, 416–421. DOI: 10.1016/j.snb.2018.03.133.

[61] Wu, L.; Wang, Y.; James, T. D.; Jia, N.; Huang, C. A Hemicyanine Based Ratiometric Fluorescence Probe for Mapping Lysosomal pH during Heat Stroke in Living Cells. *Chem. Commun.* **2018**, *54*, 5518–5521. DOI: 10.1039/C8CC02330A.

[62] Zhang, Y.; Xia, S.; Fang, M.; Mazi, W.; Zeng, Y.; Johnston, T.; Pap, A.; Luck, R.; Liu, H. New Near-Infrared Rhodamine Dyes with Large Stokes Shifts for Sensitive Sensing of Intracellular pH Changes and Fluctuations. *Chem. Commun.* **2018**, *54*, 7625–7628. DOI: 10.1039/C8CC03520B.

[63] Zhu, M.; Xing, P.; Zhou, Y.; Gong, L.; Zhang, J.; Qi, D.; Bian, Y.; Du, H.; Jiang, J. Lysosome-Targeting Ratiometric Fluorescent pH Probes Based on Long-Wavelength BODIPY. *J. Mater. Chem. B.* **2018**, *6*, 4422–4426. DOI: 10.1039/C8TB00883C.

[64] Wang, C.; Dong, B.; Kong, X.; Zhang, N.; Song, W.; Lin, W. Dual Site-Controlled Two-Photon Fluorescent Probe for the Imaging of Lysosomal pH in Living Cells. *Luminescence* **2018**, *33*, 1275–1280. DOI: 10.1002/bio.3546.

[65] Liu, H.; Chen, T. H.; Zhang, S.; Jaishi, M.; Adhikari, R.; Bi, J.; Fang, M.; Xia, S.; Zhang, Y.; Luck, R. L.; et al. New Near-Infrared Fluorescent Probes with Single-Photon Anti-Stokes-Shift Fluorescence for Sensitive Determination of pH Variances in Lysosomes with a Double-Checked Capability. *ACS Appl. Bio. Mater.* **2018**, *1*, 549–560. DOI: 10.1021/acsabm.8b00020.

[66] Zhang, Y.; Bi, J.; Xia, S.; Mazi, W.; Wan, S.; Mikesell, L.; Luck, R. L.; Liu, H. A Near-Infrared Fluorescent Probe Based on a FRET Rhodamine Donor Linked to a Cyanine Acceptor for Sensitive Detection of Intracellular pH Alternations. *Molecules* **2018**, *23*, 2679. DOI: 10.3390/molecules23102679.

[67] Wang, J.; Xia, S.; Bi, J.; Zhang, Y.; Fang, M.; Luck, R. L.; Zeng, Y.; Chen, T. H.; Lee, H. M.; Liu, H. Near-Infrared Fluorescent Probes Based on TBET and FRET Rhodamine Acceptors with Different pKa Values for Sensitive Ratiometric Visualization of pH Changes in Live Cells. *J. Mater. Chem. B.* **2019**, *7*, 198–209. DOI: 10.1039/C8TB01524D.

[68] Ning, P.; Hou, L.; Feng, Y.; Xu, G.; Bai, Y.; Yu, H.; Meng, X. Real-Time Visualizing Autophagy by Monitoring the Fluctuation of Lysosomal pH with a Ratiometric Two-Photon Fluorescent Probe. *Chem. Commun.* **2019**, *55*, 1782–1785. DOI: 10.1039/C8CC09517E.

[69] Li, J.; Li, X.; Jia, J.; Chen, X.; Lv, Y.; Guo, Y.; Li, J. A Ratiometric near-Infrared Fluorescence Strategy Based on Spiropyran in Situ Switching for Tracking Dynamic Changes of Live-Cell Lysosomal pH. *Dyes Pigm.* **2019**, *166*, 433–442. DOI: 10.1016/j.dyepig.2019.03.060.

[70] Shi, Y.; Meng, X.; Yang, H.; Song, L.; Liu, S.; Xu, A.; Chen, Z.; Huang, W.; Zhao, Q. Lysosome-Specific Sensing and Imaging of pH Variations in Vitro and in-Vivo Utilizing a Near-Infrared Boron Complex. *J. Mater. Chem. B.* **2019**, *7*, 3569–3575. DOI: 10.1039/C8TB03353F.

[71] Xia, S.; Fang, M.; Wang, J.; Bi, J.; Mazi, W.; Zhang, Y.; Luck, R. L.; Liu, H. Near-Infrared Fluorescent Probes with BODIPY Donors and Rhodamine and Merocyanine Acceptors for Ratiometric Determination of Lysosomal pH Variance. *Sens. Actuators B Chem.* **2019**, *294*, 1–13. DOI: 10.1016/j.snb.2019.05.005.

[72] Ge, J.; Zhang, K.; Fan, L.; Wang, X.; Zhang, C.; Dong, C.; Wong, M. S.; Shuang, S. Novel Long-Wavelength Emissive Lysosome-Targeting Ratiometric Fluorescent Probes for Imaging in Live Cells. *Analyst* **2019**, *144*, 4288–4294. DOI: 10.1039/C9AN00697D.

[73] Zhang, T.; Zhang, Y.; Wang, R.; Xu, D. Tuning Dual-Channel Fluorescence-Enhanced Chemosensor for Imaging of Living Cells in Extreme Acidity. *Dyes Pigm.* **2019**, *171*, 107672. DOI: 10.1016/j.dyepig.2019.107672.

[74] Niu, W.; Jia, J.; Li, J.; Zhang, C.; Yun, K. Ratiometric Emission NIR-Fluorescent Probe for the Detection of Lysosomal pH in Living Cells and in Vivo. *New J. Chem.* **2019**, *43*, 13363–13370. DOI: 10.1039/C9NJ02771H.

[75] Yuan, G.; Ding, H.; Zhou, L. An Effective FRET-Based Two-Photon Ratiometric Fluorescent Probe with Double Well-Resolved Emission Bands for Lysosomal pH Changes in Living Cells and Zebrafish. *Spectrochim. Acta A* **2020**, *224*, 117397. DOI: 10.1016/j.saa.2019.117397.

[76] Mazi, W.; Adhikari, R.; Zhang, Y.; Xia, S.; Fang, M.; Luck, R. L.; Tajiri, M.; Tiwari, A.; Tanasova, M.; Liu, H. Fluorescent Probes with High pKa Values Based on Traditional, Near-Infrared Rhodamine, and Hemicyanine Fluorophores for Sensitive Detection of Lysosomal pH Variations. *Methods* **2019**, *168*, 40–50. DOI: 10.1016/j.ymeth.2019.07.012.

[77] Tian, M.; Liu, C.; Dong, B.; Zuo, Y.; Lin, W. A Dual-Site Controlled Ratiometric Probe Revealing the Simultaneous Down-Regulation of pH in Lysosomes and Cytoplasm during Autophagy. *Chem. Commun.* **2019**, *55*, 10440–10443. DOI: 10.1039/C9CC03679B.

[78] Mao, G. J.; Liang, Z. Z.; Gao, G. Q.; Wang, Y. Y.; Guo, X. Y.; Su, L.; Zhang, H.; Ma, Q. J.; Zhang, G. A Photostable Si-Rhodamine-Based Near-Infrared Fluorescent Probe for Monitoring Lysosomal pH during Heat Stroke. *Anal. Chim. Acta.* **2019**, *1092*, 117–125. DOI: 10.1016/j.aca.2019.09.053.

[79] Yan, Y.; Zhang, X.; Zhang, X.; Li, N.; Man, H.; Chen, L.; Xiao, Y. Ratiometric Sensing Lysosomal pH in Inflammatory Macrophages by a BODIPY-Rhodamine Dyad with Restrained FRET. *Chin. Chem. Lett.* **2020**, *31*, 1091–1094. DOI: 10.1016/j.cclet.2019.10.025.

[80] Yu, F.; Jing, X.; Lin, W. Single-/Dual-Responsive pH Fluorescent Probes Based on the Hybridization of Unconventional Fluorescence and Fluorophore for Imaging Lysosomal pH Changes in HeLa Cells. *Anal. Chem.* **2019**, *91*, 15213–15219. DOI: 10.1021/acs.analchem.9b04088.

[81] Zhang, X. F.; Wang, T. R.; Cao, X. Q.; Shen, S. L. A near-Infrared Rhodamine-Based Lysosomal pH Probe and Its Application in Lysosomal pH Rise during Heat Shock. *Spectrochim. Acta A* **2020**, *227*, 117761. DOI: 10.1016/j.saa.2019.117761.

[82] Zhang, Y.; Zhao, Y.; Wu, Y.; Zhao, B.; Wang, L.; Song, B. Hemicyanine Based Naked-Eye Ratiometric Fluorescent Probe for Monitoring Lysosomal pH and Its Application. *Spectrochim. Acta A* **2020**, *227*, 117767. DOI: 10.1016/j.saa.2019.117767.

[83] Dong, Y.; Xiao, H.; Xing, L.; Wu, C.; Zhou, J.; Zhou, Z.; Liu, Y.; Zhuo, S.; Li, P. Two-Photon Fluorescence Visualization of Lysosomal pH Changes during Mitophagy and Cell Apoptosis. *Talanta* **2020**, *209*, 120549. DOI: 10.1016/j.talanta.2019.120549.

[84] Zhang, Y.; Bu, F.; Zhao, Y.; Zhao, B.; Wang, L.; Song, B. A Hemicyanine Fluorescent Probe with Intramolecular Charge Transfer (ICT) Mechanism for Highly Sensitive and Selective Detection of Acidic pH and Its Application in Living cells. *Anal. Chim. Acta.* **2020**, *1098*, 155–163. DOI: 10.1016/j.aca.2019.11.040.

[85] Wang, X.; Fan, L.; Wang, Y.; Zhang, C.; Liang, W.; Shuang, S.; Dong, C. Visual Monitoring of the Lysosomal pH Changes during Autophagy with a Red-Emission Fluorescent Probe. *J. Mater. Chem. B.* **2020**, *8*, 1466–1471. DOI: 10.1039/C9TB02551K.

[86] Zhang, J.; Zhu, M.; Cui, J.; Wang, C.; Zhou, Z.; Wang, T.; Gong, L.; Su, C.; Qi, D.; Bian, Y.; et al. A Porphyrin-Pyranine Dyad for Ratiometric Fluorescent Sensing of Intracellular pH. *J. Photochem. Photobiol. A* **2020**, *396*, 112524. DOI: 10.1016/j.jphotochem.2020.112524.

[87] Li, L.; Li, Y.; Dang, Y.; Chen, T.; Zhang, A.; Ding, C.; Xu, Z. Imidazole-Fused Benzothiadiazole-Based Red-Emissive Fluorescence Probe for Lysosomal pH Imaging in Living Cells. *Talanta* **2020**, *217*, 121066. DOI: 10.1016/j.talanta.2020.121066.

[88] Li, L.; Xiong, Z.; Dang, Y.; Li, Y.; Zhang, A.; Ding, C.; Xu, Z.; Zhang, W. A Red-Emissive D-A-D Type Fluorescent Probe for Lysosomal pH Imaging. *Anal. Methods* **2020**, *12*, 2978–2984. DOI: 10.1039/D0AY00418A.

[89] Wang, X.; Fan, L.; Wang, Y.; Zhang, C.; Liang, W.; Shuang, S.; Dong, C. A Red-Emission Fluorescent Probe for Visual Monitoring of the Lysosomal pH Changes during Mitophagy and Cell Apoptosis. *J. Mater. Chem. B.* **2020**, *8*, 1466–1471. DOI: 10.1039/C9TB02551K.

[90] Ernster, L.; Schatz, G. Mitochondria: A Historical Review. *J. Cell Biol.* **1981**, *91*, 227s–255s. DOI: 10.1083/jcb.91.3.227s.

[91] Zhu, L. P.; Yu, X. D.; Ling, S.; Brown, R. A.; Kuo, T. H. Mitochondrial Ca^{2+} Homeostasis in the Regulation of Apoptotic and Necrotic Cell Deaths. *Cell Calcium* **2000**, *28*, 107–117. DOI: 10.1054/ceca.2000.0138.

[92] Desagher, S.; Martinou, J. C. Mitochondria as the Central Control Point of Apoptosis. *Trends Cell Biol.* **2000**, *10*, 369–377. DOI: 10.1016/S0962-8924(00)01803-1.

[93] Andreyev, A. Y.; Kushnareva, Y. E.; Starkov, A. A. Mitochondrial Metabolism of Reactive Oxygen Species. *Biochemistry* **2005**, *70*, 200–214. DOI: 10.1007/s10541-005-0102-7.

[94] Nakagawa, T.; Guarente, L. Urea Cycle Regulation by Mitochondrial Sirtuin, SIRT5. *Aging* **2009**, *1*, 578–581. DOI: 10.18632/aging.100062.

[95] Singh, H.; Beckman, K.; Poulos, A. Peroxisomal Beta-Oxidation of Branched Chain Fatty Acids in Rat Liver. Evidence That Carnitine Palmitoyltransferase I Prevents Transport of Branched Chain Fatty Acids into Mitochondria. *J. Biol. Chem.* **1994**, *269*, 9514–9520. DOI: 10.1016/S0021-9258(17)36911-9.

[96] Nie, G. J.; Sheftel, A. D.; Kim, S. F.; Ponka, P. Overexpression of Mitochondrial Ferritin Causes Cytosolic Iron Depletion and Changes Cellular Iron Homeostasis. *Blood* **2005**, *105*, 2161–2167. DOI: 10.1182/blood-2004-07-2722.

[97] Wu, H.; Chen, Q. Hypoxia Activation of Mitophagy and Its Role in Disease Pathogenesis. *Antioxid. Redox Signaling* **2015**, *22*, 1032–1046. DOI: 10.1089/ars.2014.6204.

[98] Youle, R. J.; Narendra, D. P. Mechanisms of Mitophagy. *Nat. Rev. Mol. Cell Biol.* **2011**, *12*, 9–14. DOI: 10.1038/nrm3028.

[99] Kim, J. H.; Kim, H. Y.; Lee, Y. K.; Yoon, Y. S.; Xu, W. G.; Yoon, J. K.; Choi, S. E.; Ko, Y. G.; Kim, M. J.; Lee, S. J.; et al. Involvement of Mitophagy in Oncogenic K-Ras-Induced Transformation: Overcoming a Cellular Energy Deficit from Glucose Deficiency. *Autophagy* **2011**, *7*, 1187–1198. DOI: 10.4161/auto.7.10.16643.

[100] Lin, M. T.; Beal, M. F. Mitochondrial Dysfunction and Oxidative Stress in Neurodegenerative Diseases. *Nature* **2006**, *443*, 787–795. DOI: 10.1038/nature05292.

[101] Trincado, C. V.; Carvajal, I. G.; Pennanen, C.; Parra, V.; Hill, J. A.; Rothermel, B. A.; Lavandero, S. Mitochondrial Dynamics, Mitophagy and Cardiovascular Disease. *J. Physiol.* **2016**, *594*, 509–525. DOI: 10.1113/JP271301.

[102] Wrighton, K. H. Putting Energy into Mitophagy. *Nat. Rev. Mol. Cell Biol.* **2013**, *14*, 325–325. DOI: 10.1038/nrm3586.

[103] Wisnovsky, S.; Lei, E. K.; Jean, S. R.; Kelley, S. O. Mitochondrial Chemical Biology: New Probes Elucidate the Secrets of the Powerhouse of the Cell. *Cell Chem. Biol.* **2016**, *23*, 917–927. DOI: 10.1016/j.chembiol.2016.06.012.

[104] Li, K.; Feng, Q.; Niu, G.; Zhang, W.; Li, Y.; Kang, M.; Xu, K.; He, J.; Hou, H.; Tang, B. Z. Benzothiazole-Based AIEgen with Tunable Excited-State Intramolecular Proton Transfer and Restricted Intramolecular Rotation Processes for Highly Sensitive Physiological pH Sensing. *ACS Sens.* **2018**, *3*, 920–928. DOI: 10.1021/acssensors.7b00820.

[105] Podder, A.; Won, M.; Kim, S.; Verwilst, P.; Maiti, M.; Yang, Z.; Qu, J.; Bhuniya, S.; Kim, J. S. A Two-Photon Fluorescent Probe Records the Intracellular pH through 'OR' Logic Operation via Internal Calibration. *Sens. Actuators B Chem.* **2018**, *268*, 195–204. DOI: 10.1016/j.snb.2018.04.092.

[106] Qi, S.; Li, Q.; Liu, W.; Ren, H.; Zhang, H.; Wu, J.; Ge, J.; Wang, P. Coumarin/Fluorescein-Fused Fluorescent Dyes for Rapidly Monitoring Mitochondrial pH Changes in Living Cells. *Spectrochim. Acta A* **2018**, *204*, 590–597. DOI: 10.1016/j.saa.2018.06.095.

[107] Gui, L.; Yuan, Z.; Kassaye, H.; Zheng, J.; Yao, Y.; Wang, F.; He, Q.; Shen, Y.; Liang, L.; Chen, H. Correction: A Tumor-Targeting Probe Based on a Mitophagy Process for Live Imaging. *Chem. Commun.* **2018**, *54*, 10774. DOI: 10.1039/C8CC04246B.

[108] Niu, L. Q.; Huang, J.; Yan, Z. J.; Men, Y. H.; Luo, Y.; Zhou, X. M.; Wang, J. M.; Wang, J. H. Fluorescence Detection of Intracellular pH Changes in the Mitochondria-Associated Process of Mitophagy Using a Hemicyanine-Based Fluorescent Probe. *Spectrochim. Acta A* **2019**, *207*, 123–131. DOI: 10.1016/j.saa.2018.09.015.

[109] Hong, K. I.; Park, S. H.; Lee, S. M.; Shin, I.; Jang, W. D. A pH-Sensitive Excited State Intramolecular Proton Transfer Fluorescent Probe for Imaging Mitochondria and Helicobacter pylori. *Sens. Actuators B Chem.* **2019**, *286*, 148–153. DOI: 10.1016/j.snb.2019.01.101.

[110] Liu, X.; Wang, L.; Bing, T.; Zhang, N; Shangguan, D. A Mitochondria-Targeted Ratiometric Fluorescent pH Probe. *ACS Appl. Bio Mater.* **2019**, *2*, 1368–1375. DOI: 10.1021/acsabm.9b00061.

[111] Wang, F.; Liu, D.; Shen, Y.; Liu, J.; Li, D.; Tian, X.; Zhang, Q.; Wu, J.; Li, S.; Tian, Y. A Two-Photon Mitochondria-Targeted Fluorescent Probe for the Detection of pH Fluctuation in Tumor and Living Cells. *Dyes Pigm.* **2019**, *166*, 92–97. DOI: 10.1016/j.dyepig.2019.03.033.

[112] Xiao, H.; Dong, Y.; Zhou, J.; Zhou, Z.; Wu, X.; Wang, R.; Miao, Z.; Liu, Y.; Zhuo, S. Monitoring Mitochondrial pH with a Hemicyanine-Based Ratiometric Fluorescent Probe. *Analyst* **2019**, ***144***, 3422–3427. DOI: 10.1039/C9AN00422J.

[113] Jiang, X.; Liu, Z.; Yang, Y.; Li, H.; Qi, X.; Ren, W. X.; Deng, M.; Lü, M.; Wu, J.; Liang, S. A Mitochondria-Targeted Two-Photon Fluorescent Probe for Sensing and Imaging pH Changes in Living Cells. *Spectrochim. Acta A* **2020**, *224*, 117435. DOI: 10.1016/j.saa.2019.117435.

[114] Li, X.; Hu, Y.; Li, X.; Ma, H. Mitochondria-Immobilized Near-Infrared Ratiometric Fluorescent pH Probe to Evaluate Cellular Mitophagy. *Anal. Chem.* **2019**, *91*, 11409–11416. DOI: 10.1021/acs.analchem.9b02782.

[115] Zhang, Y.; Xia, S.; Mikesell, L.; Whisman, N.; Fang, M.; Steenwinkel, T. E.; Chen, K.; Luck, R. L.; Werner, T.; Liu, H. Near-Infrared Hybrid Rhodol Dyes with Spiropyran Switches for Sensitive Ratiometric Sensing of pH Changes in Mitochondria and Drosophila melanogaster First-Instar Larvae. *ACS Appl. Bio Mater.* **2019**, *2*, 4986–4997. DOI: 10.1021/acsabm.9b00710.

[116] Tang, W.; Dai, Y.; Gu, B.; Liu, M.; Yi, Z.; Li, Z.; Zhang, Z.; He, H.; Zeng, R. A near Infrared Fluorescent Probe Based on ICT for Monitoring Mitophagy in Living Cells. *Analyst* **2020**, *145*, 1427–1432. DOI: 10.1039/C9AN02053E.

[117] Xia, S.; Wang, J.; Zhang, Y.; Whisman, N.; Bi, J.; Steenwinkel, T. E.; Wan, S.; Medford, J.; Tajiri, M.; Luck, R. L.; et al. Ratiometric Fluorescent Probes Based on Through-Bond Energy Transfer of Cyanine Donors to Near-Infrared Hemicyanine Acceptors for Mitochondrial pH Detection and Monitoring of Mitophagy. *J. Mater. Chem. B.* **2020**, *8*, 1603–1615. DOI: 10.1039/C9TB02302J.

[118] Palokangas, H.; Ying, M.; VäÄnäNen, K.; Saraste, J. Retrograde Transport from the Pre-Golgi Intermediate Compartment and the Golgi Complex Is Affected by the

Vacuolar H+-ATPase Inhibitor Bafilomycin A1. *Mol. Biol. Cell.* **1998**, *9*, 3561–3578. DOI: 10.1091/mbc.9.12.3561.

[119] Campbell, B. J.; Rowe, G. E.; Leiper, K.; Rhodes, J. M. Increasing the Intra-Golgi pH of Cultured LS174T Goblet-Differentiated Cells Mimics the Decreased Mucin Sulfation and Increased Thomsen-Friedenreich Antigen (Galβ1-3GalNacα-) Expression Seen in Colon Cancer. *Glycobiology* **2001**, *11*, 385–393. DOI: 10.1093/glycob/11.5.385.

[120] Schindler, M.; Grabski, S.; Hoff, E.; Simon, S. M. Defective pH Regulation of Acidic Compartments in Human Breast Cancer Cells (MCF-7) Is Normalized in Adriamycin-Resistant Cells (MCF-7adr). *Biochemistry* **1996**, *35*, 2811–2817. DOI: 10.1021/bi952234e.

[121] Rivinoja, A.; Pujol, F. M.; Hassinen, A.; Kellokumpu, S. Golgi pH, Its Regulation and Roles in Human Disease. *Ann. Med.* **2012**, *44*, 542–554. DOI: 10.3109/07853890.2011.579150.

[122] Xue, F.; Wen, Y.; Wei, P.; Gao, Y.; Zhou, Z.; Xiao, S.; Yi, T. A Smart Drug: A pH-Responsive Photothermal Ablation Agent for Golgi Apparatus Activated Cancer Therapy. *Chem. Commun.* **2017**, *53*, 6424–6427. DOI: 10.1039/C7CC03168H.

[123] Yamashiro, D. J.; Tycko, B.; Fluss, S. R.; Maxfield, F. R. Segregation of Transferrin to a Mildly Acidic (pH 6.5) Para-Golgi Compartment in the Recycling Pathway. *Cell* **1984**, *37*, 789–800. DOI: 10.1016/0092-8674(84)90414-8.

[124] Kellokumpu, S.; Sormunen, R.; Kellokumpu, I. Abnormal Glycosylation and Altered Golgi Structure in Colorectal Cancer: Dependence on intra-Golgi pH. *FEBS Lett.* **2002**, *516*, 217–224. DOI: 10.1016/S0014-5793(02)02535-8.

[125] Barasch, J.; Kiss, B.; Prince, A.; Saiman, L.; Gruenert, D.; Al-Awqati, Q. Defective Acidification of Intracellular Organelles in Cystic Fibrosis. *Nature* **1991**, *352*, 70–73. DOI: 10.1038/352070a0.

[126] Morava, E.; Guillard, M.; Lefeber, D. J.; Wevers, R. A. Autosomal Recessive Cutis Laxa Syndrome Revisited. *Eur. J. Hum. Genet.* **2009**, *17*, 1099–1110. DOI: 10.1038/ejhg.2009.22.

[127] Vanoevelen, J.; Dode, L.; Raeymaekers, L.; Wuytack, F.; Missiaen, L. Diseases Involving the Golgi Calcium Pump. *Subcell. Biochem.* **2007**, *45*, 385–404. DOI: 10.1007/978-1-4020-6191-2_14.

[128] Fan, L.; Wang, X.; Ge, J.; Li, F.; Zhang, C.; Lin, B.; Shuang, S.; Dong, C. A Golgi-Targeted Off-On Fluorescent Probe for Real-Time Monitoring of pH Changes in Vivo. *Chem. Commun.* **2019**, *55*, 6685–6688. DOI: 10.1039/C9CC02511A.

[129] Wang, H.; Yang, Y.; Huang, F.; He, Z.; Li, P.; Zhang, W.; Zhang, W.; Tang, B. In Situ Fluorescent and Photoacoustic Imaging of Golgi pH to Elucidate the Function of Transmembrane Protein 165. *Anal. Chem.* **2020**, *92*, 3103–3110. DOI: 10.1021/acs.analchem.9b04709.

[130] Xu, W.; Zeng, Z.; Jiang, J. H.; Chang, Y. T.; Yuan, L. Discerning the Chemistry in Individual Organelles with Small-Molecule Fluorescent Probes. *Angew. Chem. Int. Ed. Engl.* **2016**, *55*, 13658–13699. DOI: 10.1002/anie.201510721.

[131] Qiu, K.; Chen, Y.; Rees, T. W.; Ji, L.; Chao, H. Organelle-Targeting Metal Complexes: From Molecular Design to Bio-Applications. *Coord. Chem. Rev.* **2019**, *378*, 66–86. DOI: 10.1016/j.ccr.2017.10.022.

[132] Wu, H. L.; Duan, Z. T.; Jiang, Z. D.; Cao, W. J.; Wang, Z. B.; Hu, K. W.; Gao, X.; Wang, S. K.; He, B. S.; Zhang, Z. Y.; Xie, H. G. Increased Endoplasmic Reticulum Stress Response is Involved in Clopidogrel-Induced Apoptosis of Gastric Epithelial Cells. *PLoS One* **2013**, *8*, e74381. DOI: 10.1371/journal.pone.0074381.

[133] Braakman, I.; Bulleid, N. J. Protein Folding and Modification in the Mammalian Endoplasmic Reticulum. *Annu. Rev. Biochem.* **2011**, *80*, 71–99. DOI: 10.1146/annurev-biochem-062209-093836. [21495850]

[134] Wu, M. M.; Llopis, J.; Adams, S.; McCaffery, J. M.; Kulomaa, M. S.; Machen, T. E.; Moore, H. P. H.; Tsien, R. Y. Organelle pH Studies Using Targeted Avidin and fluorescein-biotin. *Chem. Biol.* **2000**, *7*, 197–209. DOI: 10.1016/S1074-5521(00)00088-0. [10712929]

[135] Paroutis, P.; Touret, N.; Grinstein, S. The pH of the Secretory Pathway: Measurement, Determinants, and Regulation. *Physiology* **2004**, *19*, 207–215. [Database] DOI: 10.1152/physiol.00005.2004.

[136] Sano, R.; Reed, J. C. ER Stress-Induced Cell Death Mechanisms. *Biochim. Biophys. Acta Mol. Cell Res.* **2013**, *1833*, 3460–3470. DOI: 10.1016/j.bbamcr.2013.06.028.

[137] Özcan, U.; Cao, Q.; Yilmaz, E.; Lee, A. H.; Iwakoshi, N. N.; ÖZdelen, E.; Tuncman, G.; GörgüN, C.; Glimcher, L. H.; Hotamisligil, G. S. Endoplasmic Reticulum Stress Links Obesity, Insulin Action, and Type 2 Diabetes. *Science* **2004**, *306*, 457–461. DOI: 10.1126/science.1103160.

[138] Eizirik, D. L.; Cardozo, A. K.; Cnop, M. The Role for Endoplasmic Reticulum Stress in Diabetes Mellitus. *Endocr. Rev.* **2008**, *29*, 42–61. DOI: 10.1210/er.2007-0015.

[139] Xiao, H.; Zhang, R.; Wu, C.; Li, P.; Zhang, W.; Tang, B. A New pH-Sensitive Fluorescent Probe for Visualization of Endoplasmic Reticulum Acidification during Stress. *Sens. Actuators B Chem.* **2018**, *273*, 1754–1761. DOI: 10.1016/j.snb.2018.07.059.

[140] Zhang, N.; Dong, B.; Kong, X.; Song, W.; Lin, W. A Two-Photon Endoplasmic Reticulum-Targeting Fluorescent Probe for the Imaging of pH in Living Cells and Zebrafish. *Anal. Methods* **2018**, *10*, 5702–5706. DOI: 10.1039/C8AY02199F.

[141] Dong, B.; Song, W.; Lu, Y.; Kong, X.; Mehmood, A. H.; Lin, W. An Ultrasensitive Ratiometric Fluorescent Probe Based on ICT-PETFRET Mechanism for the Quantitative Measurement of pH Values in Endoplasmic Reticulum (ER). *Chem. Commun.* **2019**, *55*, 10776–10779. DOI: 10.1039/C9CC03114F.

[142] Fang, M.; Xia, S.; Bi, J.; Wigstrom, T. P.; Valenzano, L.; Wang, J.; Mazi, W.; Tanasova, M.; Luo, F. T.; Liu, H. A Cyanine-Based Fluorescent Cassette with Aggregation-Induced Emission for Sensitive Detection of pH Changes in Live Cells. *Chem. Commun.* **2018**, *54*, 1133–1136. DOI: 10.1039/C7CC08986D.

[143] Wang, L.; Cui, M.; Tang, H.; Cao, D. A BODIPY- 2-(2'-Hydroxyphenyl) Benzothiazole Conjugate with Solid State Emission and Used as a Fluorescent pH Probe. *Anal. Methods* **2018**, *10*, 1633–1639. DOI: 10.1039/C8AY00053K.

[144] Tang, X.; Zhu, Z.; Wang, Y.; Han, J.; Ni, L.; Wang, L.; Zhang, H.; Li, J.; Qiu, Y. A Dual Site-Controlled Probe for Fluorescent Monitoring of Intracellular pH and Colorimetric Monitoring of Cu^{2+}. *Sens. Actuators B Chem.* **2018**, *270*, 35–44. DOI: 10.1016/j.snb.2018.04.173.

[145] Chao, J.; Song, K.; Zhang, Y.; Yin, C.; Huo, F.; Wang, J.; Zhang, T. A Pyrene-Based Colorimetric and Fluorescent pH Probe with Large Stokes Shift and Its Application in Bioimaging. *Talanta* **2018**, *189*, 150–156. DOI: 10.1016/j.talanta.2018.06.073.

[146] Georgiev, N. I.; Said, A. I.; Toshkova, R. A.; Tzoneva, R. D.; Bojinov, V. B. A Novel Water-Soluble Perylenetetracarboxylic Diimide as a Fluorescent pH Probe: Chemosensing, Biocompatibility and Cell Imaging. *Dyes Pigm.* **2019**, *160*, 28–36. DOI: 10.1016/j.dyepig.2018.07.048.

[147] Liu, Z.; Li, G.; Wang, Y.; Li, J.; Mi, Y.; Zou, D.; Li, T.; Wu, Y. Quinoline-Based Ratiometric Fluorescent Probe for Detection of Physiological pH Changes in Aqueous Solution and Living Cells. *Talanta* **2019**, *192*, 6–13. DOI: 10.1016/j.talanta.2018.09.026.

[148] Wang, S.; Fan, Y.; Li, D.; Sun, C.; Lei, Z.; Lu, L.; Wang, T.; Zhang, F. Anti-Quenching NIR-II Molecular Fluorophores for in Vivo High-Contrast Imaging and pH Sensing. *Nat. Commun.* **2019**, *10*, 1058 DOI: 10.1038/s41467-019-09043-x.

[149] Jiang, T.; Wang, X.; Wang, G.; Wang, Y.; Wang, K.; Xuan, X.; Chen, C.; Jiang, K.; Zhang, H. Light-Activated "Cycle-Reversible Intramolecular Charge Transfer" Fluorescent Probe: Monitoring of pHi Trace Change Induced by UV Light in

Programmed Cell Death. *Chem. Commun.* **2019**, ***55***, 5279–5282. DOI: 10.1039/C9CC01451A.

[150] Song, W.; Dong, B.; Lu, Y.; Lin, W. Developing a Novel Ratiometric Fluorescent Probe Based on ESIPT for the Detection of pH Changes in Living Cells. *Tetrahedron Lett.* **2019**, *60*, 1696–1701. DOI: 10.1016/j.tetlet.2019.05.047.

[151] Mai, H.; Wang, Y.; Li, S.; Jia, R.; Li, S.; Peng, Q.; Xie, Y.; Hu, X.; Wu, S. A pH-Sensitive near-Infrared Fluorescent Probe with Alkaline pKa for Chronic Wound Monitoring in Diabetic Mice. *Chem. Commun.* **2019**, *55*, 7374–7377. DOI: 10.1039/C9CC02289A.

[152] Jin, D.; Wang, B.; Hou, Y.; Du, Y.; Li, X.; Chen, L. Novel Near-Infrared pH-Sensitive Cyanine-Based Fluorescent Probes for Intracellular pH Monitoring. *Dyes Pigm.* **2019**, *170*, 107612. DOI: 10.1016/j.dyepig.2019.107612.

[153] Lin, B.; Fan, L.; Ying, Z.; Ge, J.; Wang, X.; Zhang, T.; Dong, C.; Shuang, S.; Wong, M. S. The Ratiometric Fluorescent Probe with High Quantum Yield for Quantitative Imaging of Intracellular pH. *Talanta* **2020**, *208*, 120279. DOI: 10.1016/j.talanta.2019.120279.

[154] Zhu, J.; Gao, Q.; Tong, Q.; Wu, G. Fluorescent Probes Based on Benzothiazole-Spiropyran Derivatives for pH Monitoring in Vitro and in Vivo. *Spectrochim. Acta A* **2020**, *225*, 117506. DOI: 10.1016/j.saa.2019.117506.

[155] Yin, H.; Zhao, B.; Kan, W.; Ding, L.; Wang, L.; Song, B.; Wang, W.; Deng, Q. A Phenanthro[9,10-d]Imidazole-Based Optical Sensor for Dual-Responsive Turn-on Detection of Acidic pH and Cu^{2+} in Chicken Blood and Living Cells. *Dyes Pigm.* **2020**, *173*, 107916. DOI: 10.1016/j.dyepig.2019.107916.

[156] Yuan, X.; Zhang, T.; Yan, J.; Chen, X.; Wang, L.; Liu, X.; Zheng, K.; Zhang, N. A Simple Acidic 'Turn-On' Fluorescent pH Probe Based on BOPYIN and Its Visual Detection and Cellular Imaging. *Dyes Pigm.* **2020**, *177*, 108318. DOI: 10.1016/j.dyepig.2020.108318.

[157] Mohamed, M. B. I.; Aysha, T. S.; Elmorsi, T. M.; El-Sedik, M.; Omara, S. T.; Shaban, E.; Kandil, O. M.; Bedair, A. H. Colorimetric Chemosensor and Turn on Fluorescence Probe for pH Monitoring Based on Xanthene Dye Derivatives and Its Bioimaging of Living *Escherichia coli* Bacteria. *J. Fluoresc.* **2020**, *30*, 601–612. DOI: 10.1007/s10895-020-02522-1.

[158] Benitez-Martin, C.; Guadix, J. A.; Pearson, J. R.; Najera, F.; Perez-Pomares, J. M.; Perez-Inestrosa, E. Indolenine-Based Derivatives as Customizable Two-Photon Fluorescent Probes for pH Bioimaging in Living Cells. *ACS Sens.* **2020**, *5*, 1068–1074. DOI: 10.1021/acssensors.9b02590.

[159] He, X.; Xu, W.; Xu, C.; Ding, F.; Chen, H.; Shen, J. Reversible Spiropyran-Based Chemosensor with pH-Switches and Application for Bioimaging in Living Cells, *Pseudomonas aeruginosa* and Zebrafish. *Dyes Pigm.* **2020**, *180*, 108497. DOI: 10.1016/j.dyepig.2020.108497.

[160] Haldar, U.; Chaudhury, S. S.; Sharma, R.; Ruidas, B.; Patra, S. G.; Mukhopadhyay, C. D.; Lee, H. A Fluorimetric Water-Soluble Polymeric pH Chemosensor for Extremely Acidic Conditions: Live-Cell and Bacterial Imaging Application. *Sens. Actuators B Chem.* **2020**, *320*, 128379. DOI: 10.1016/j.snb.2020.128379.

[161] He, X.; Ding, F.; Xu, W.; Xu, C.; Li, Y.; Qian, Y.; Zhao, S.; Chen, H.; Shen, J. FRET-Based Colorimetric and Ratiometric Sensor for Visualizing pH Change and Application for Bioimaging in Living Cells, Bacteria and Zebrafish. *Anal. Chim. Acta.* **2020**, *1127*, 29–38. DOI: 10.1016/j.aca.2020.06.031.

[162] Yang, J.; Li, M.; Zhu, W. H. Dicyanomethylene-4H-Pyran-Based NIR Fluorescent Ratiometric Chemosensor for pH Measurement. *Res. Chem. Intermed.* **2018**, *44*, 3959–3969. DOI: 10.1007/s11164-018-3334-z.

[163] Wang, Z.; Zhang, Y.; Li, M.; Yang, Y.; Xu, X.; Xu, H.; Liu, J.; Fang, H.; Wang, S. Two D-π-a Type Fluorescent Probes Based on Isolongifolanone for Sensing Acidic pH with Large Stokes Shifts. *Tetrahedron* **2018**, *74*, 3030–3037. DOI: 10.1016/j.tet.2018.05.008.

[164] Hwang, S. M.; Kim, C. Fluorescent Detection of Zn^{2+} and Cu^{2+} by a Phenanthrene-Based Multifunctional Chemosensor That Acts as a Basic pH Indicator. *Inorg. Chim. Acta* **2018**, *482*, 375–383. DOI: 10.1016/j.ica.2018.06.039.

[165] Yuan, C.; Li, J.; Xi, H.; Li, Y. A Sensitive Pyridine-Containing Turn-off Fluorescent Probe for pH Detection. *Mater. Lett.* **2019**, *236*, 9–12. DOI: 10.1016/j.matlet.2018.10.060.

[166] Li, J.; Zhuge, X.; Yan, X.; Li, Y.; Yuan, C. Two pH-Responsive Fluorescence Probes Based on Indole Derivatives. *Opt. Mater.* **2019**, *90*, 257–263. DOI: 10.1016/j.optmat.2019.03.001.

[167] Ye, F.; Liang, X. M.; Wu, N.; Li, P.; Chai, Q.; Fu, Y. A New Perylene-Based Fluorescent pH Chemosensor for Strongly Acidic Condition. *Spectrochim. Acta A* **2019**, *216*, 359–364. DOI: 10.1016/j.saa.2019.03.049.

[168] Georgiev, N. I.; Krasteva, P. V.; Bojinov, V. B. A Ratiometric 4-Amido-1,8-Naphthalimide Fluorescent Probe Based on Excimer-Monomer Emission for Determination of pH and Water Content in Organic Solvents. *J. Lumin.* **2019**, *212*, 271–278. DOI: 10.1016/j.jlumin.2019.04.053.

[169] Aysha, T. S.; Sedik, M. S.; Mohamed, M. B. I.; Gaballah, S. T.; Kamel, M. M. Dual Functional Colorimetric and Turn-off Fluorescence Probe Based on Pyrrolinone Ester Hydrazone Dye Derivative for Cu^{2+} Monitoring and pH Change. *Dyes Pigm.* **2019**, *170*, 107549. DOI: 10.1016/j.dyepig.2019.107549.

[170] Wang, Y.; Zeng, L.; Zhou, J.; Jiang, B.; Zhao, L.; Wang, C.; Xu, B. A Dansyl Fluorescent pH Probe with Wide Responsive Range in Aqueous Solution. *Spectrochim. Acta A* **2019**, *223*, 117348. DOI: 10.1016/j.saa.2019.117348.

[171] Hazra, A.; Roy, A.; Bhattacharjee, A.; Barma, A.; Roy, P. Quinoline Based Chromogenic and Fluorescence Chemosensor for pH: Effect of Isomer. *J. Mol. Struct.* **2020**, *1201*, 127173. DOI: 10.1016/j.molstruc.2019.127173.